DOKUZ EYLÜL UNIVERSITY

GRADUATE SCHOOL OF NATURAL AND APPLIED SCIENCES

INVESTIGATING THE EFFECT OF MISALIGNMENT ON ROTOR-BEARING SYSTEM CONNECTED WITH HELICAL COUPLING

by

Timuçin ERİŞ

July, 2008

İZMİR

INVESTIGATING THE EFFECT OF MISALIGNMENT ON ROTOR-BEARING SYSTEM CONNECTED WITH HELICAL COUPLING

A Thesis Submitted to the
Graduate School of Natural and Applied Sciences of Dokuz Eylül University In Partial Fulfillment of the Requirements for the Degree of Doctor of Philosophy in Mechanical Engineering, Machine Theory and Dynamics Program

by
Timuçin ERİŞ

July, 2008
İZMİR

Ph.D. THESIS EXAMINATION RESULT FORM

We have read the thesis entitled **"INVESTIGATING THE EFFECT OF MISALIGNMENT ON ROTOR-BEARING SYSTEM CONNECTED WITH HELICAL COUPLING"** completed by **TİMUÇİN ERİŞ** under supervision of **PROF. DR. HİRA KARAGÜLLE** and we certify that in our opinion it is fully adequate, in scope and in quality, as a thesis for the degree of Doctor of Philosophy.

Prof. Dr. Hira KARAGÜLLE

_____

_____

Supervisor

Yard. Doç. Dr. Zeki KIRAL	Yard. Doç. Dr. Yavuz ŞENOL
_____	_____
_____	_____
Thesis Committee Member	Thesis Committee Member
Prof. Dr. Mustafa SABUNCU	Prof. Dr. Vedat KARADAĞ
_____	_____
_____	_____
Examining Committee Member	Examining Committee Member

_____

Prof.Dr. Cahit HELVACI

Director

Graduate School of Natural and Applied Sciences

ACKNOWLEDGMENTS

I would like to express my gratitude to my supervisor, Prof. Dr. Hira Karagülle, whose expertise, understanding, and patience, made this study possible. I would like to thank the other members of my committee, Assist. Prof. Dr. Zeki Kıral, and Assist. Prof. Dr. Yavuz Şenol for the assistance they provided at all levels of the research project.

A very special thanks goes out to Prof. Dr. Semra Ülkü of Izmir Institute of Technology, without whose motivation and encouragement I would not have been able to attend this program.

I must acknowledge the patience of Mechanical Engineering Department of Izmir Institute of Technology, of which members were always patience and tolerated my lack of attendance to the my duties.

Timuçin ERİŞ

INVESTIGATING THE EFFECT OF MISALIGNMENT ON ROTOR-BEARING SYSTEMS CONNECTED WITH HELICAL COUPLING

ABSTRACT

In this thesis, helical coupling is modeled with the gemetrically exact beam theory in order to investigate the effect of misalignment on rotor-bearing systems. A new approach based on using constitutive equations as constraint was developed. Comparison with previous results showed that proposed approach was able to predict the frequency components associated with misalignment. Results indicated that misalignment causes driven shaft velocity to fluctuate around that of driving shaft for any misalignment type. However variations observed in velocity are not constant for given misalignment value but dependent on inertia and coupling geometry. Large inertia causes rotor velocity to converge to that motor. Results showed that reaction loads are also dependent on inertia and coupling geometry.

Keywords: Misalignment, helical coupling, geometrically exact beam theory.

EKSEN KAÇIKLIĞIN HELİSEL KAPLİNLE BAĞLI ROTOR- YATAK SİSTEMİNE ETKİSİNİN İNCELENMESİ

ÖZ

Bu tez çalışmasında, eksenel kaçıklığın bir rotor-yatak sistemine etkisini incelemek için helisel kaplin, geometrik tam kiriş teorisi ile modellenmiştir. Bünye denklemlerini kısıtlama olarak kullanan yeni bir yaklaşım geliştirilmiştir. Literatürdeki çalışmalarla yapılan karşılaştırmalar, önerilen yaklaşımın eksenel kaçıklığa bağlı frekans bileşenlerini tahmin edebildiğini göstermiştir. Sonuçlar, eksenel kaçıklığın her tipi için, tahrik edilen şaftın hızının tahrik şaftının hızı etrafında salınım yaptığını göstermiştir. Hızda gözlenen salınımların belirli bir eksenel kaçıklık değeri için sabit olmayıp, atalet ve kaplin geometrisine de bağlı olduğu gözlemlenmiştir. Atalet arttıkça rotor hızının motor hızına yaklaştığı gözlemlenmiştir. Sonuçlar, reaksiyon kuvvetlerinin de atalet ve kaplin geometrisine bağlı olduğunu göstermiştir.

Anahtar Kelimeler: Eksenel kaçıklık, helisel kaplin, geometrik tam kiriş teorisi.

CONTENTS

Page

CHAPTER ONE
INTRODUCTION

Misalignment is one of the most common causes of vibration in rotating machinery. Shaft misalignment causes additional loads on structure and, in return, decreases operating lives of parts (Piotrowski, 1995). A poorly aligned machine can cost a factory 20% to 30% in machine down time, replacement parts, inventory, and energy consumption (Ganeriwala, Patel & Hartung, 1999). Misalignment is the condition in which driving and driven shafts connected by coupling are not collinear at the point of power transition (Piotrowski, 1995). There are basically two types of misalignment: angular and parallel. A combination of angular and parallel misalignment in the vertical and horizontal directions is observed in applications. Despite the best efforts, it is almost impossible to achieve perfect alignment between driving and driven shafts. Even if perfect alignment was obtained initially, it could not be maintained over extended period of time due to various effects, such as heat generated in casings, from bearings, lubrication systems, compression of gases and foundation movements (Xu & Marangoni, 1994a). For this reason, flexible couplings are used in industry to accommodate unavoidable misalignment. Although flexible coupling help power train to tolerate misalignment, they do not completely eliminate detrimental effects of misalignment on system. Thus detection of misalignment is crucial to guarantee continuous operation.

In spite of the importance of misalignment, few researchers from academic world have paid attention to this phenomenon due to complexity in modeling.

Dewel & Mitchell (1984) predicted that bending moment produced by angularly misaligned four bolt metallic disc coupling has frequency components which are the multiples of four times the driving shaft's rotation frequency (called 4X component), due to variation in coupling stiffness and changing bolt positions for every quarter turn of driving shaft. Moreover they assumed that coupling in case of angular misalignment behaves exactly as universal joint. Thus they concluded that bending moment has additional frequency components which are the multiples of twice the

driving shaft's speed (called 2X component). Their experiments showed that 2X and 4X components produced the largest changes in frequency spectrum.

Xu & Marangoni (1994a, 1994b) investigated the effect of angular misalignment on rotor-flexible coupling- rotor system. They assumed that flexible coupling in case of angular misalignment behaves exactly as universal joint (i.e. Cadan joint). Thus they estimated that bending moment caused by misaligned coupling has frequency of twice the motor speed (2X component). They concluded that although 2X component can be used as the indication of angular misalignment, it may not always show up in vibration spectrum if it is not close enough to one of the system natural frequencies.

Sekhar & Parbhu (1995) studied the misalignment effects on rotor- bearing system by developing a theoretical model using higher order finite elements. They assumed that misaligned coupling behaves as linear spring element, of which stiffness coefficients vary with frequency of twice the motor speed. They also assumed that unbalance force has 1X and 2X components. They observed that while system response in 2X component was increased with increasing misalignment, response in 1X component was altered significantly.

Lee & Lee (1999) investigated the effects of misalignment on the natural frequency of misaligned rotor system by deriving a dynamic model for misaligned rotor-ball bearing system driven through flexible coupling. They treated the reaction loads and deformations at bearing and coupling elements as the misalignment effect. Forces and moments due to deformation of coupling element are described by modeling the coupling as beam element with the effective flexural and axial rigidity. Both experimental and simulation results agree that, as angular misalignments increases, natural frequency associate with the misalignment direction increases largely. On the other hand natural frequencies are not changed for parallel misalignment.

Saavendra and Ramirez (2004a, 2004b) developed a theoretical model of rotor bearing system with a flexible coupling to investigate the shaft misalignment. They

considered the coupling as couple of rigid blocks connected with ideal spring elements. They presented an experimental method to construct the coupling stiffness matrix. They showed that frequencies generated by shaft misalignment are directly dependent on the frequencies of the variation in coupling stiffness.

Misalignment results in reaction loads on system due to relative deformation between coupling faces. Since most of the couplings are not uniform but rather has certain geometric symmetry around their rotation axes, magnitude of reaction loads at given instant of time depend on the angular position of driving shaft. As driving shaft rotates with constant speed, deformed coupling repeats its configuration. Thus reaction loads change periodically. If misaligned coupling causes driving and driven shaft speeds to differ as universal joint does in case of angular misalignment, relative deformation between coupling faces would be different as compared to the case when driving and driven shafts have same speeds. Since reaction loads depend on the relative position between couplings faces, periods as well as the magnitude of reaction loads would also be different. Moreover motor produces additional torque in order to compensate inertial effect resulted from driven shaft's rotary inertia and acceleration. In return this torque, depending on the deformed coupling configuration, may result in additional reaction loads on driven shaft. Thus behavior of the rotating coupling should be identified in order to understand effect of the misalignment on system.

In previous studies mentioned above, rotating coupling behavior is always assumed to be known a priori, and reaction loads generated by misaligned coupling on system are estimated accordingly. Behaviors which are assumed to be exhibited by deformed coupling are a) universal joint (Dewel & Mitchell, 1984, Xu & Marangoni, 1994a 1994b) b) ideal spring elements with periodic stiffness which has frequencies of integer multiply of motor speed (Sekhar & Prabu, 1995). Although vibration spectrum of misaligned system given in literature and/or obtained by above mentioned researchers justifies these assumptions, there are some points to be considered:

a) Universal joint effect is borrowed from rigid body dynamics. It states that two rigid shafts connected by rigid coupling (Cardan joint) should have same rotation angle for one full rotation (i.e. 2Π). If angular misalignment is present, full circle in the plane perpendicular to driving shaft axis is manifested as ellipse in the plane perpendicular to driven shaft axis. Therefore driven shaft speed fluctuates around that of driving shaft. However couplings (considered in above studies) are flexible elements and they do not necessarily behave as rigid ones. Also (if applicable) universal joint effect considers only pure angular misalignment. Moreover, if angularly misaligned coupling behaves exactly as universal joint same vibration pattern should be observed for all angularly misaligned systems. However, systems connected with different coupling type exhibit different vibration spectrum in case of angular misalignment.
b) Modeling flexible coupling as ideal spring element requires determination of stiffness coefficients for different rotation angles. Even if this can be accomplished, measuring stiffness for different misalignment conditions would be difficult. In addition to that, methods employed for that purpose should also consider certain dynamical effects (i.e. variation of driven shaft speed, friction and loads resulted from operation) since they may change the relative deformation between coupling faces, thereby altering the reaction loads.

As mentioned above developing models for misaligned systems is difficult due to complexity of the phenomena. Thus a priori assumptions for misaligned coupling behavior in rotating system are required. However, as explained in previous paragraph, validity of previously employed assumptions is in question. For this reason new method which can calculate the deformed coupling behavior without any a priori assumptions is necessary to identify characteristics of misalignment. Driven shaft moves due to loads which are transferred through coupling. Since coupling is a flexible element, transferred loads could be calculated by employing constitutive equations. If one uses constitutive equation with proper assumptions as constraints,

deformed coupling behavior can be computed directly. This is the main theme of this study and details are presented in subsequent chapters.

Rotating coupling exhibits the motion known as three dimensional finite rotations. Displacements and rotations experienced by structure undergoing finite rotation are not only deformations but include rigid body motion as well. Thus deformations should be extracted from displacements to determine the structures behavior correctly. Classical example of finite rotation is a swinging beam. Some methods pertaining to finite rotation can be found in the literature. In this study helical coupling is used. Since helical coupling is nothing more than helical beam, computationally simple method known as geometrically exact beam theory is used to model its behavior. Details of geometrically exact beam theory are presented in subsequent chapter.

CHAPTER TWO
MISALIGNMENT

2.1 Definition of Shaft Misalignment

Shaft misalignment is defined as “the deviation of relative shaft position from a collinear axis of rotation measured at the points of power transmission when equipment is running at normal operating conditions” (Piotrowski, 1995). If driving and driven shafts are collinear, then they are said to be aligned. If misalignment is present, centerline of one shaft deviates with respect to the centerline of the other shaft. Figure 2.1 depicts the typical misalignment condition. Since misalignment occurs in 3D space, misalignment between two shafts is determined by projecting drive train to the two different planes which are perpendicular (Figure 2.2).

There are basically two types of shaft misalignment: Angular and parallel. If axes of rotation of two shafts intersect with one another at an angle, misalignment is termed angular misalignment (Figure 2.3a). If centerlines of two shafts are parallel but do not intersect, misalignment is called parallel misalignment (Figure 2.3b). In practice combination of both angular and parallel misalignment is encountered in machine assemblies.

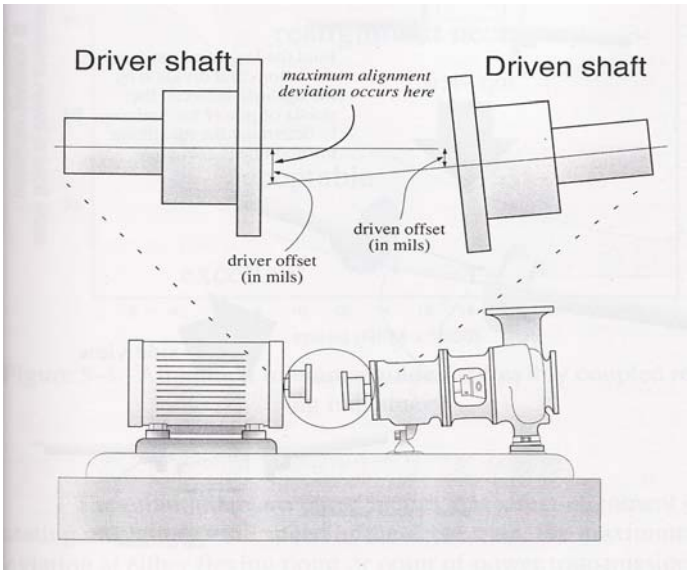

Figure 2.1 Typical misalignment conditions. Adapted from Piotrowski, (1995), page 143.

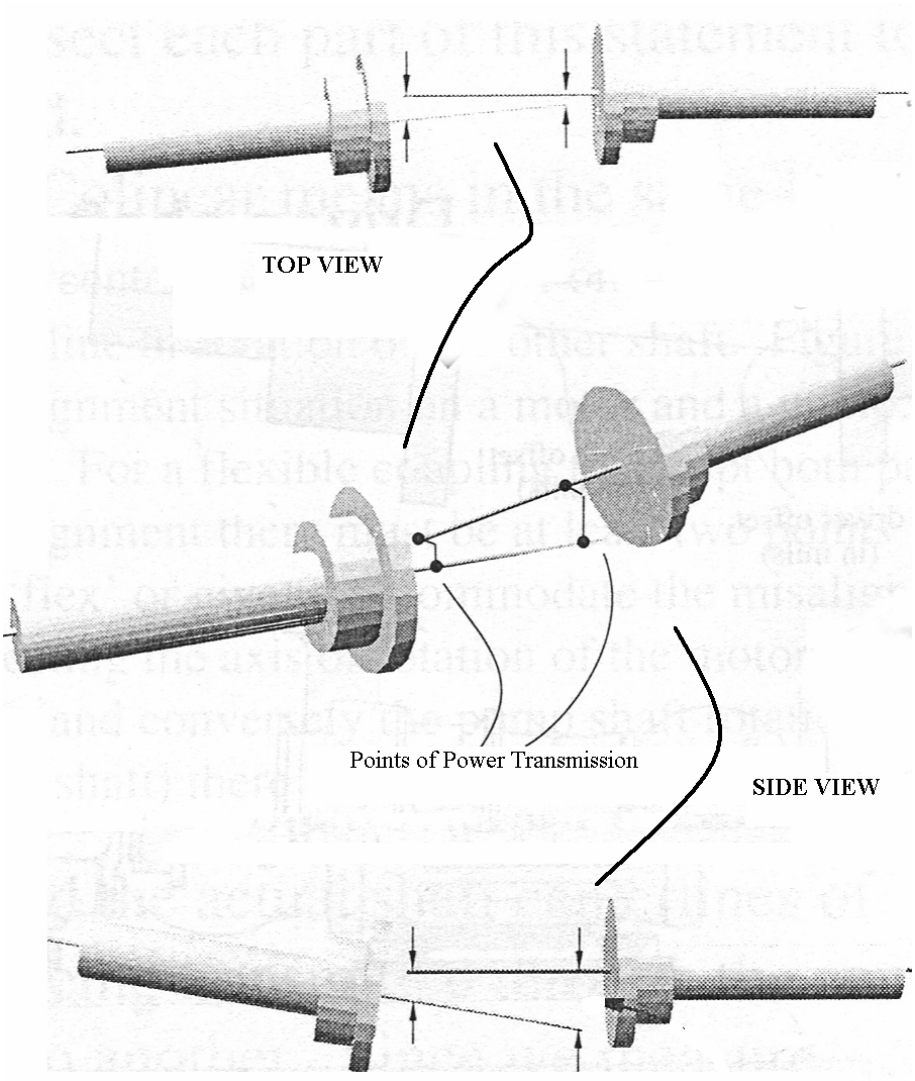

Figure 2.2 Determination of misalignment. Adapted from Piotrowski (195) page 144.

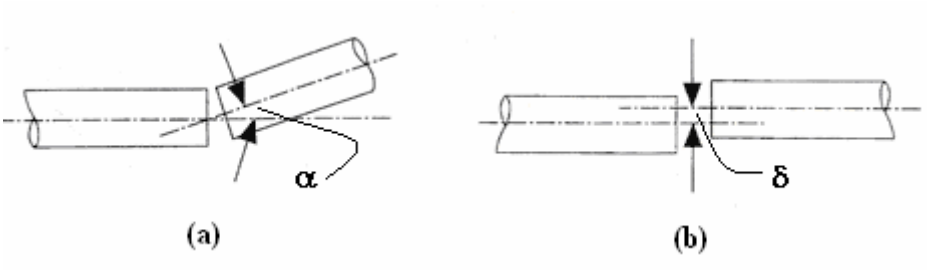

Figure 2.3 Misalignment types: (a) Angular misalignment. α is the misalignment angle. (b) Parallel misalignment. δ is the misalignment offset.

2.2 Importance of Shaft Misalignment

When shafts are misaligned, the reaction loads are generated in system. These loads produce stresses as well as the vibration on the rotating and stationary components and cause some parts to fail. To emphasize the detrimental effects of misalignment on field applications, two examples will be discussed. First, an ammonia plant in USA was shut down for an extended period when a compressor shaft failed catastrophically due to excessive coupling misalignment. This failure resulted in the process upset and substantial economic losses for that company (Dewel & Mitchel, 1984). The second example concerns a steel company. According to predictive maintenance department of that company, misalignment made up of 23% of vibration related faults in production lines.

Despite the best efforts, perfect alignment of rotating machinery shafts cannot be achieved in practical application. Even if perfect alignment was achieved initially, it could not be maintained over an extended period of time because of the dynamic movements caused by the thermal growth of machinery casing (Piotrowski, 1995). Thus flexible couplings are used in industry to accommodate unavoidable misalignment. Although flexible couplings help the power-train to tolerate misalignment, they do not completely eliminate the negative effects of misalignment.

2.3 Symptoms of Shaft Misalignment

Reaction loads generated by misalignment are typically static and difficult to measure. Therefore what really seen in practical applications are the secondary effects of these loads which exhibit many of the following symptoms (Piotrowski, 1995):

- Excessive radial and axial vibration
- Premature bearing, seal, shaft, or coupling failure
- Excessive amount of oil leakage at the bearing seals
- Loose foundation bolts
- Loose or broken coupling bolts.
- High casing temperature.

CHAPTER THREE
GEOMETRICALLY EXACT BEAM THEORY

3.1 Introduction

G*eometrically exact beam theory* states that configurations of the beam are completely defined by specifying evolution of an *orthogonal transformation* and position vector of the line of centroit of the beam cross sections. *Orthogonal transformation* takes the 3D orthogonal moving frame defined on the current configuration and places it on the next configuration. Moving frame is defined so that one of its vectors remains normal to the cross section in any configuration. Thus *orthogonal transformation* gives the rotation of a cross section. Orthogonal transformation of this kind is referred as SO(3) which stands for the Special Orthogonal (Lie) group. Matrix components of o*rthogonal transformation* are called *rotation matrix*.

Representing beam configuration with *rotation matrix* is attractive from the computational standpoint because it allows complete freedom on choosing the parametization schemes. Euler angles and use of queternions are two of the possibilities. In this study computationally much simpler approach is used: Incremental rotation vector.

3.2 Kinematics of 3D Beam

For a given parameter $S\in[0,L]\subset R$, $L\in R$, r*eference* (initial or undeformed) *configuration* of the beam is described by defining a family of cross-sections the centroids of which are connected by a space curve $S \rightarrow \boldsymbol{\varphi}_0(S)\in R^3$ in a three dimensional ambient space R^3 with a right-handed inertial Cartesian (*material*) frame, $\mathbf{E_i}$ i=1,2,3. The parameter S represents the arc-length of the line of centroids in the *reference* (unstressed) *configuration*. The parameter L is referred to as the initial length of the beam (Figure 3.1). Cross sections of the beam in reference configuration is defined by the unit vectors $S\rightarrow \mathbf{t}_{i,0}(S)\in R^3$ i=1,2,3 with unit vector $\mathbf{t}_{1,0}(S)$ being tangent to the line of centroids and normal to the cross section such that

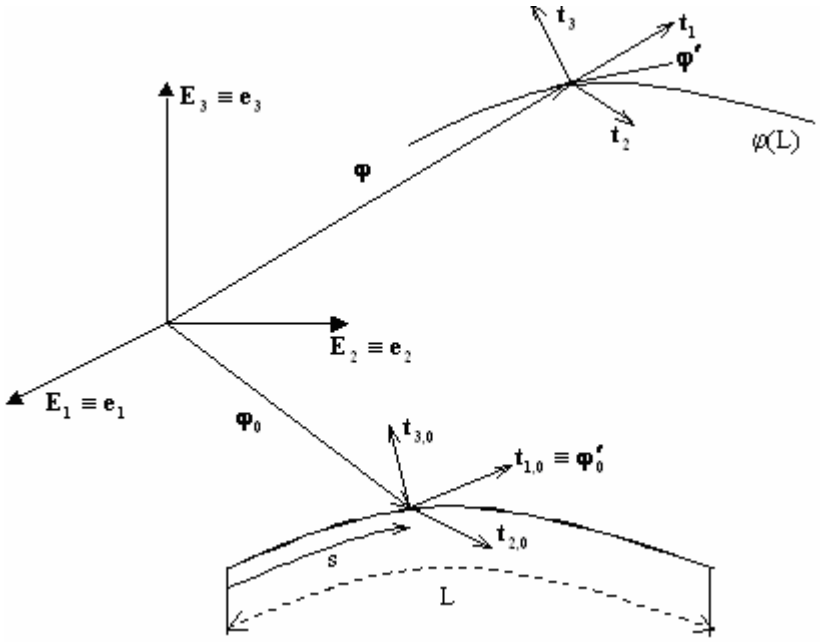

Figure 3.1 Initial and deformed configuration of three-dimensional beam. In figure, material ($\mathbf{E_1E_2E_3}$) and spatial ($\mathbf{e_1e_2e_3}$) frames are chosen to coincide.

$$\mathbf{t_{1,0}}(S)= \boldsymbol{\varphi}_0'(S) \tag{3.1}$$

and with unit vectors $\mathbf{t_{2,0}}$ and $\mathbf{t_{3,0}}$ being directed along the principle axis of inertia of the cross-section at S. In Equation 3.1 and in the foregoing prime (′) denotes the derivative with respect to the undeformed arc-length parameter S. Thus unit vectors $\mathbf{t_{i,0}}(S)$ i=1,2,3 form the right-handed orthonormal triad such that

$$\mathbf{t_{i,0}}(S) \cdot \mathbf{t_{j,0}}(S)=\delta_{i,j} \quad i,j=1,2,3 \tag{3.2a}$$

$$\left|\left|\mathbf{t_{i,0}}(S)\right|\right|=1 \quad i=1,2,3 \tag{3.2b}$$

$$\mathbf{t_{1,0}}(S)= \mathbf{t_{3,0}}(S)\mathbf{X}\, \mathbf{t_{2,0}}(S) \tag{3.2c}$$

where $\delta_{i,j}$ is the Knocker delta, i.e. $\delta_{i,j}=1$ i=j and $\delta_{i,j}=0$ i≠j. Body attached frame $\mathbf{t_{i,0}}(S)$, i=1,2,3 and *material* inertial frame $\mathbf{E_i}$, i=1,2,3 are related through a linear transformation $S\rightarrow\boldsymbol{\Lambda_0}(S)\in SO(3)$

$$\mathbf{t_{i,0}}(S) =\boldsymbol{\Lambda_0}(S)\cdot\mathbf{E_i} \quad i=1,2,3 \tag{3.3}$$

where SO(3) is the Special Orthogonal (Lie) group of the proper *orthogonal transformation* and $\boldsymbol{\Lambda_0}(S)$ is the orthogonal tensor defined as

$$\boldsymbol{\Lambda_0}(S)= \Lambda_{0;j,i}\mathbf{E_j}\otimes\mathbf{E_i} \quad i,j=1,2,3 \tag{3.4}$$

In Equation 3.4 and in the foregoing symbol ($\otimes$) denotes the tensor products of vectors. Matrix representation of $\mathbf{\Lambda_0}(S)$ satisfies $\det(\mathbf{\Lambda_0}(S))=1$ and $\mathbf{\Lambda_0}(S)\mathbf{\Lambda_0^T}(S)=\mathbf{I}$ with $\mathbf{I}$ being the 3x3 identity matrix. The matrix representation of tensor $\mathbf{\Lambda_0}(S)$ is referred to as the *initial rotation matrix*. The initial position vector of an arbitrary point on cross-section at S, $\mathbf{r_0}(S)$ may be defined as

$$\mathbf{r_0}(S,\xi_2,\xi_3)=\boldsymbol{\varphi}_0(S)+\sum_{i=2}^{3}\xi_i\mathbf{t}_{i,0}(S), \qquad S\in[0,L]\subset R, \qquad (\xi_2,\xi_3)\in R \tag{3.5a}$$

or with substituting Equation 3.3 into Equation 3.5a

$$\mathbf{r_0}(S,\xi_2,\xi_3)=\boldsymbol{\varphi}_0(S)+\sum_{i=2}^{3}\xi_i\mathbf{\Lambda_0}(S)\mathbf{E}_i(S) \tag{3.5b}$$

where ξ_2 and ξ_3 are the co-ordinates of the arbitrary point within a cross-section at S with respect to the its centroid (Figure 3.1). It should be emphasized that cross-section are assumed arbitrary and constant along the line of centroids. Thus initial position vector of centroids $\boldsymbol{\varphi_0}(S)$ and the orthogonal transformation $\mathbf{\Lambda_0}(S)$ at $S\in[0,L]$ completely define the initial configuration of the beam $S\rightarrow C_0=(\boldsymbol{\varphi_0}, \mathbf{\Lambda_0})\in R^3 x SO(3)$.

Similarly, deformed (*current*) configuration of the beam is defined by family of cross-sections connected through deformed beam centroid axis given by a space curve $S\rightarrow \boldsymbol{\varphi}(S)\in R^3$ in three dimensional space R^3 with inertial Cartesian (*spatial*) frame, $\mathbf{e_i}$ i=1,2,3 (Figure 3.1). Cross-sections in *current configuration* is described by orthonormal traid of unit vectors $\mathbf{t_i}(S)$ i=1,2,3 satisfying

$$\mathbf{t_i}(S)\cdot\mathbf{t_j}(S)=\delta_{i,j} \quad i,j=1,2,3 \tag{3.6a}$$

$$||\mathbf{t_i}(S)||=1 \quad i=1,2,3 \tag{3.6b}$$

$$\mathbf{t_1}(S)=\mathbf{t_3}(S)X\,\mathbf{t_2}(S) \tag{3.6c}$$

Unit vector $\mathbf{t_1}(S)$ is normal to the cross-section but not tangent to the line of centroids due to shear deformation. Unit vectors $\mathbf{t_2}(S)$ and $\mathbf{t_3}(S)$ are still directed along the principle axes of inertia of the cross-section at S. Although material inertial frame $\mathbf{E_i}$ i=1,2,3 is chosen to coincide with spatial inertial frame $\mathbf{e_i}$ i=1,2,3 in Figure 3.1 for clarity they do not necessarily coincide. Since unit vectors $\mathbf{t_{i,0}}$ i=1,2,3 and $\mathbf{t_j}$

j=1,2,3 form orthonormal frames they could be related with an orthogonal transformation $\mathbf{\Lambda}(S)\in SO(3)$ such that

$$\mathbf{t_i}(S) = \mathbf{\Lambda}(S)\cdot \mathbf{t_{i,0}}(S) \quad i=1,2,3 \tag{3.7}$$

where $\mathbf{\Lambda}(S)$ is the two-point orthogonal tensor defined as

$$\mathbf{\Lambda}(S)= \mathbf{t_i}(S)\otimes \mathbf{t_{i,0}}(S)= \Lambda_{j,i}\mathbf{e_j}\otimes\mathbf{E_i} \qquad i,j=1,2,3 \tag{3.8}$$

with $\Lambda_{j,i}$ being the co-ordinate representation in the inertial frames of the *reference* and *current configurations.* As mentioned above, matrix representation of $\mathbf{\Lambda}(S)$ satisfies $\det(\mathbf{\Lambda}(S))=1$ and $\mathbf{\Lambda(S)\Lambda^T(S)=I}$ with **I** being the 3x3 identity matrix.

If Bernoulli hypothesis of plane cross sections remaining planar after deformation and retaining their shapes is assumed to hold the position vector of an arbitrary point on cross-section at S, $\mathbf{r}(S)$ may be given as

$$\mathbf{r}(S,\xi_2,\xi_3) = \boldsymbol{\varphi}(S) + \sum_{i=2}^{3}\xi_i\mathbf{t}_i(S), \qquad S\in[0,L]\subset R, \qquad (\xi_2,\xi_3)\in R \tag{3.9a}$$

where $\boldsymbol{\varphi}(S)$ is position vectors of centroids and $\mathbf{t_i}$ i=1,2,3 are the unit vectors of body attached frame in *current configuration* (Figure 3.1). Substituting Equation 3.7 into Equation 3.9a yields

$$\mathbf{r}(S,\xi_2,\xi_3) = \boldsymbol{\varphi}(S) + \sum_{i=2}^{3}\xi_i\mathbf{\Lambda}(s)\mathbf{t}_{i,0}(S) \tag{3.9b}$$

Thus *current configuration* of the beam at $S\in[0,L]$ is fully described by position vector of centroids $\boldsymbol{\varphi}(S)$ and orthogonal transformation $\mathbf{\Lambda}(S)$: $S\rightarrow C=(\boldsymbol{\varphi}, \mathbf{\Lambda})\in R^3 x SO(3)$.

3.3 Derivatives of the Moving Frame

Since body attached frame $\mathbf{t_i}(S)$ i=1,2,3 changes its orientation with deformation of the beam it is also referred to as *moving frame* or *moving basis*. In order to derive the *stress-strain* relation one needs to calculate the derivatives of the moving basis (Equation 3.7) with respect to the (undeformed) arc-length parameter S; i.e.

$$\frac{d\mathbf{t}_i(S)}{dS} = \frac{d\mathbf{\Lambda}(S)}{dS}\cdot\mathbf{t}_{i,0}(S) + \mathbf{\Lambda}(S)\cdot\frac{d\mathbf{t}_{i,0}(S)}{dS} \quad i=1,2,3 \tag{3.10}$$

Taking the derivative of Equation 3.3 and substituting into Equation 3.10 together with Equation 3.3 and Equation 3.7 (by employing the property of $\mathbf{\Lambda}^{-1}(S) = \mathbf{\Lambda}^{T}(S)$) one obtains

$$\frac{d\mathbf{t}_i(S)}{dS} = \left(\mathbf{\Omega}(S) + \mathbf{\Lambda}(S)\cdot\mathbf{\Omega}_o(S)\cdot\mathbf{\Lambda}^{T}(S)\right)\cdot\mathbf{t}_i(S) = \overline{\mathbf{\Omega}}(S)\cdot\mathbf{t}_i(S) \qquad i=1,2,3 \qquad (3.11)$$

where

$$\mathbf{\Omega}(S) = \frac{d\mathbf{\Lambda}(S)}{dS}\cdot\mathbf{\Lambda}^{T}(S) \qquad (3.12a)$$

and

$$\mathbf{\Omega}_0(S) = \frac{d\mathbf{\Lambda}_0(S)}{dS}\cdot\mathbf{\Lambda}_0^{T}(S) \qquad (3.12b)$$

are the *skew-symmetric* tensors; i.e. $\mathbf{\Omega}(S) + \mathbf{\Omega}^{T}(S) = \mathbf{0}$, $\mathbf{\Omega}_0(S) + \mathbf{\Omega}_0^{T}(S) = \mathbf{0}$. Substituting Equation 3.8 and its derivative relative to arc-length parameter $S\in R$ into Equation 3.12a yields

$$\mathbf{\Omega}(S) = \left(\frac{d\Lambda_{j,i}}{dS}\cdot\mathbf{e}_j\otimes\mathbf{E}_i\right)\cdot\left(\Lambda_{k,l}\cdot\mathbf{E}_k\otimes\mathbf{e}_l\right) = \frac{d\Lambda_{j,i}}{dS}\Lambda_{k,l}\cdot\mathbf{e}_j\otimes\mathbf{e}_l \quad i,j,k,l=1,2,3 \qquad (3.13)$$

Similarly, substituting Equation 3.4 and its derivative into Equation 3.12b with Equation 3.8, one finds

$$\begin{aligned}\mathbf{\Lambda}(S)\cdot\Omega(S)\cdot\mathbf{\Lambda}^{T}(S) &= \left(\Lambda_{j,i}\cdot\mathbf{e}_j\otimes\mathbf{E}_i\right)\cdot\left(\frac{d\Lambda_{0;k,l}}{dS}\Lambda_{0;m,n}\mathbf{E}_k\otimes\mathbf{E}_n\right)\cdot\left(\Lambda_{p,q}\mathbf{E}_p\otimes\mathbf{e}_q\right)\\ &= \left(\Lambda_{j,i}\frac{d\Lambda_{k,l}}{dS}\Lambda_{m,n}\Lambda_{p,q}\cdot\mathbf{e}_j\otimes\mathbf{e}_q\right) \qquad i,j,k,l,m,n,p,q = 1,2,3\end{aligned} \qquad (3.14)$$

Thus $\overline{\mathbf{\Omega}}(S)$ is *spatial* tensor for each $S\in R$ and its components may be given relative to the moving frame $\mathbf{t}_i(S)$ i=1,2,3 as

$$\overline{\mathbf{\Omega}}(S) = \overline{\Omega}_{i,j}\mathbf{t}_i(s)\otimes\mathbf{t}_j(S) \qquad i,j=1,2,3 \qquad (3.15)$$

with

$$\overline{\Omega}_{i,j} = 0 \qquad i = j \qquad \text{and} \qquad \overline{\Omega}_{i,j} = -\overline{\Omega}_{j,i} \qquad i \neq j$$

Matrix representation of Equation 3.15 is more convenient and given as

$$\overline{\mathbf{\Omega}}(S) = \begin{bmatrix} 0 & -\omega_3 & \omega_2 \\ \omega_3 & 0 & -\omega_1 \\ -\omega_2 & \omega_1 & 0 \end{bmatrix} \qquad (3.16)$$

If one introduces the vector $S \rightarrow \boldsymbol{\omega}(S) = \omega_i(S)\mathbf{t}_i(S)$ $i = 1,2,3$, vector $\boldsymbol{\omega}(S)$ and skew-symmetric tensor $\overline{\boldsymbol{\Omega}}(S)$ satisfy

$$\overline{\boldsymbol{\Omega}}(S) \cdot \boldsymbol{\omega}(S) = \mathbf{0} \tag{3.17}$$

Vector $\boldsymbol{\omega}(S)$ is called the *axial vector* of the skew-symmetric tensor $\overline{\boldsymbol{\Omega}}(S)$. The derivatives of moving frame (Equation 3.11) may be recast into another expression with axial vector given in Equation 3.17 as

$$\frac{d\mathbf{t}_i(S)}{dS} = \boldsymbol{\omega}(S) \times \mathbf{t}_i(S) \quad i=1,2,3 \tag{3.18}$$

It should be noted that although axial vector $\boldsymbol{\omega}(S)$ is parametized by reference arc-length S it is a spatial vector (Equation 3.17 and Equation 3.18). Alternatively axial vector $\boldsymbol{\omega}(S)$ may be expressed relative to $\mathbf{t}_{i,0}$ i=1,2,3 or $\mathbf{E}_j$ j=1,2,3 by employing Equation 3.10; i.e. *material* form of axial vector such that

$$\mathbf{K}(S) = \boldsymbol{\Lambda}^T(S) \cdot \boldsymbol{\omega}(S) \tag{3.19}$$

The axial vector $\mathbf{K}(S)$ appears in the material form of internal power expression and its derivation presented in derived in section 3.4.

Note: Property of

$$(\boldsymbol{\Lambda})^{-1} = \boldsymbol{\Lambda}^T = \left(\Lambda_{j,i}\mathbf{e}_j \otimes \mathbf{E}_i\right)^T = \Lambda_{i,j}\mathbf{E}_i \otimes \mathbf{e}_j \qquad i,j = 1,2,3 \tag{3.20}$$

is used in above equations.

3.4 The Linear and Angular Momentum

In case of motion, configuration of the beam is not only parametized by reference arc-length $S \in [0,L]$ also with time $t \in R^+$; that is

$$t \rightarrow \mathbf{r}_t(S,\xi_2,\xi_3;t) = \boldsymbol{\varphi}(S,t) + \sum_{i=2}^{3} \xi_i \mathbf{t}_i(S,t) \tag{3.21a}$$

or with Equation 3.9b

$$t \rightarrow \mathbf{r}_t(S,\xi_2,\xi_3;t) = \boldsymbol{\varphi}(S,t) + \sum_{i=2}^{3} \xi_i \boldsymbol{\Lambda}(S,t) \cdot \mathbf{t}_{i,0}(S) \tag{3.21b}$$

Before introducing the linear and angular momentum vectors associated with the motion (Equation 3.21) material time derivative of the moving frame $\mathbf{t_i}(S,t)$ i=1,2,3 needs to be calculated; that is

$$\dot{\mathbf{t}}_i(S,t) = \left(\dot{\mathbf{\Lambda}}(S,t)\cdot\mathbf{\Lambda}^T(S,t)\right)\cdot\mathbf{t}_i(S,t) = \mathbf{W}(S,t)\cdot\mathbf{t}_i(S,t) \qquad i=1,2,3 \tag{3.22}$$

where $\mathbf{W}(S,t)$ is the *spin* of the moving frame and it is a *spatial skew symmetric* tensor; i.e. $\mathbf{W}(S,t) = -\mathbf{W}^T(S,t)$. The associated axial vector $\mathbf{w}(S,t)$ is the *vorticity* of the moving frame $\mathbf{t_i}(S,t)$ i=1,2,3 and satisfies the relation $\mathbf{W}(S,t)\cdot\mathbf{w}(S,t) = 0$. In Equation 3.22 and in the foregoing superposed dot ($\dot{}$) denotes the material time derivative.

In terms of vorticity vector Equation 3.22 may be written as

$$\dot{\mathbf{t}}_i(S,t) = \mathbf{w}(S,t)\times\mathbf{t}_i(S,t) \qquad i=1,2,3 \tag{3.23}$$

Taking the material time derivative of Equation 3.21a yields

$$\dot{\mathbf{r}}_t(S,\xi_2,\xi_3;t) = \dot{\boldsymbol{\varphi}}(S,t) + \sum_{i=2}^{3}\xi_i\dot{\mathbf{t}}_i(S,t) \tag{3.24a}$$

Substituting Equation 3.23 into Equation 3.24a one obtains

$$\dot{\mathbf{r}}_t(S,\xi_2,\xi_3;t) = \dot{\boldsymbol{\varphi}}(S,t) + \mathbf{w}(s,t)\times\left(\sum_{i=2}^{3}\xi_i\mathbf{t}_i(S,t)\right) \tag{3.24b}$$

If kinematic assumption given in Equation 3.21a is used in Equation 3.24b one has

$$\dot{\mathbf{r}}_t(S,\xi_2,\xi_3;t) = \dot{\boldsymbol{\varphi}}(S,t) + \mathbf{w}(s,t)\times\left(\mathbf{r}_t(S,t) - \boldsymbol{\varphi}(S,t)\right) \tag{3.24c}$$

Linear momentum per unit of reference arc-length $S\in[0,L]$ of an arbitrary cross-section $A_t\in R^2$ in *current configuration* is defined as

$$\mathbf{L}_t = \int_A \rho(S,\xi_2,\xi_3)\dot{\mathbf{r}}_t(S,\xi_2,\xi_3)\,d\xi_2 d\xi_3 \tag{3.25a}$$

where $\rho(S,\xi_2\xi_3)$ is the density in reference configuration. Substituting Equation 3.24c into Equation 3.25a it is obtained

$$\mathbf{L}_t = \left(\int_A \rho(S,\xi_2,\xi_3)\,d\xi_2 d\xi_3\right)\dot{\boldsymbol{\varphi}}(S,t) + \mathbf{w}(s,t)\times\left(\int_A\left(\mathbf{r}_t(S,t) - \boldsymbol{\varphi}(S,t)\right)d\xi_2 d\xi_3\right) \tag{3.25b}$$

Since $\boldsymbol{\varphi(S,t)}$ defines the centroid of the cross section second term in Equation 3.25b equals to zero. Then *Linear momentum* per unit of reference arc-length $S\in[0,L]$ is given as

$$\mathbf{L}_t = \left(\int_A \rho(S,\xi_2,\xi_3) d\xi_2 d\xi_3 \right) \dot{\varphi}(S,t) = A_\rho \dot{\varphi}(S,t) \tag{3.26}$$

Similarly, *Linear momentum* per unit of reference arc-length $S\in[0,L]$ with respect to the centroid of cross-section $A_t \in R^2$ in *current configuration* is defined as

$$\mathbf{H}_t = \int_A \rho(S,\xi_2,\xi_3)\left(\mathbf{r}_t(S,t) - \varphi(S,t)\right) \times \dot{\mathbf{r}}_t(S,\xi_2,\xi_3) d\xi_2 d\xi_3 \tag{3.27a}$$

Substituting Equation 3.24c into Equation 3.27a yields

$$\begin{aligned} \mathbf{H}_t = & \left(\int_A \rho(S,\xi_2,\xi_3)\left(\mathbf{r}_t(S,t) - \varphi(S,t)\right) d\xi_2 d\xi_3 \right) \times \dot{\varphi}(S,t) + \\ & \int_A \rho(S,\xi_2,\xi_3)\left(\mathbf{r}_t(S,t) - \varphi(S,t)\right) \times \left[\mathbf{w}(s,t) \times \left(\mathbf{r}_t(S,t) - \varphi(S,t)\right)\right] d\xi_2 d\xi_3 \end{aligned} \tag{3.27b}$$

Since $\boldsymbol{\varphi(S,t)}$ defines the centroid of cross-section Equation 3.27b may be written as

$$\mathbf{H}_t = \int_A \rho(S,\xi_2,\xi_3)\left(\mathbf{r}_t(S,t) - \varphi(S,t)\right) \times \left[\mathbf{w}(s,t) \times \left(\mathbf{r}_t(S,t) - \varphi(S,t)\right)\right] d\xi_2 d\xi_3 \tag{3.27c}$$

By employing the relation from tensor calculus

$$\mathbf{a} \times (\mathbf{b} \times \mathbf{a}) = \left(\|\mathbf{a}\|^2 \hat{\mathbf{I}} - \mathbf{a} \otimes \mathbf{a} \right) \cdot \mathbf{b}$$

where $\hat{\mathbf{I}}$ is the identity dyadic matrix representation of which is a 3x3 identity matrix, angular momentum per unit of reference arc-length S is found as

$$\mathbf{H}_t = \left[\int_A \rho \left(\|\mathbf{r}_t - \varphi\|^2 \cdot \hat{\mathbf{I}} - (\mathbf{r}_t - \varphi) \otimes (\mathbf{r}_t - \varphi) \right) \right] \cdot \mathbf{w}(s,t) = \mathbf{I}_P \cdot \mathbf{w}(s,t) \tag{3.28}$$

where $\mathbf{I_P}$ is the *inertia tensor* with respect to the moving frame $\mathbf{t_i}(S,t)$ i=1,2,3 and has the explicit form of

$$\mathbf{I}_P = \left(\sum_{i=1}^{3} \sum_{j=1}^{3} \int_A \rho \xi_i \xi_j dA \right) \cdot \left(\delta_{i,j} \hat{\mathbf{I}} - \mathbf{t}_i \otimes \mathbf{t}_j \right) \tag{3.29}$$

It is clear from Equation 3.29 that components of inertia tensor $\mathbf{I_p}$ relative to the moving frame do not depend on time.

Since unit vectors $\mathbf{t_2}$ and $\mathbf{t_3}$ of moving frame are directed along the principle axes of inertia of the cross-section $\mathbf{I_P}$ takes the familiar form of

$$\mathbf{I}_p = J \cdot \mathbf{t}_1 \otimes \mathbf{t}_1 + I_2 \cdot \mathbf{t}_2 \otimes \mathbf{t}_2 + I_3 \cdot \mathbf{t}_3 \otimes \mathbf{t}_3 \tag{3.30}$$

where

$$J=I_2+I_3$$

$$I_2 = \int_A \xi_2^2 \rho(S,\xi_2,\xi_3) \cdot d\xi_2 \cdot d\xi_3$$

$$I_3 = \int_A \xi_3^2 \rho(S,\xi_2,\xi_3) \cdot d\xi_2 \cdot d\xi_3$$

$J=I_2+I_3$ denotes the *polar moment* of inertia of the cross-section.

Taking the material time derivative of Equation 3.28, noting that $\dot{\mathbf{w}}(S,t) = \dot{w}_i \mathrm{t}_i$ and using the Equation 3.23 one obtains

$$\dot{\mathbf{H}}_t = \mathbf{I}_P \cdot \dot{\mathbf{w}} + \mathbf{w} \times \mathbf{H}_t \tag{3.31}$$

Equation 3.31 is the identical expression found in rigid body mechanics.

3.5 Equation of Motion

In this section equation of motion for the nonlinear beam model is derived from the material form of linear and angular momentum principles of the 3 dimensional theory, which may be expressed as

$$\mathrm{DIV}\mathbf{P} + \rho\mathbf{B} = \rho\ddot{\mathbf{r}}(S,t) \tag{3.32a}$$

and

$$\mathbf{F} \cdot \mathbf{P}^T = \mathbf{P} \cdot \mathbf{F}^T \tag{3.32b}$$

where **P** is the *first Piola-Kirchoff stress* tensor, **B** is the body force vector, and **F** is the *deformation gradient*. Explicit form of the *first Piola-Kirchoff stress* tensor **P** and *deformation gradient* **F** are given as, respectively

$$P = \mathbf{T_1}(S,\xi_2,\xi_3) \otimes \mathbf{E_1} + \mathbf{T_2}(S,\xi_2,\xi_3) \otimes \mathbf{E_2} + \mathbf{T_3}(S,\xi_2,\xi_3) \otimes \mathbf{E_3} \tag{3.33}$$

and

$$\mathbf{F} = \left(\frac{\partial \varphi}{\partial S} + \omega \times (\mathbf{r}_t - \varphi) \right) \otimes \mathbf{E}_1 + \mathbf{t}_2 \otimes \mathbf{E}_2 + \mathbf{t}_3 \otimes \mathbf{E}_3 \tag{3.34}$$

where $\mathbf{T_i}(S,\xi_2,\xi_3) = \mathbf{P}(S,\xi_2,\xi_3)\cdot\mathbf{E_i}$ $i = 1,2,3$ are the stress vectors, $\boldsymbol{\omega}$ is the curvature of the beam given in Equation 3.17.

If divergence of *first Piola-Kirchoff stress* tensor **P** is calculated as

$$DIV\mathrm{P} = \left(\frac{\partial}{\partial S}\mathbf{E}_1 + \frac{\partial}{\partial S}\mathbf{E}_2 + \frac{\partial}{\partial S}\mathbf{E}_3\right)\cdot \mathrm{P} = \frac{\partial \mathbf{T}_1}{\partial S} + \frac{\partial \mathbf{T}_2}{\partial S} + \frac{\partial \mathbf{T}_3}{\partial S} \tag{3.35}$$

,and substituted into linear momentum equation (Equation 3.32a), and resultant equation is integrated over cross-section one obtains

$$\int_A \frac{\partial \mathbf{T}_1}{\partial S} d\xi_2 d\xi_3 = -\int_A \left(\frac{\partial \mathbf{T}_1}{\partial S} + \frac{\partial \mathbf{T}_2}{\partial S} + \rho\mathbf{B}\right) d\xi_2 d\xi_3 + \int_A \rho\ddot{\mathbf{r}}(S,t) d\xi_2 d\xi_3 \tag{3.36}$$

Applying the divergence theorem to the second integral in Equation 3.36 yields

$$\int_{\mathrm{A}} \frac{\partial \mathbf{T}_1}{\partial \mathrm{S}} \mathrm{d}\xi_2 \mathrm{d}\xi_3 = \int_{\partial\Gamma} \left(\mathbf{T}_2 \nu_2 + \mathbf{T}_3 \nu_3\right) \mathrm{d}\Gamma + \int_{\mathrm{A}} \rho\mathbf{B} \mathrm{d}\xi_2 \mathrm{d}\xi_3 + \int_{\mathrm{A}} \rho\ddot{\mathbf{r}}(\mathrm{S},\mathrm{t}) \mathrm{d}\xi_2 \mathrm{d}\xi_3 \tag{3.37}$$

where $\boldsymbol{\nu} = \nu_2\mathbf{E}_2 + \nu_3\mathbf{E}_3$ is the vector filed normal to the *lateral* contour $\delta\Gamma$ of the beam.

Defining the *resultant contact force* per unit of the reference arc-length as

$$\boldsymbol{f}(\mathrm{S},\mathrm{t}) = \int_{\mathrm{A}} \mathbf{P}(\mathrm{S},\xi_2,\xi_3)\cdot\mathbf{E}_1 \mathrm{d}\xi_2 \mathrm{d}\xi_3 = \int_{\mathrm{A}} \frac{\partial \mathbf{T}_1}{\partial \mathrm{S}} \mathrm{d}\xi_2 \mathrm{d}\xi_3 \tag{3.38}$$

and applied load as

$$\bar{\mathbf{q}}(\mathrm{S},\mathrm{t}) = \int_{\partial\Gamma} \left(\mathbf{T}_2 \nu_2 + \mathbf{T}_3 \nu_3\right) \mathrm{d}\Gamma + \int_{\mathrm{A}} \rho\mathbf{B} \mathrm{d}\xi_2 \mathrm{d}\xi_3 \tag{3.39}$$

linear momentum balance equation is found as, with Equation 3.26

$$\frac{\partial \boldsymbol{f}(\mathrm{S},\mathrm{t})}{\partial \mathrm{S}} + \bar{\mathbf{q}}(\mathrm{S},\mathrm{t}) = \dot{\mathbf{L}}_{\mathrm{t}} = \mathrm{A}_\rho \ddot{\boldsymbol{\varphi}}(\mathrm{S},\mathrm{t}) \tag{3.40}$$

The *resultant torque* per unit of reference arc-length over the cross-section is defined as

$$\mathbf{m}(\mathrm{S},\mathrm{t}) = \int_{\mathrm{A}} (\mathbf{r}_{\mathrm{t}} - \boldsymbol{\varphi}) \times \mathbf{T}_3(\mathrm{S},\xi_2,\xi_3) \mathrm{d}\xi_2 \mathrm{d}\xi_3 \tag{3.41}$$

Taking derivative of Equation 3.41 relative to reference arc-length S yields

$$\frac{\partial \mathbf{m}}{\partial \mathrm{S}} = \int_{\mathrm{A}} \left(\frac{\partial \mathbf{r}_{\mathrm{t}}}{\partial \mathrm{S}} \times \mathbf{T}_1\right) \mathrm{d}\xi_2 \mathrm{d}\xi_3 - \int_{\mathrm{A}} \left(\frac{\partial \boldsymbol{\varphi}}{\partial \mathrm{S}} \times \mathbf{T}_1\right) \mathrm{d}\xi_2 \mathrm{d}\xi_3 + \int_{\mathrm{A}} (\mathbf{r}_{\mathrm{t}} - \boldsymbol{\varphi}) \times \frac{\partial \mathbf{T}_1}{\partial \mathrm{S}} \mathrm{d}\xi_2 \mathrm{d}\xi_3 \tag{3.42}$$

Substituting Equation 3.36 into Equation 3.42 and making the use of the definition of resultant force, one finds

$$\frac{\partial \mathbf{m}}{\partial \mathrm{S}} = \int_{\mathrm{A}} \left(\frac{\partial \mathbf{r}_{\mathrm{t}}}{\partial \mathrm{S}} \times \mathbf{T}_1 \right) \mathrm{d}\xi_2 \mathrm{d}\xi_3 - \frac{\partial \varphi}{\partial \mathrm{S}} \times \boldsymbol{f} - \int_{\mathrm{A}} (\mathbf{r}_{\mathrm{t}} - \varphi) \times \left(\frac{\partial \mathbf{T}_2}{\partial \mathrm{S}} + \frac{\partial \mathbf{T}_3}{\partial \mathrm{S}} \right) \mathrm{d}\xi_2 \mathrm{d}\xi_3 + \int_{\mathrm{A}} (\mathbf{r}_{\mathrm{t}} - \varphi) \times (\rho \mathbf{B}) \mathrm{d}\xi_2 \mathrm{d}\xi_3 + \int_{\mathrm{A}} (\mathbf{r}_{\mathrm{t}} - \varphi) \times (\rho \ddot{\mathbf{r}}(\mathrm{S}, \mathrm{t})) \mathrm{d}\xi_2 \mathrm{d}\xi_3 \tag{3.43}$$

If Equation 3.31 is used in Equation 3.43 and divergence theorem is applied to the second integral, one obtains

$$\frac{\partial \mathbf{m}}{\partial S} = \dot{\mathbf{H}}_{\mathrm{t}} + \int_A \left(\left\{ \frac{\partial \varphi}{\partial S} + \boldsymbol{\omega} \times (\mathbf{r}_{\mathrm{t}} - \varphi) \right\} \times \mathbf{T}_1 + \frac{\partial \mathbf{r}_{\mathrm{t}}}{\partial \xi_2} \times \mathbf{T}_2 + \frac{\partial \mathbf{r}_{\mathrm{t}}}{\partial \xi_3} \times \mathbf{T}_3 \right) \mathrm{d}\xi_2 d\xi_3 - \frac{\partial \varphi}{\partial S} \times \boldsymbol{f} - \overline{\mathbf{m}}(S, t) \tag{3.44}$$

where $\overline{\mathbf{m}}(\mathrm{S}, \mathrm{t})$ is the applied moment and given as

$$\overline{\mathbf{m}}(\mathrm{S}, \mathrm{t}) = \int_{\partial \Gamma} (\mathbf{r}_{\mathrm{t}} - \varphi) \times (\mathbf{T}_2 \mathrm{v}_2 + \mathbf{T}_3 \mathrm{v}_3) \mathrm{d}\Gamma + \int_{\mathrm{A}} (\mathbf{r}_{\mathrm{t}} - \varphi) \times (\rho \mathbf{B}) \mathrm{d}\xi_2 \mathrm{d}\xi_3 \tag{3.45}$$

From Equation 3.9a unit vectors $\mathbf{t_2}$ and $\mathbf{t_3}$ can be expressed as

$$\mathbf{t}_{\mathbf{k}} = \frac{\partial \varphi}{\partial \xi_{\mathrm{k}}} \qquad \mathrm{k} = 2,3 \tag{3.46}$$

Then deformation gradient $\mathbf{F}$ can be recast into alternative expression with Equation 3.46

$$\mathbf{F} = \left(\frac{\partial \varphi}{\partial \mathrm{S}} + \boldsymbol{\omega} \times (\mathbf{r}_{\mathrm{t}} - \varphi) \right) \otimes \mathbf{E}_1 + \frac{\partial \varphi}{\partial \xi_2} \otimes \mathbf{E}_2 + \frac{\partial \varphi}{\partial \xi_3} \otimes \mathbf{E}_3 \tag{3.47}$$

Substituting Equation 3.47 and Equation 3.33 into angular momentum balance equation (Equation 3.32b) it is obtained

$$\sum_{j=2}^{3} \left(\frac{\partial \mathbf{r}_{\mathrm{t}}}{\partial \xi_{\mathrm{j}}} \otimes \mathbf{T}_{\mathrm{j}} - \mathbf{T}_{\mathrm{j}} \otimes \frac{\partial \mathbf{r}_{\mathrm{t}}}{\partial \xi_{\mathrm{j}}} \right) + \left(\frac{\partial \varphi}{\partial S} + \boldsymbol{\omega} \times (\mathbf{r}_{\mathrm{t}} - \varphi) \right) \otimes \mathbf{T}_{\mathrm{l}} - \mathbf{T}_{\mathrm{l}} \otimes \left(\frac{\partial \varphi}{\partial S} + \boldsymbol{\omega} \times (\mathbf{r}_{\mathrm{t}} - \varphi) \right) = 0 \tag{3.48}$$

By scalar-multiplying of Equation 3.48 with any nonzero vector $\mathbf{e} \neq \mathbf{0}$, one has

$$\sum_{j=2}^{3} \left(\frac{\partial \mathbf{r}_{\mathrm{t}}}{\partial \xi_{\mathrm{j}}} (\mathbf{T}_{\mathrm{j}} \cdot \mathbf{e}) - \mathbf{T}_{\mathrm{j}} \left(\frac{\partial \mathbf{r}_{\mathrm{t}}}{\partial \xi_{\mathrm{j}}} \cdot \mathbf{e} \right) \right) + \left(\frac{\partial \varphi}{\partial S} + \boldsymbol{\omega} \times (\mathbf{r}_{\mathrm{t}} - \varphi) \right) (\mathbf{T}_{\mathrm{l}} \cdot \mathbf{e}) - \mathbf{T}_{\mathrm{l}} \left(\left(\frac{\partial \varphi}{\partial S} + \boldsymbol{\omega} \times (\mathbf{r}_{\mathrm{t}} - \varphi) \right) \cdot \mathbf{e} \right) = 0 \tag{3.49}$$

Taking the note of vector identity

$$\mathbf{A} \times (\mathbf{B} \times \mathbf{C}) = \mathbf{B}(\mathbf{A} \cdot \mathbf{C}) - \mathbf{C}(\mathbf{A} \cdot \mathbf{B}) \tag{3.50}$$

one obtains

$$\sum_{j=2}^{3}\left(\mathbf{e}\times\left(\frac{\partial \mathbf{r_t}}{\partial \xi_j}\times\mathbf{T_j}\right)\right)+\mathbf{e}\times\left(\left(\frac{\partial \boldsymbol{\varphi}}{\partial S}+\boldsymbol{\omega}\times(\mathbf{r_t}-\boldsymbol{\varphi})\right)\times\mathbf{T_1}\right)=\mathbf{0} \tag{3.51}$$

Equation 3.51 holds for any nonzero vector $\mathbf{e}\neq\mathbf{0}$ thus

$$\sum_{j=2}^{3}\left(\frac{\partial \mathbf{r_t}}{\partial \xi_j}\times\mathbf{T_j}\right)+\left(\frac{\partial \boldsymbol{\varphi}}{\partial S}+\boldsymbol{\omega}\times(\mathbf{r_t}-\boldsymbol{\varphi})\right)\times\mathbf{T_1}=\mathbf{0} \tag{3.52}$$

By substituting Equation 3.52 into Equation 3.44 angular momentum balance equation is obtained as

$$\frac{\partial \mathbf{m}}{\partial S}+\frac{\partial \varphi}{\partial S}\times \boldsymbol{f}+\overline{\mathbf{m}}(S,t)=\dot{\mathbf{H}}_t=\mathbf{I}_P\cdot\dot{\mathbf{w}}+\mathbf{w}\times\mathbf{H}_t \tag{3.53}$$

Linear and angular momentum balance equations (Equation 3.40 and Equation 3.53, respectively), although parameterized by the reference arc-length, take values on the current configuration; i.e. their components are expressed in the spatial basis, either $\mathbf{e}_i$ or $\mathbf{t}_i$ i=1,2,3. Alternatively their material forms may be found by defining the material vectors

$$\mathbf{N}=\Lambda^T\cdot\mathbf{f}=\Lambda^T\cdot(f_i\mathbf{t}_i)=f_i(\Lambda^T\cdot\mathbf{t}_i)=f_i\mathbf{t}_{i,0}\quad i=1,2,3 \tag{3.54a}$$

$$\mathbf{M}=\Lambda^T\cdot\mathbf{m}=\Lambda^T\cdot(m_i\mathbf{t}_i)=m_i(\Lambda^T\cdot\mathbf{t}_i)=m_i\mathbf{t}_{i,0}\quad i=1,2,3 \tag{3.54b}$$

From Equation 3.54a and 3.54b it is clear that "components of the force and moment vectors **f** and **m** relative to the moving frame $\mathbf{t}_i$ i=1,2,3 equal those of **N** and **M** relative to the reference frame $\mathbf{t}_i$ i=1,2,3" (Simo, 1985).

Material forms of the linear and angular momentum balance equations are obtained by substituting Equation 3.54a into Equation 3.40 and Equation 3.54b into Equation 3.53.

3.6 Internal Power and Strain Measures

In this section, *strain measures* are obtained from the *internal power* expression of the 3-dimensional theory, which is given as

$$\P=\int_{AxS}\left(\mathbf{P}:\dot{\mathbf{F}}\right)dS d\xi_2 d\xi_3 \tag{3.55}$$

where **P** is the *first Piola-Kirchoff* stress tensor (Equation 3.33) and $\dot{\mathbf{F}}$ is the *material* time derivative of the *deformation gradient* (Equation 3.34). In Equation 3.55 column (:) denotes the double contraction of the tensors defined as

$$(\mathbf{a}\otimes\mathbf{b}):(\mathbf{c}\otimes\mathbf{d})=(\mathbf{a}\cdot\mathbf{c})(\mathbf{b}\cdot\mathbf{d}) \tag{3.56}$$

Taking the material time derivative of deformation gradient and making the use of Equation 3.23 one finds

$$\dot{\mathbf{F}}=\left(\frac{\partial\dot{\varphi}}{\partial S}+\dot{\omega}\times(\mathbf{r}_t-\varphi)+\dot{\omega}\times\left(\mathbf{w}\times(\mathbf{r}_t-\varphi)\right)\right)\otimes\mathbf{E}_1+\sum_{i=2}^{3}\left(\mathbf{w}\times\mathbf{t}_i\right)\otimes\mathbf{E}_i \tag{3.57}$$

From Equation 3.33 and Equation 3.57, noting Equation 3.56, $\mathbf{P}:\dot{\mathbf{F}}$ is obtained as

$$\mathbf{P}:\dot{\mathbf{F}}=\mathbf{T}_1\cdot\frac{\partial\varphi}{\partial S}+\mathbf{T}_1\cdot\left[\omega\times\{w\times(\mathbf{r}_t-\varphi\}\right]+\left[(\mathbf{r}_t-\varphi)\times\mathbf{T}_3\right]\cdot\dot{\omega}+\sum_{i=2}^{3}w\cdot\left(\mathbf{t}_i\times\mathbf{T}_i\right) \tag{3.58}$$

where the following vector manipulation is used

$$\mathbf{a}\cdot(\mathbf{b}\times\mathbf{c})=(\mathbf{a}\cdot\mathbf{b})\mathbf{c}=\mathbf{c}(\mathbf{b}\cdot\mathbf{a})=(\mathbf{c}\times\mathbf{a})\cdot\mathbf{b} \tag{3.59}$$

The last term in Equation 3.58 can be written in alternative form by using Equation 3.46 as

$$\sum_{i=2}^{3}w\cdot\left(\mathbf{t}_i\times\mathbf{T}_i\right)=w\cdot\left(\sum_{i=2}^{3}\frac{\partial\varphi}{\partial\xi_i}\times\mathbf{T}_i\right) \tag{3.60}$$

By using angular momentum balance condition (Equation 3.52) and vector manipulation given in Equation 3.59, one finds

$$\sum_{i=2}^{3}w\cdot\left(\mathbf{t}_i\times\mathbf{T}_i\right)=-\mathbf{T}_1\cdot\left(w\times\frac{\partial\varphi}{\partial S}+w\times\{\omega\times(\mathbf{r}_t-\varphi)\}\right) \tag{3.61}$$

Another form of Equation 3.60 may be obtained by making the use of the identity, noting the Equation 3.50

$$\begin{aligned}\omega\times\{w\times(\mathrm{r}_t-\varphi)\}-w\times\{\omega\times(\mathrm{r}_t-\varphi)\}=\\ \left[w\otimes\omega-\omega\otimes w\right]\cdot(\mathrm{r}_t-\varphi)=\left[\omega\times w\right]\times(\mathrm{r}_t-\varphi)\end{aligned} \tag{3.62}$$

as

$$\sum_{i=2}^{3}w\cdot\left(\mathbf{t}_i\times\mathbf{T}_i\right)=-\mathbf{T}_1\cdot\left(w\times\frac{\partial\varphi}{\partial S}+\omega\times\{w\times(\mathbf{r}_t-\varphi)\}-\left[\omega\times w\right]\times(\mathbf{r}_t-\varphi)\right) \tag{3.63}$$

Substituting Equation 3.63 into Equation 3.58 and integrating yields

$$\P = \int_{AxS} \left(\mathrm{P} : \dot{\mathrm{F}}\right) dS d\xi_2 d\xi_3 = \int_S \left[\int_A \mathrm{T}_1 d\xi_2 d\xi_3\right] \cdot \left[\frac{\partial \dot{\varphi}}{\partial S} - \boldsymbol{w} \times \frac{\partial \varphi}{\partial S}\right] dS + \int_S \left[\int_A (\mathrm{r}_t - \varphi) \cdot \mathrm{T}_1 d\xi_2 d\xi_3\right] \left[\dot{\omega} - \boldsymbol{w} \times \omega\right] dS \tag{3.64}$$

Using the definitions for resultant force and moment, *reduced internal power* is obtained as

$$\P = \int_{\mathrm{AxS}} \left(\mathbf{P} : \dot{\mathbf{F}}\right) \mathrm{dS} \mathrm{d}\xi_2 \mathrm{d}\xi_3 = \int_{\mathrm{S}} \left(\mathbf{f} \cdot \overset{\nabla}{\boldsymbol{\gamma}} + \mathbf{m} \cdot \overset{\nabla}{\boldsymbol{\omega}}\right) \mathrm{dS} \tag{3.65}$$

where

$$\overset{\nabla}{\boldsymbol{\gamma}} = \frac{\partial}{\partial \mathrm{t}} \left(\frac{\partial \boldsymbol{\varphi}}{\partial \mathrm{S}}\right) - \boldsymbol{w} \times \frac{\partial \boldsymbol{\varphi}}{\partial \mathrm{S}} \tag{3.66a}$$

is the time rate of change of the *spatial strain measure* corresponding to the resultant force **f**(S,t), and

$$\overset{\nabla}{\boldsymbol{\omega}} = \frac{\partial}{\partial \mathrm{t}} (\dot{\boldsymbol{\omega}}) - \boldsymbol{w} \times \dot{\boldsymbol{\omega}} \tag{3.66b}$$

is the time rate of change of the *spatial strain measure* corresponding to the resultant moment **m**(S,t).

Material time derivative of any moving generic vector **V**(t) is given by

$$\frac{\mathrm{D}\mathbf{V}}{\mathrm{D}t} = \frac{\partial \mathbf{V}}{\partial t} + \boldsymbol{w} \times \mathbf{V} \qquad \mathbf{V} \in \mathrm{R}^3 \tag{3.67}$$

where $\frac{\partial \mathbf{V}}{\partial \mathrm{t}}$ is the rate due to change in vector length and $\boldsymbol{w} \times \mathbf{V}$ is the rate due to change in vector direction imposed by the spin of the moving frame. Thus while calculating the time rate of strain measures, effect of the spin of the moving frame $\mathbf{t_i}$ i=1,2,3 should be subtracted from the material time derivatives. This explains the using of symbol ($\overset{\nabla}{\cdot}$) instead of superposed dot ($\dot{\cdot}$) which stands for the material time derivative.

Spatial strain measure, $\boldsymbol{\gamma}$ accounts for axial and shear deformation of the beam as can be seen from its explicit form:

$$\boldsymbol{\gamma} = \frac{\partial \boldsymbol{\varphi}}{\partial \mathrm{S}} - \mathrm{t}_1(\mathrm{S}) \tag{3.68}$$

and $\boldsymbol{\omega}$ is the bending strain.

Material form of the reduced internal power equation my be obtained by introducing the following vectors, noting the Equation 3.7

$$\Gamma(S,t) = \Lambda^T \cdot \gamma = \Lambda^T \cdot \frac{\partial \varphi}{\partial S} + \Lambda^T \cdot \mathbf{t}_1 = \Lambda^T \cdot \frac{\partial \varphi}{\partial S} + \mathbf{t}_{1,0} \tag{3.69a}$$

and

$$\mathbf{K}(S,t) = \Lambda^T \cdot \omega \tag{3.69b}$$

From Equation 3.66a and Equation 3.69a, by making the use of Equation 3.22 and axial vector definition of spin tensor:

$$\overset{\nabla}{\gamma} = \frac{\partial \gamma}{\partial S} - \mathbf{w} \times \gamma = \frac{\partial \gamma}{\partial S} - \mathbf{W} \cdot \gamma = \Lambda \cdot \frac{\partial(\Lambda^T \cdot \gamma)}{\partial S} = \Lambda \cdot \frac{\partial(\Gamma)}{\partial S} \qquad \Rightarrow \dot{\Gamma} = \Lambda \cdot \overset{\nabla}{\gamma} \tag{3.70a}$$

and similarly from Equation 3.66b and Equation 69b, by noting $\mathbf{W}(t,s) \cdot \mathbf{w}(t,s) = \mathbf{0}$

$$\overset{\nabla}{\omega} = \frac{\partial \omega}{\partial S} - \mathbf{w} \times \omega = \frac{\partial \omega}{\partial S} - \mathbf{W} \cdot \omega = \Lambda \cdot \frac{\partial(\Lambda^T \cdot \omega)}{\partial S} = \Lambda \cdot \frac{\partial(\mathbf{K})}{\partial S} \qquad \Rightarrow \dot{\mathbf{K}} = \Lambda \cdot \overset{\nabla}{\omega} \tag{3.70b}$$

Substituting Equations 3.70a and 3.70b into Equation 3.65 and noting Equation 3.54 and the orthogonally of $\Lambda(t,s)$, one finds the material form of the reduced internal power as:

$$¶ = \int_{AxS} \left(\mathbf{P} : \dot{\mathbf{F}}\right) dS d\xi_2 d\xi_3 = \int_S \left(\mathbf{N} \cdot \dot{\Gamma} + \mathbf{M} \cdot \dot{\mathbf{K}}\right) dS \tag{3.71}$$

In finite element implementation internal energy (*virtual work*) is preferred over internal power expression and it may be given as, for material description

$$\Pi = \int_S \left(\mathbf{N} \cdot \Gamma + \mathbf{M} \cdot \mathbf{K}\right) dS \tag{3.72a}$$

and for spatial description

$$\Pi = \int_S \left(\mathbf{f} \cdot \gamma + \mathbf{m} \cdot \omega\right) dS \tag{3.72b}$$

3.7 Parametization of Finite Rotation

3.7.1 Total Rotation Vector

Consider 3-D beam in Figure 3.1 undergoing large displacements and finite 3-D rotations. $\mathbf{t}_{i,0}$ $_{i=1,2,3}$ is the local Cartesian frame located at the centroid of the cross-section of the beam in the reference configuration. Similarly $\mathbf{t}_i$ $_{i=1,2,3}$ is the local

Cartesian frame positioned at the centroid of the beam on the current configuration, $\boldsymbol{\varphi}(S)$. Relation between $\mathbf{t}_{i,0}$ $_{i=1,2,3}$ and $\mathbf{t}_i$ $_{i=1,2,3}$ can be represented by an orthogonal tensor $\boldsymbol{\Lambda} \in SO(3)$ as

$$\mathbf{t}_i = \boldsymbol{\Lambda} \cdot \mathbf{t}_{i,0} \tag{3.73}$$

As mentioned above SO(3) stands for the Special Orthogonal (Lie) group. Thus $\boldsymbol{\Lambda}$ is a two-point tensor and can be defined as

$$\boldsymbol{\Lambda} = \mathbf{t}_i \otimes \mathbf{t}_{j,0} = \Lambda_{ji} \mathbf{e}_j \otimes \mathbf{E}_i \tag{3.74}$$

where Λ_{ji} is the coordinate representation in the inertial frames of the reference and current configurations with $\mathbf{E}_i$ and $\mathbf{e}_j$ being the corresponding unit vectors. Tensor $\boldsymbol{\Lambda}$ rotates the unit vector $\mathbf{t}_{i,0}$ in the reference configuration to the unit vector $\mathbf{t}_i$ in current configuration.

The unit vectors of inertial frames of reference and current configurations are chosen to coincide (Figure 3.1) but different symbols are used for clarity. Thus one has

$$\mathbf{e}_i = \hat{\mathbf{I}} \cdot \mathbf{E}_i \qquad \Rightarrow \hat{\mathbf{I}} = \mathbf{e}_i \otimes \mathbf{E}_i \tag{3.75}$$

where $\hat{\mathbf{I}}$ is the identity dyadic matrix representation of which is 3x3 identity matrix. Euler's Theorem for the finite rotation of rigid body states that there is vector $\boldsymbol{\theta}$ which is not affected by the rotation such that

$$\boldsymbol{\theta} = \boldsymbol{\Lambda} \cdot \boldsymbol{\vartheta} = \hat{\mathbf{I}} \cdot \boldsymbol{\vartheta} \tag{3.76}$$

where $\boldsymbol{\theta}$ is the spatial vector field corresponding to the material vector field $\boldsymbol{\vartheta}$. $\boldsymbol{\theta}$ is called *total rotation vector*. Hence inertial frames of reference and current configurations are chosen to coincide, the components of $\boldsymbol{\theta}$ and $\boldsymbol{\vartheta}$ are equal; i.e.

$$\boldsymbol{\theta} \cdot \mathbf{e}_i = \boldsymbol{\vartheta} \cdot \mathbf{E}_i = \theta_i \tag{3.77}$$

where dot $(\cdot)$ denotes the scalar vector product. Therefore, $\boldsymbol{\theta}$ and $\boldsymbol{\vartheta}$ are used interchangeable whenever there is not danger of confusion.

Two-point tensor $\boldsymbol{\Lambda}$can also be represented with *Rodrigues formula* (Goldstein, 1980) such that

$$\boldsymbol{\Lambda} = \cos(\theta)\cdot\left[\hat{\mathbf{I}} - \mathbf{n}\otimes\mathbf{n}\right] + \sin(\theta)\cdot\left[\mathbf{n}\times\hat{\mathbf{I}}\right] + \left[\mathbf{n}\otimes\mathbf{n}\right]$$
$$\boldsymbol{\Lambda} = \cos(\theta)\cdot\hat{\mathbf{I}} + \frac{\sin(\theta)}{\theta}\cdot\boldsymbol{\Theta} + \frac{1-\sin(\theta)}{\theta^2}\cdot\boldsymbol{\theta}\otimes\boldsymbol{\theta} \tag{3.78}$$

where $\theta = \sqrt{\theta\cdot\theta} = \sqrt{\theta_1^2+\theta_2^2+\theta_2^2}$ is the magnitude of the rotation vector, $\mathbf{n} = \boldsymbol{\theta}/\theta$ is a unit vector along the rotation axis and $\boldsymbol{\Theta}$ is the skew-symmetric tensor corresponding to the axial vector $\boldsymbol{\theta}$ defined as $\boldsymbol{\Theta}\cdot\boldsymbol{\theta}=\mathbf{0}$.

Using vector identity

$$\boldsymbol{\Theta}\cdot\left(\boldsymbol{\Theta}\cdot\mathbf{b}\right) = \left[\boldsymbol{\theta}\otimes\boldsymbol{\theta} - \theta^2\hat{\mathbf{I}}\right]\cdot\mathbf{b} \qquad \mathbf{b}\in R^3 \tag{3.79}$$

leads to the closed form of the Rodrigues formula given by exponential mapping

$$\boldsymbol{\Lambda} = \exp(\boldsymbol{\Theta}) = \cos(\theta)\cdot\hat{\mathbf{I}} + \frac{\sin(\theta)}{\theta}\cdot\boldsymbol{\Theta} + \frac{1-\cos(\theta)}{\theta^2}\cdot\boldsymbol{\theta}\otimes\boldsymbol{\theta} \tag{3.80}$$

where $\exp(\boldsymbol{\Theta}) = \sum_{n=1}^{\infty}\left(\frac{\boldsymbol{\theta}^n}{n!}\right)$.

If $\delta\mathbf{W}(S)$ is the superposed infitesimal rotation onto the moving frame defined by $\boldsymbol{\Lambda}(S)$, then admissible variation $\delta\boldsymbol{\Lambda}$ of orthogonal tensor $\boldsymbol{\Lambda}$, for $\in>0$, may be calculated by using exponential mapping as:

$$\delta\boldsymbol{\Lambda} = \frac{d}{d\in}\left(\exp(\in\delta\mathbf{W})\cdot\boldsymbol{\Lambda}\right) = \delta\mathbf{W}\cdot\boldsymbol{\Lambda} \tag{3.81}$$

Differentiating orthogonality condition of $\boldsymbol{\Lambda}$; i.e. $\boldsymbol{\Lambda}^T\cdot\boldsymbol{\Lambda}=\boldsymbol{\Lambda}\cdot\boldsymbol{\Lambda}^T=\mathbf{I}$, one finds that

$$\delta\boldsymbol{\Lambda}\cdot\boldsymbol{\Lambda}^T + \boldsymbol{\Lambda}\cdot\delta\boldsymbol{\Lambda}^T = \boldsymbol{\Lambda}^T\cdot\delta\boldsymbol{\Lambda} + \delta\boldsymbol{\Lambda}^T\cdot\boldsymbol{\Lambda} = \mathbf{0} \tag{3.82a}$$

$$\delta\mathbf{W} + \delta\mathbf{W}^T = \delta\boldsymbol{\Psi} + \delta\boldsymbol{\Psi}^T = \mathbf{0} \tag{3.82b}$$

Hence $\delta\mathbf{W}$ is a skew-symmetric tensor and spatial object components of which are given in spatial inertial frame as

$$\delta\mathbf{W} = \left(\delta\Lambda_{ij}\mathbf{e}_i\otimes\mathbf{E}_j\right)\cdot\left(\Lambda_{kl}\mathbf{E}_k\otimes\mathbf{e}_l\right) = \delta W_{il}\mathbf{e}_i\otimes\mathbf{e}_l \qquad i,j,k,l = 1,2,3 \tag{3.83}$$

It should be pointed out that infitesimal rotations are skew-symmetric transformation (see Goldstein, 1980). One recovers the orthogonal transformation by exponenting of skew-symmetric matrix (infititesimal rotation).

NOTE: Since numerical implementation of finite element formulation is considered in this study, “matrix” and “tensor” are used interchangeable whenever there is no danger of confusion.

Alternatively, admissible variation $\delta\mathbf{\Lambda}$ can be constructed by translating $\delta\mathbf{W}$ into material inertial frame such as

$$\delta\mathbf{\Psi} = \mathbf{\Lambda}^{T} \cdot \delta\mathbf{W} \cdot \mathbf{\Lambda} \tag{3.84}$$

Substituting Equation 3.84 into Equation 3.81 yields

$$\delta\mathbf{\Lambda} = \frac{\partial}{\partial S}\left[\exp\left(\mathbf{\Lambda} \cdot \in \delta\mathbf{\Psi} \cdot \mathbf{\Lambda}^{T}\right) \cdot \mathbf{\Lambda}\right]_{\varepsilon=0} = \mathbf{\Lambda} \cdot \delta\mathbf{\Psi} \tag{3.85}$$

where property of the exponential mapping

$$\exp\left(\mathbf{\Lambda} \cdot \in \delta\mathbf{\Psi} \cdot \mathbf{\Lambda}^{T}\right) = \mathbf{\Lambda} \cdot \exp\left(\in \delta\mathbf{\Psi}\right) \cdot \mathbf{\Lambda}^{T} \tag{3.86}$$

is employed.

From Equation 3.82b it is can be seen that $\delta\mathbf{\Psi}$ is also skew-symmetric tensor and material object; i.e.

$$\delta\mathbf{\Psi} = \left(\Lambda_{ij}\mathbf{E}_i \otimes \mathbf{e}_j\right) \cdot \left(\delta\Lambda_{kl}\mathbf{e}_k \otimes \mathbf{E}_l\right) = \delta\Psi_{il}\mathbf{E}_i \otimes \mathbf{E}_l \qquad i,j,k,l = 1,2,3 \tag{3.87}$$

From Equation 3.83 it is clear that $\delta\mathbf{W}$ is an element of tangent space of SO(3) at point $\mathbf{\Lambda}$ ($T_{\Lambda}(SO(3))$, and similarly, from Equation 3.87, $\delta\mathbf{\Psi}$ is an element of tangent space of SO(3) at the identity ($T_{I}(SO(3))$. Geometric interpretation of $\delta\mathbf{\Psi}$ and $\delta\mathbf{W}$ is shown in Figure 3.3**.**

Since $\delta\mathbf{\Psi}$ and $\delta\mathbf{W}$ are skew-symmetric tensors they can be represented by axial vectors defined by $\delta\mathbf{\Psi} \cdot \delta\psi = \mathbf{0}$ and $\delta\mathbf{W} \cdot \delta\mathbf{w} = \mathbf{0}$, respectively. The relation of two axial vectors follows from the Equation 3.84 as

$$\delta\mathbf{\Psi} = \mathbf{\Lambda}^{T} \cdot \delta\mathbf{W} \cdot \mathbf{\Lambda} \quad \Rightarrow \quad \delta\mathbf{w} = \mathbf{\Lambda}^{T} \cdot \delta\psi \quad \Rightarrow \quad \delta\psi = \mathbf{\Lambda} \cdot \delta\mathbf{w} \tag{3.88}$$

Admissible variation $\delta\mathbf{\Lambda}$ **of** $\mathbf{\Lambda}$can also be constructed by means of material rotation vector ϑ and its variation $\delta\vartheta$ such that

$$\exp\left(\mathbf{\Phi} + \in \delta\mathbf{\Phi}\right) = \exp\left(\mathbf{\Phi}\right) \cdot \exp\left(\in \delta\mathbf{\Psi}\right) \tag{3.89}$$

where $\mathbf{\Phi}$ is the skew-symmetric tensor defined by relation . Geometric interpretation of Equation 3.89 is given in Figure 3.4. By using the observation given in Goldstein, (1980); i.e. $\left[\exp\left(\mathbf{\Phi}\right)\right]^{-1} = \exp\left(-\mathbf{\Phi}\right)$, Equation 3.89 may be written as

$$\exp\left(\in \delta\mathbf{\Psi}\right) = \exp\left(-\mathbf{\Phi}\right) \cdot \exp\left(\mathbf{\Phi} + \in \delta\mathbf{\Phi}\right) \tag{3.90}$$

Taking the derivative with respect to $\in$ and setting $\in$=0; i.e.

$$\frac{\partial}{\partial \in}\left(\exp\left(\in \delta\boldsymbol{\Psi}\right)\right)\Big|_{\in=0} = \frac{\partial}{\partial \in}\left(\exp\left(-\boldsymbol{\Phi}\right)\cdot\exp\left(\boldsymbol{\Phi}+\in\delta\boldsymbol{\Phi}\right)\right)\Big|_{\in=0} \tag{3.91}$$

one finds

$$\delta\boldsymbol{\psi} = \mathbf{T}^{\mathrm{T}}(\boldsymbol{\vartheta})\cdot\delta\boldsymbol{\vartheta} \tag{3.92}$$

where skew-symmetric tensor $\mathbf{T}^{\mathrm{T}}$ is given in explicit form as

$$\mathbf{T}^{\mathrm{T}}(\boldsymbol{\vartheta}) = \frac{\sin\vartheta}{\vartheta}\mathbf{I} - \frac{1-\cos\vartheta}{\vartheta^2}\boldsymbol{\Phi} + \frac{\vartheta-\sin\vartheta}{\vartheta^3}\boldsymbol{\vartheta}\otimes\boldsymbol{\vartheta} \tag{3.93}$$

By using the same procedure; i.e.

$$\exp\left(\in\delta\mathbf{W}\right) = \exp\left(\boldsymbol{\Theta}+\in\delta\boldsymbol{\Theta}\right)\cdot\exp\left(-\boldsymbol{\Theta}\right) \qquad \boldsymbol{\Theta}\cdot\boldsymbol{\theta} = 0 \tag{3.94a}$$

$$\frac{\partial}{\partial \in}\left(\exp\left(\in\delta\mathbf{W}\right)\right)\Big|_{\in=0} = \frac{\partial}{\partial \in}\left(\exp\left(\boldsymbol{\Theta}+\in\delta\boldsymbol{\Theta}\right)\exp\left(-\boldsymbol{\Theta}\right)\right)\Big|_{\in=0} \tag{3.94b}$$

one finds the relation between spatial rotation vector ($\boldsymbol{\theta}$) variation $\delta\boldsymbol{\theta}$ and superposed rotation $\delta\mathbf{W}$ as

$$\delta\mathbf{w} = \mathbf{T}(\boldsymbol{\theta})\cdot\delta\boldsymbol{\theta} \tag{3.95}$$

where $\mathbf{T}(\boldsymbol{\theta})$ is the skew-symmetric tensor given explicitly in Equation 3.93. Properties of $\mathbf{T}(\boldsymbol{\theta})$ can be found in Ibrahimbegovic, (1995) .

If Equation 3.92 and 3.95 are substituted into Equation 3.88, one gets

$$\delta\boldsymbol{\theta} = \mathbf{T}^{-1}\cdot\boldsymbol{\Lambda}\cdot\mathbf{T}^{-1}\cdot\mathbf{T}^{\mathrm{T}}\cdot\delta\boldsymbol{\vartheta} = \mathbf{I}\cdot\delta\boldsymbol{\vartheta} \tag{3.96}$$

where relations $\mathbf{T}^{-1}\cdot\boldsymbol{\Lambda} = \boldsymbol{\Lambda}\cdot\mathbf{T}^{-1}$ and $\mathbf{T}^{-\mathrm{T}}\cdot\mathbf{T}^{-1} = \boldsymbol{\Lambda}^{\mathrm{T}}$ are used (Ibrahimbegovic, 1995). Equation 3.96 confirms the relation given in Equation 3.76

By employing the similar calculation procedure given above, the following results are also obtained:

$$\boldsymbol{\kappa} = \mathbf{T}^{\mathrm{T}}(\boldsymbol{\theta})\cdot\boldsymbol{\vartheta}' \tag{3.97a}$$

$$\boldsymbol{\omega} = \mathbf{T}(\boldsymbol{\theta})\cdot\boldsymbol{\theta}' \tag{3.97b}$$

where $\boldsymbol{\kappa}$ and $\boldsymbol{\omega}$ are the material and spatial bending measures (see Equations 3.72a and 3.72b.

The parameterization of finite rotation given above can handle the any 3-D rotation as long as magnitude of rotation is smaller that 2Π. In case where rotation is

greater than 2Π, parameterization will be ill defined; i.e. non-unique. This deficiency can be overcome by restricting the size of rotation being smaller that 2Π and using the incremental rotation vector for constructing admissible variation $\delta\boldsymbol{\Lambda}$. This is considered in the next section.

3.7.2 Incremental Rotation Vector

As mentioned in previous section total rotation vector parameterization of finite rotation cannot handle large rotations; i.e. cases encountered in dynamic problems. If one partitions the configuration space into a number of time steps: $0<t_1<t_2<\ldots<t_n\ldots.<T$ and uses the incremental procedure, the deficiency can be overcome. If the value of rotation at a typical time t_n is denoted as

$$\boldsymbol{\Lambda}_n=\boldsymbol{\Lambda}(t_n) \tag{3.98}$$

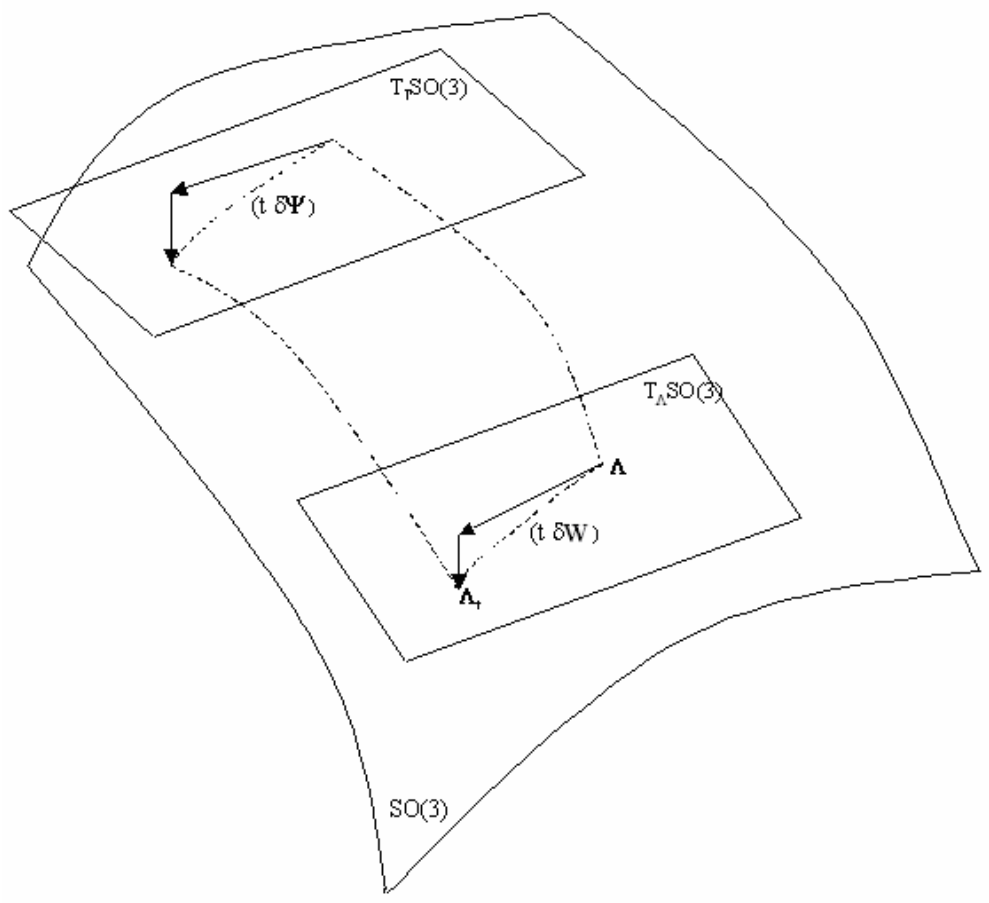

Figure 3.2 Finite rotation decomposition: Infitesimal rotation

the rotation update at time t_{n+1} can be carried out as

$$\mathbf{\Lambda_{n+1}} = \widetilde{\mathbf{\Lambda}}(\boldsymbol{\theta}_{n+1}) \cdot \mathbf{\Lambda_n} = \mathbf{\Lambda_n} \cdot \widetilde{\mathbf{\Lambda}}(\boldsymbol{\vartheta}_{n+1}) \tag{3.99}$$

where $\boldsymbol{\theta}_{n+1}$ is the *spatial incremental rotation* vector and $\boldsymbol{\vartheta}_{n+1}$ is the its *materia*l counterpart. $\widetilde{\mathbf{\Lambda}}(\boldsymbol{\theta}_{n+1}) = \exp(\boldsymbol{\theta}_{n+1})$ is the exponential mapping given by Equation 3.80. Since $\mathbf{\Lambda_n}$ is an orthogonal tensor; i.e. $\mathbf{\Lambda_n^T} = \mathbf{\Lambda_n^{-1}}$, one obtains the relations

$$\widetilde{\mathbf{\Lambda}}(\boldsymbol{\theta}_{n+1}) = \mathbf{\Lambda_n} \cdot \widetilde{\mathbf{\Lambda}}(\boldsymbol{\vartheta}_{n+1}) \cdot \mathbf{\Lambda_n^T} \tag{3.100a}$$

$$\widetilde{\mathbf{\Lambda}}(\boldsymbol{\vartheta}_{n+1}) = \mathbf{\Lambda_n^T} \cdot \widetilde{\mathbf{\Lambda}}(\boldsymbol{\theta}_{n+1}) \cdot \mathbf{\Lambda_n} \tag{3.100b}$$

By taking into that skew-symmetric tensor shares the same eigenvectors with orthogonal tensor obtained by exponentiating it, one finds from Equations 3.100a and 3.100b

$$\mathbf{\Theta}_{n+1} = \mathbf{\Lambda_n} \cdot \mathbf{\Phi}_{n+1} \cdot \mathbf{\Lambda_n^T} \tag{3.101a}$$

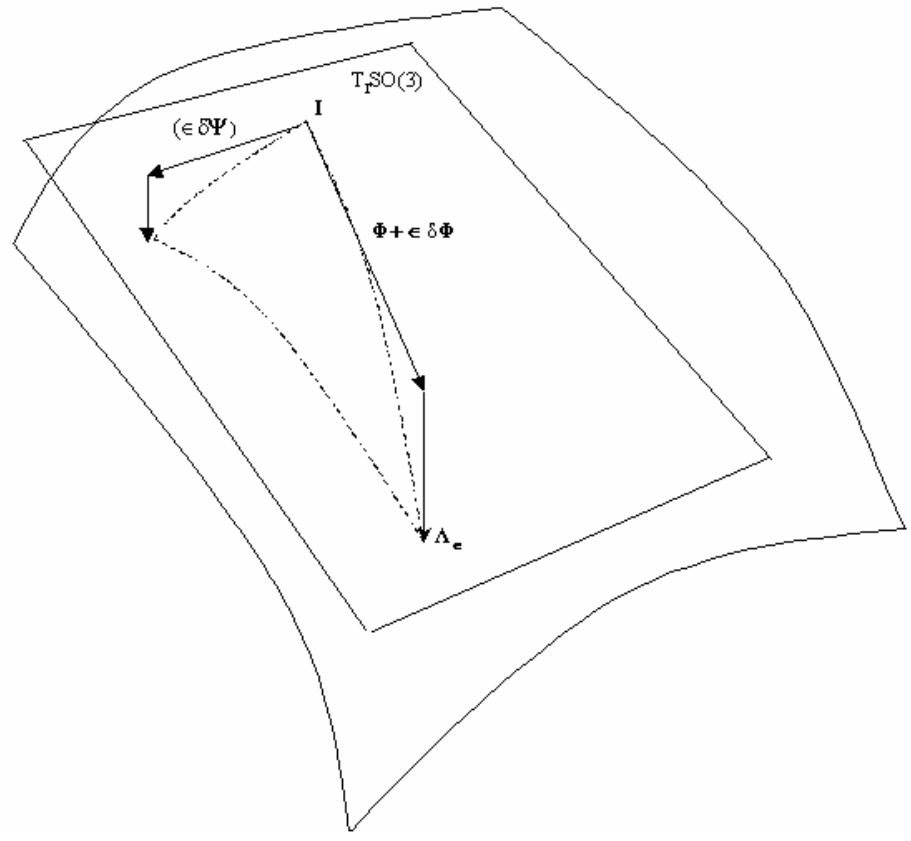

Figure 3.3 Finite rotation decomposition: Rotation vector variation

$$\boldsymbol{\Phi}_{n+1} = \boldsymbol{\Lambda}_n^T \cdot \boldsymbol{\Theta}_{n+1} \cdot \boldsymbol{\Lambda}_n \tag{3.101b}$$

where $\boldsymbol{\Theta}_{n+1} \cdot \mathbf{b} = \boldsymbol{\theta}_{n+1} \times \mathbf{b}$ and $\boldsymbol{\Phi}_{n+1} \cdot \mathbf{b} = \boldsymbol{\vartheta}_{n+1} \times \mathbf{b} \quad \forall \mathbf{b} \in \mathbf{R}^3$. Equations 3.101a and 3.101b lead to the relation between *spatial* and *material incremental rotation vectors* such that

$$\boldsymbol{\theta}_{n+1} = \boldsymbol{\Lambda}_n \cdot \boldsymbol{\vartheta}_{n+1} \tag{3.102a}$$

$$\boldsymbol{\vartheta}_{n+1} = \boldsymbol{\Lambda}_{n+1}^T \cdot \boldsymbol{\theta}_{n+1} \tag{3.102b}$$

The graphical representation of the relation between $\boldsymbol{\vartheta}_{n+1}$ and $\boldsymbol{\theta}_{n+1}$ is given in Figure 3.3. It should be noted that $\boldsymbol{\theta}_{n+1}$ belongs to the tangent space of SO(3) at point $\boldsymbol{\Lambda}_n$ $\left[T_{\Lambda}(SO(3))\right]$ and $\boldsymbol{\vartheta}_{n+1}$ belongs to the tangent space of SO(3) at identity $\left[T_I(SO(3))\right]$. In sharp contrast with *total rotation vector* given in Equation 3.76, the spatial and material representation of the *incremental rotation vector* is not identical.

When *incremental rotation vector* is used for parameterization of finite rotation, final values of the state variables are calculated by an iterative procedure carried over each increment.

The *iterative update* of finite rotation is more involved than *total rotation vector* procedure because one not only chooses between spatial and material representation but also between different iterative rotation parameters. Let superscript (i) denote the iteration counter. Consider the rotation update:

$$\boldsymbol{\Lambda}_{n+1}^{i+1} = \widetilde{\boldsymbol{\Lambda}}_{n+1}(\in \delta \mathbf{w}_{n+1}^i) \cdot \boldsymbol{\Lambda}_{n+1}^i \tag{3.103}$$

where $\delta \mathbf{w}_{n+1}^i$ is the infitesimal rotation superposed on existing rotation $\boldsymbol{\Lambda}_{n+1}^i$ (Figure 3.4). The same value of total rotation $\boldsymbol{\Lambda}_{n+1}^{i+1}$ can be obtained by making use of spatial incremental rotation vector $\boldsymbol{\theta}_{n+1}^i$ and its variation $\delta\boldsymbol{\theta}_{n+1}^i$ as

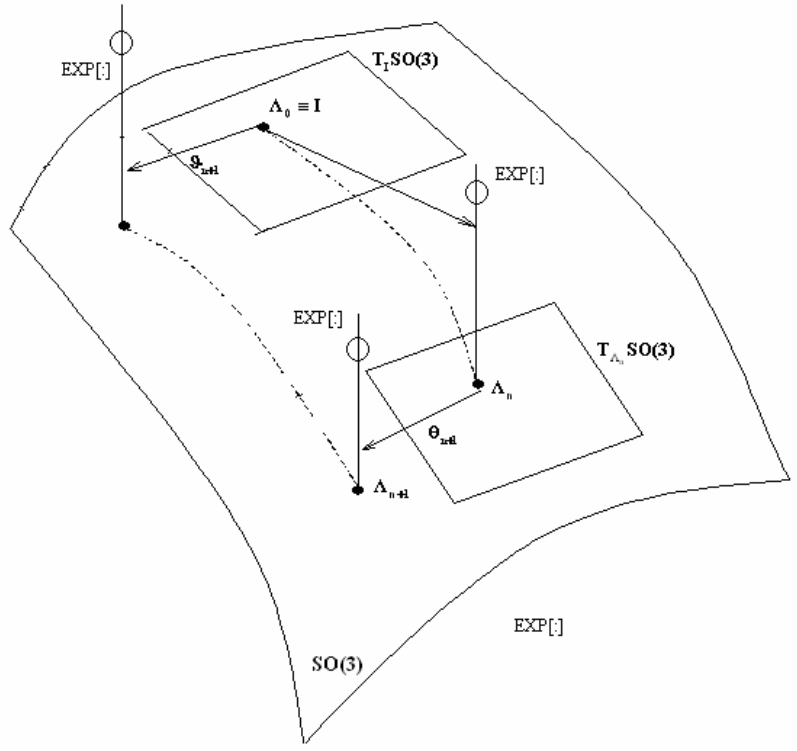

Figure 3.4 Incremental rotation vector in spatial and material representation

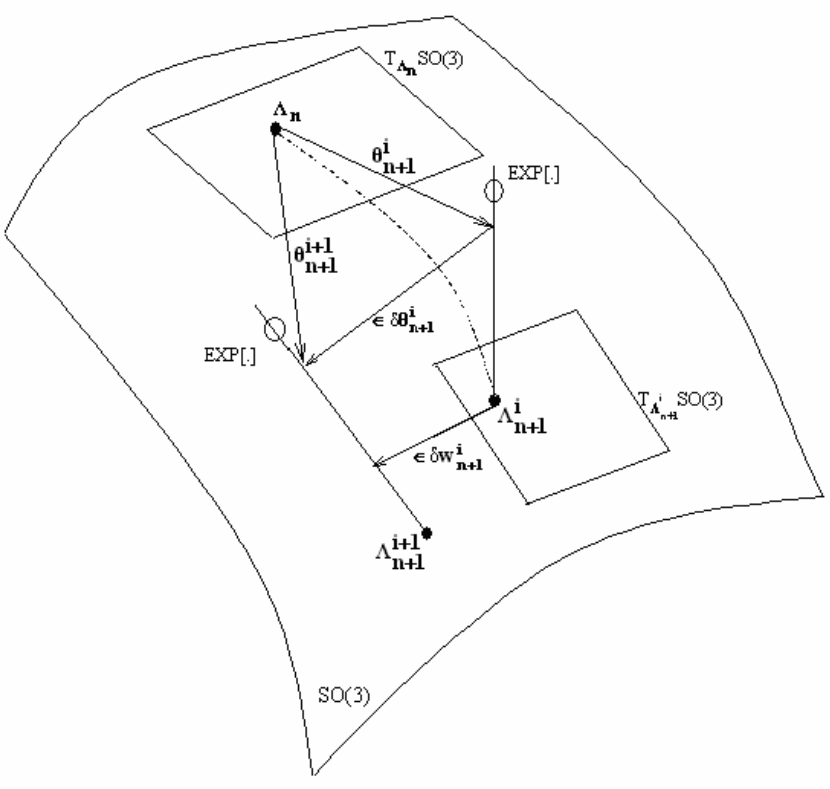

Figure 3.5 Iterative updates of the rotation

$$\mathbf{\Lambda}_{n+1}^{i+1} = \widetilde{\mathbf{\Lambda}}(\boldsymbol{\theta}_{n+1}^{i} + \in \delta\boldsymbol{\theta}_{n+1}^{i}) \cdot \mathbf{\Lambda}_{n} \tag{3.104}$$

From Equations 3.103, 3.104 and spatial incremental rotation vector definition in 3.100b one obtains

$$\widetilde{\mathbf{\Lambda}}(\in \delta\mathbf{w}_{n+1}^{i}) = \widetilde{\mathbf{\Lambda}}(\boldsymbol{\theta}_{n+1}^{i} + \in \delta\boldsymbol{\theta}_{n+1}^{i}) \cdot \widetilde{\mathbf{\Lambda}}^{T}(\boldsymbol{\theta}_{n+1}^{i}) \tag{3.105}$$

which by following the same procedure given in previous section; i.e.

$$\frac{d}{d\in}\left(\widetilde{\mathbf{\Lambda}}(\in \delta\mathbf{w}_{n+1}^{i})\right)\Big|_{\in=0} = \frac{d}{d\in}\left(\widetilde{\mathbf{\Lambda}}(\boldsymbol{\theta}_{n+1}^{i} + \in \delta\boldsymbol{\theta}_{n+1}^{i}) \cdot \widetilde{\mathbf{\Lambda}}^{T}(\boldsymbol{\theta}_{n+1}^{i})\right)\Big|_{\in=0} \tag{3.106}$$

leads to the admissible variation in terms of spatial incremental rotation vector:

$$\delta\mathbf{w}_{n+1}^{i} = \widetilde{\mathbf{T}}(\boldsymbol{\theta}_{n+1}^{i}) \cdot \delta\boldsymbol{\theta}_{n+1}^{i} \tag{3.107}$$

Similarly, the rotation update can be carried out with material rotation parameters as

$$\widetilde{\mathbf{\Lambda}}(\in \delta\boldsymbol{\psi}_{n+1}^{i}) = \widetilde{\mathbf{\Lambda}}^{T}(\boldsymbol{\vartheta}_{n+1}^{i}) \cdot \widetilde{\mathbf{\Lambda}}(\boldsymbol{\vartheta}_{n+1}^{i} + \in \delta\boldsymbol{\vartheta}_{n+1}^{i}) \tag{3.108}$$

from where one obtains the relation

$$\delta\boldsymbol{\psi}_{n+1}^{i} = \widetilde{\mathbf{T}}^{T}(\boldsymbol{\vartheta}_{n+1}^{i}) \cdot \delta\boldsymbol{\vartheta}_{n+1}^{i} \tag{3.109}$$

In Equation 3.109, $\delta\boldsymbol{\psi}_{n+1}^{i}$ is the material form of the infitesimal rotation $\delta\mathbf{w}_{n+1}^{i}$. The graphic illustration of iterative update procedure is presented in Figure 3.3.

3.8 Weak Form of Balance Equation

The potential energy of the beam is found in section 3.6 as

$$\mathbf{\Pi} = \int_{S} (\mathbf{N} \cdot \mathbf{\Gamma} + \mathbf{M} \cdot \mathbf{K}) dS \tag{3.110}$$

where **N** and **M** are energy conjugate stress resultants with corresponding strain measures **Γ** and **K**, respectively. If the simplest constitutive equations are chosen, one may obtain the stress resultants as

$$\mathbf{N}=\mathbf{C_n}\cdot\mathbf{\Gamma} \tag{3.111a}$$

$$\mathbf{M}=\mathbf{C_m}\cdot\mathbf{K} \tag{3.111b}$$

where $\mathbf{C_n}$ and $\mathbf{C_m}$ are the constitutive matrices with constant diagonal entries for linear elastic beam given as

$$\mathbf{C_n}=\text{diag}([\mathbf{EA},\mathbf{GA_2},\mathbf{GA_3}]) \tag{3.112a}$$

$$\mathbf{C_m}=\text{diag}([\mathbf{GJ},\mathbf{EI_2},\mathbf{EI_3}]) \tag{3.112b}$$

Here, **EA** is the axial stiffness, $\mathbf{GA_2}$ and $\mathbf{GA_3}$ denote shear stiffness, **GJ** is the torsional stiffness, and $\mathbf{EI_2}$ and $\mathbf{EI_3}$ are principle bending stiffness relative to $\mathbf{t_{2,0}}$ and $\mathbf{t_{3,0}}$ of the beam cross-section.

Explicit form of the strain measures are given in section 3.6 as

$$\boldsymbol{\Gamma}(S,t)_1 = \boldsymbol{\Lambda}^T(\theta)\cdot\frac{\partial\boldsymbol{\varphi}}{\partial S} + \mathbf{t}_{1,0} \tag{3.113a}$$

$$\mathbf{K}(S,t) = \boldsymbol{\Lambda}^T(\theta)\cdot\boldsymbol{\Lambda}'(\theta) + \boldsymbol{\Omega}_0(S) \tag{3.113b}$$

where prime (‘) denotes the derivative with respect to the arc-length parameter S.

From Equation (3..112) and Equation (3.113), it is clear that potential energy is the functional of dependent variables $\boldsymbol{\varphi}$ and $\boldsymbol{\theta}$**.** Hence the virtual work equations can be obtained by the directional derivative of the potential energy in the direction of virtual displacement $\delta\boldsymbol{\varphi}$ and rotation vectors $\delta\boldsymbol{\theta}$ such that

$$\delta\Pi(\boldsymbol{\varphi},\boldsymbol{\theta})\cdot(\delta\boldsymbol{\varphi},\delta\boldsymbol{\theta}) = \frac{d}{d\in}\left[\Pi(\boldsymbol{\varphi}+\delta\boldsymbol{\varphi},\boldsymbol{\theta}+\delta\boldsymbol{\theta})\right]\Big|_{\in=0} = \int_S(\delta\boldsymbol{\Gamma}\cdot\mathbf{N}+\delta\mathbf{k}\cdot\mathbf{M}) \tag{3.114}$$

In Equation (3.114) $\delta\boldsymbol{\Gamma}$ corresponding to the axial and shear strains is computed as

$$\delta\boldsymbol{\Gamma} = \frac{d}{d\in}\left[\left(\boldsymbol{\Lambda}^T+\in\delta\boldsymbol{\Lambda}^T\right)\cdot\left(\boldsymbol{\varphi}+\in\delta\boldsymbol{\varphi}\right)-\mathbf{t}_{1,0}\right]\Big|_{\in=0} = \boldsymbol{\Lambda}^T\cdot\delta\boldsymbol{\varphi}'+\delta\boldsymbol{\Lambda}^T\cdot\boldsymbol{\varphi} \tag{3.115}$$

By making use the results given in section 3.7; i.e. $\delta\boldsymbol{\Lambda}^T = \delta\boldsymbol{\Psi}^T\cdot\boldsymbol{\Lambda}^T$ and $\delta\boldsymbol{\Psi}\cdot\delta\boldsymbol{\psi}=\mathbf{0}$ one obtains

$$\delta\boldsymbol{\Gamma} = \boldsymbol{\Lambda}^T\cdot\delta\boldsymbol{\varphi}'+\boldsymbol{\Lambda}^T\cdot\boldsymbol{\varphi}'\times\delta\boldsymbol{\psi} \tag{3.116}$$

Similarly, virtual bending strain $\delta\mathbf{K}$ is calculated as

$$\delta\mathbf{K} = \frac{d}{d\in}\left[\left(\boldsymbol{\Lambda}^T+\in\delta\boldsymbol{\Lambda}^T\right)\cdot\left(\boldsymbol{\Lambda}'+\in\delta\boldsymbol{\Lambda}'\right)-\boldsymbol{\Omega}_0\right]\Big|_{\in=0} = \boldsymbol{\Lambda}^T\cdot\delta\boldsymbol{\Lambda}'+\delta\boldsymbol{\Lambda}^T\cdot\boldsymbol{\Lambda}' \tag{3.117}$$

From Equation (3.117) one finds

$$\delta\mathbf{K} = \delta\boldsymbol{\Psi}'+\mathbf{K}\cdot\delta\boldsymbol{\Psi}-\delta\boldsymbol{\Psi}\cdot\mathbf{K} \tag{3.118}$$

Since $\delta\mathbf{K}$ is a skew-symmetric tensor, Equation (3.118) can be written in terms of axial vector $\delta\mathbf{K}\cdot\delta\mathbf{k}=\mathbf{0}$ and $\delta\boldsymbol{\Psi}\cdot\delta\boldsymbol{\psi}=\mathbf{0}$ as

$$\delta\mathbf{k} = \delta\boldsymbol{\psi}'+\mathbf{k}\cdot\delta\boldsymbol{\psi} \tag{3.119}$$

By making use of the Equation (3.68) spatial form of virtual strains can be obtained as

$$\boldsymbol{L}_{\delta}(\gamma) = \delta\boldsymbol{\varphi}' + \boldsymbol{\varphi}' \times \delta\mathbf{w} \tag{3.120}$$

And

$$\boldsymbol{L}_{\delta}(\omega) = \delta\boldsymbol{\omega} + \boldsymbol{\omega} \times \delta\mathbf{w} \tag{3.121}$$

Alternative form of the spatial bending strain measure can be recovered by making use of Equation (3.9) as

$$\boldsymbol{L}_{\delta}(\omega) = \delta\mathbf{w}' \tag{3.122}$$

Symbol $\boldsymbol{L}_{\delta}$ stands for the Lie derivative and is explained later.

Finally by using Equation (3.114) through Equation (3.122) virtual work equations in terms of spatial objects can be expressed as

$$\delta\Pi(\boldsymbol{\varphi},\boldsymbol{\theta})\cdot(\delta\boldsymbol{\varphi},\delta\boldsymbol{\theta}) = \int_{S}\left(\mathbf{L}_{\delta}(\gamma)\cdot\mathbf{n} + \mathbf{L}_{\delta}(\omega)\cdot\mathbf{m}\right)ds = 0 \tag{3.123}$$

Virtual work equation given in Equation (3.123) is highly nonlinear and one needs iterative procedure to obtain its solution. If Newton procedure is employed for that purpose one needs *consistent linearization* to ensure *objectivity* and to guarantee quadratic convergence rate. This is automatically enforced with *Lie derivative formularization where the spatial objects are first pulled-back to the reference configuration, and the derivative is then pushed-forward to the current configuration*; i.e.

$$\boldsymbol{L}_{\Delta}\left(\delta\Pi^{i}_{n+1}\right) = \boldsymbol{\Lambda}^{i}_{n+1}\cdot\frac{d}{d\in}\left[\boldsymbol{\Lambda}^{(i),T}_{n+1,\in}\cdot(\bullet)\big|_{\in}\right] \tag{3.124}$$

Then *consistent linerization* formulation for Virtual work can be obtained as

$$L\left(\delta\Pi^{i}_{n+1}\right) = \delta\Pi^{i}_{n+1} + \boldsymbol{L}_{\Delta}\left(\delta\Pi^{i}_{n+1}\right) \tag{3.125}$$

where subscript (n+1) is used to point out that proposed formulation is employed only spatial incremental rotation vector parameterization scheme, and L(•) denotes the linear part of the functional.

By introducing the spatial incremental rotation vector given in Equation (3.26a), the last term in Equation (3.125) can be simplified to obtain

$$\boldsymbol{L}_{\Delta}\left(\delta\Pi^{i}_{n+1}\right)=\left(\widetilde{\boldsymbol{\Lambda}}_{\mathbf{n+1}}(\boldsymbol{\theta}_{n+1})\cdot\boldsymbol{\Lambda}_{\mathbf{n}}\right)\cdot\frac{\mathrm{d}}{\mathrm{d}\in}\left[\boldsymbol{\Lambda}^{\mathrm{T}}_{\mathbf{n}}\cdot\widetilde{\boldsymbol{\Lambda}}^{\mathrm{T}}_{\mathbf{n+1,\in}}(\boldsymbol{\theta}_{n+1,\in})\cdot\left(\bullet\big|_{n+1,\in}\right)\right] \tag{3.126}$$

and using the orthogonality condition $\boldsymbol{\Lambda}_{\mathbf{n}}\cdot\boldsymbol{\Lambda}^{\mathrm{T}}_{\mathbf{n}}=\mathbf{I}$

$$\boldsymbol{L}_{\Delta}\left(\delta\Pi^{i}_{n+1}\right)=\left(\widetilde{\boldsymbol{\Lambda}}_{\mathbf{n+1}}(\boldsymbol{\theta}_{n+1})\right)\cdot\frac{\mathrm{d}}{\mathrm{d}\in}\left[\widetilde{\boldsymbol{\Lambda}}^{\mathrm{T}}_{\mathbf{n+1,\in}}(\boldsymbol{\theta}_{n+1,\in})\cdot\left(\bullet\big|_{n+1,\in}\right)\right] \tag{3.127}$$

The linearized form of the virtual work equations can be written as

$$\begin{aligned}\mathrm{L}\left(\delta\Pi\left(\boldsymbol{\varphi}^{i}_{n+1},\boldsymbol{\theta}^{i}_{n+1}\right)\cdot\left(\delta\boldsymbol{\varphi}^{i}_{n+1},\delta\boldsymbol{\theta}^{i}_{n+1}\right)\right)=&\int_{S}\left(\boldsymbol{L}_{\delta}\left(\boldsymbol{\gamma}^{i}_{n+1}\right)\cdot\mathbf{n}^{i}_{n+1}+\boldsymbol{L}_{\delta}\left(\boldsymbol{\omega}^{i}_{n+1}\right)\cdot\mathbf{m}^{i}_{n+1}\right)\mathrm{d}s+\\&\int_{S}\left(\boldsymbol{L}_{\delta}\left(\boldsymbol{\gamma}^{i}_{n+1}\right)\cdot\boldsymbol{L}_{\Delta}\left(\mathbf{n}^{i}_{n+1}\right)+\mathbf{L}_{\delta}\left(\boldsymbol{\omega}^{i}_{n+1}\right)\cdot\boldsymbol{L}_{\Delta}\left(\mathbf{m}^{i}_{n+1}\right)\right)\mathrm{d}s+\\&\int_{S}\left(\boldsymbol{L}_{\Delta}\left(\boldsymbol{L}_{\delta}\left(\boldsymbol{\gamma}^{i}_{n+1}\right)\right)\cdot\mathbf{n}^{i}_{n+1}+\boldsymbol{L}_{\Delta}\left(\boldsymbol{L}_{\delta}\left(\boldsymbol{\omega}^{i}_{n+1}\right)\right)\cdot\mathbf{m}^{i}_{n+1}\right)\mathrm{d}s\end{aligned} \tag{3.128}$$

In Equation (3.128) above, $\mathbf{n}^{i}_{n+1}$ and $\mathbf{m}^{i}_{n+1}$ are spatial representation of material stress resultants **N** and **M**, respectively and given as

$$\mathbf{n}^{i}_{n+1}=\left(\boldsymbol{\Lambda}^{i}_{\mathbf{n+1}}\cdot\mathbf{C}_{\mathbf{n}}\cdot\boldsymbol{\Lambda}^{(i),\mathrm{T}}_{\mathbf{n+1}}\right)\cdot\boldsymbol{\gamma}^{i}_{n+1} \tag{3.129}$$

$$\mathbf{m}^{i}_{n+1}=\left(\boldsymbol{\Lambda}^{i}_{\mathbf{n+1}}\cdot\mathbf{C}_{\mathbf{m}}\cdot\boldsymbol{\Lambda}^{(i),\mathrm{T}}_{\mathbf{n+1}}\right)\cdot\boldsymbol{\omega}^{i}_{n+1} \tag{3.130}$$

By applying the Lie derivative formulation given in Equation (3.124) to Equations (3.129) and (3.130), one obtains

$$\boldsymbol{L}_{\Delta}\left(\mathbf{n}^{i}_{n+1}\right)=\left(\boldsymbol{\Lambda}^{i}_{\mathbf{n+1}}\cdot\mathbf{C}_{\mathbf{n}}\cdot\boldsymbol{\Lambda}^{(i),\mathrm{T}}_{\mathbf{n+1}}\right)\cdot\boldsymbol{L}_{\Delta}\left(\boldsymbol{\gamma}^{i}_{n+1}\right) \tag{3.131}$$

$$\boldsymbol{L}_{\Delta}\left(\mathbf{m}^{i}_{n+1}\right)=\left(\boldsymbol{\Lambda}^{i}_{\mathbf{n+1}}\cdot\mathbf{C}_{\mathbf{m}}\cdot\boldsymbol{\Lambda}^{(i),\mathrm{T}}_{\mathbf{n+1}}\right)\cdot\boldsymbol{L}_{\Delta}\left(\boldsymbol{\omega}^{i}_{n+1}\right) \tag{3.132}$$

where the following should be noted

$$\boldsymbol{L}_{\Delta}\left(\boldsymbol{\Lambda}^{i}_{\mathbf{n+1}}\cdot\mathbf{C}_{\mathbf{n}}\cdot\boldsymbol{\Lambda}^{(i),\mathrm{T}}_{\mathbf{n+1}}\right)=\boldsymbol{\Lambda}^{i}_{\mathbf{n+1}}\frac{\mathrm{d}}{\mathrm{d}\in}\left(\boldsymbol{\Lambda}^{(i)\mathrm{T}}_{\mathbf{n+1,\in}}\boldsymbol{\Lambda}^{i}_{\mathbf{n+1,\in}}\cdot\mathbf{C}_{\mathbf{n}}\cdot\boldsymbol{\Lambda}^{(i),\mathrm{T}}_{\mathbf{n+1,\in}}\boldsymbol{\Lambda}^{(i)}_{\mathbf{n+1,\in}}\right)\cdot\boldsymbol{\Lambda}^{(i),\mathrm{T}}_{\mathbf{n+1}}=\mathbf{0} \tag{3.133}$$

When additive update procedure is used, one may write

$$\boldsymbol{\varphi}^{i}_{n+1,\in}=\boldsymbol{\varphi}_{n}+\boldsymbol{\varphi}^{i}_{n+1}+\in\Delta\boldsymbol{\varphi}^{i}_{n+1} \tag{3.134a}$$

$$\boldsymbol{\theta}^{i}_{n+1,\in}=\boldsymbol{\theta}^{i}_{n+1}+\in\Delta\boldsymbol{\theta}^{i}_{n+1} \tag{3.134b}$$

where rotation parameters belong to the tangent space $\left[\mathrm{T}_{\boldsymbol{\Lambda}_{\mathbf{n}}}(\mathrm{SO}(3)\right]$ (Figure 5.7). By making use the Lie derivative formulation given in Equation (3.123), virtual (*spatial*) strain measures and their linearized forms are found as:

$$\boldsymbol{L}_{\delta}\left(\boldsymbol{\gamma}^{i}_{n+1}\right)=\left(\delta\boldsymbol{\varphi}'\right)^{i}_{n+1}+\left(\boldsymbol{\varphi}'\right)^{i}_{n+1}\times\delta\mathbf{w}^{i}_{\mathbf{n+1}} \tag{3.135}$$

$$\boldsymbol{L}_{\delta}\left(\boldsymbol{\omega}^{i}_{n+1}\right)=\delta\boldsymbol{\omega}^{i}_{n+1}+\boldsymbol{\omega}^{i}_{n+1}\times\delta\mathbf{w}^{i}_{n+1} \tag{3.136}$$

$$\boldsymbol{L}_{\Delta}(\boldsymbol{\gamma}^{i}_{\mathrm{n+1}}) = (\Delta\boldsymbol{\varphi}')^{i}_{n+1} + (\boldsymbol{\varphi}')^{i}_{n+1} \times \Delta\mathbf{w}^{i}_{\mathbf{n+1}} \tag{3.137}$$

$$\boldsymbol{L}_{\Delta}(\boldsymbol{\omega}^{i}_{n+1}) = \Delta\boldsymbol{\omega}^{i}_{n+1} + \boldsymbol{\omega}^{i}_{n+1} \times \Delta\mathbf{w}^{i}_{\mathrm{n+1}} \tag{3.138}$$

$$\begin{aligned}\boldsymbol{L}_{\Delta}\left(\boldsymbol{L}_{\delta}(\boldsymbol{\gamma}^{i}_{\mathrm{n+1}})\right) = &-\Delta\mathbf{w}^{i}_{\mathbf{n+1}} \times \left((\delta\boldsymbol{\varphi}')^{i}_{n+1} + (\boldsymbol{\varphi}')^{i}_{n+1} \times \delta\mathbf{w}^{i}_{\mathbf{n+1}}\right) \\ &+ (\Delta\boldsymbol{\varphi}')^{i}_{n+1} \times \delta\mathbf{w}^{i}_{\mathbf{n+1}} + (\boldsymbol{\varphi}')^{i}_{n+1} \times \Delta\delta\mathbf{w}^{i}_{\mathbf{n+1}}\end{aligned} \tag{3.139}$$

$$\begin{aligned}\boldsymbol{L}_{\Delta}\left(\boldsymbol{L}_{\delta}(\boldsymbol{\omega}^{i}_{n+1})\right) = &-\Delta\mathbf{w}^{i}_{\mathbf{n+1}} \times \left[\delta\boldsymbol{\omega}^{i}_{n+1} + \boldsymbol{\omega}^{i}_{n+1} \times \delta\mathbf{w}^{i}_{\mathrm{n+1}}\right] \\ &+ \Delta\delta\boldsymbol{\omega}^{i}_{n+1} + \Delta\boldsymbol{\omega}^{i}_{n+1} \times \delta\mathbf{w}^{i}_{\mathrm{n+1}} + \boldsymbol{\omega}^{i}_{n+1} \times \Delta\delta\mathbf{w}^{i}_{\mathrm{n+1}}\end{aligned} \tag{3.140}$$

It should be noted that all the rotation parameters in Equations 3.135 to 3.140 is expressed in terms of incremental rotation vector $\boldsymbol{\theta}^{i}_{n+1}$, its variations $\delta\boldsymbol{\theta}^{i}_{n+1}$ and its incremental values $\Delta\boldsymbol{\theta}^{i}_{n+1}$, i.e.

$$\delta\mathbf{w}^{\mathrm{i}}_{\mathbf{n+1}} = \widetilde{\mathbf{T}}(\boldsymbol{\theta}^{\mathrm{i}}_{\mathrm{n+1}}) \cdot \delta\boldsymbol{\theta}^{\mathrm{i}}_{\mathrm{n+1}} \tag{3.107}$$

$$\Delta\mathbf{w}^{i}_{\mathrm{n+1}} = \widetilde{\mathbf{T}}(\boldsymbol{\theta}^{i}_{n+1}) \cdot \Delta\boldsymbol{\theta}^{i}_{n+1} \tag{3.141}$$

$$\begin{aligned}\Delta\delta\mathbf{w}^{i}_{\mathrm{n+1}} = &\left(\widetilde{\mathbf{T}}(\boldsymbol{\theta}^{i}_{n+1}) \cdot \delta\boldsymbol{\theta}^{i}_{n+1}\right)^{\mathbf{T}} \times \left(\widetilde{\mathbf{T}}(\boldsymbol{\theta}^{i}_{n+1}) \cdot \delta\boldsymbol{\theta}^{i}_{n+1}\right) \\ &+ \left.\frac{\mathrm{d}}{\mathrm{d}\varepsilon}\right|_{\varepsilon=0} \left[\widetilde{\mathbf{T}}(\boldsymbol{\theta}^{i}_{n+1})\right] \cdot \delta\boldsymbol{\theta}^{i}_{n+1}\end{aligned} \tag{3.142}$$

and

$$\left.\frac{\mathrm{d}}{\mathrm{d}\varepsilon}\right|_{\varepsilon=0} \left[\widetilde{\mathbf{T}}(\boldsymbol{\theta}^{i}_{n+1})\right] \cdot \mathbf{a} = \boldsymbol{\Sigma}(\mathbf{a}) \cdot \Delta\boldsymbol{\theta}^{i}_{n+1} \tag{3.143}$$

where

$$\begin{aligned}\boldsymbol{\Sigma}(\mathbf{a}) = &\left[\mathrm{c}_1\mathbf{a} - \mathrm{c}_2\left(\boldsymbol{\theta}^{i}_{n+1} \times \mathbf{a}\right) + \mathrm{c}_3\left(\boldsymbol{\theta}^{i}_{n+1} \cdot \mathbf{a}\right)\boldsymbol{\theta}^{i}_{n+1}\right] \otimes \boldsymbol{\theta}^{i}_{n+1} + \mathrm{c}_4[\mathbf{a}\times] \\ &+ \mathrm{c}_5\left[\left(\boldsymbol{\theta}^{i}_{n+1} \times \mathbf{a}\right)\mathbf{I} + \left(\boldsymbol{\theta}^{i}_{n+1} \otimes \mathbf{a}\right)\right]\end{aligned} \tag{3.144}$$

$$\begin{aligned}&\mathrm{c}_1 = \frac{\theta\cos\theta - \sin\theta}{\theta^3} \qquad \mathrm{c}_2 = \frac{\theta\sin\theta + 2\cos\theta - 2}{\theta^4} \\ &\mathrm{c}_3 = \frac{3\sin\theta - 2\theta - \theta\cos\theta}{\theta^5} \qquad \mathrm{c}_4 = \frac{1-\cos\theta}{\theta^2} \qquad \mathrm{c}_5 = \frac{\theta - \sin\theta}{\theta^3}\end{aligned} \tag{3.145}$$

The explicit form of linearized virtual work equation presented in Appendix 1.

CHAPTER FOUR
SYSTEM EQUATION OF MOTION

4.1 Mechanical Model of the System

System considered in this study is illustrared in Figure 4.1. It consists of a motor, a helical coupling and a Jeffcott rotor. System is supported with idendical self aligning ball bearings. In order to callculate the system response in case of misalignment its mechanical model is developed with the following assumptions:

a) Helical coupling is made up of rigid and flexible components. Rigid components are the coupling ends where other machine parts such as rotor and motor are attached to. Flexible component is helical part of the coupling where streching and contraction take place. It is also assumed that helical part is welded to the rigid ones, so that its ends follow the motion of rigid parts (see Figure 4.2).

b) Stiffness of shafts connected to coupling and of bearings are much greater than helical part, in foregoing called helical beam or simply beam, then axes of motor and rotor may be assumed to be fixed in space. In other words coupling rotates around the space fixed axes. For this reason motor and rotor contribute to the mechanical model only with rotory inertias around their axes.

c) Misalignment values and their directions are supposed to be known. Thus locations and directions of rotational axes of coupling are defined (see below).

d) Misalignment values are measured at the point where coupling and rotor are connected (see Figure 4.3).

e) Friction is ignored. However frictional forces and moments could be easily integrated to the proposed scheme details of which are presented subsequent sections.

f) Angular speed of motor is presumed to be known explicitly. Thus motor rotation angle and its angular acceleration are also known.

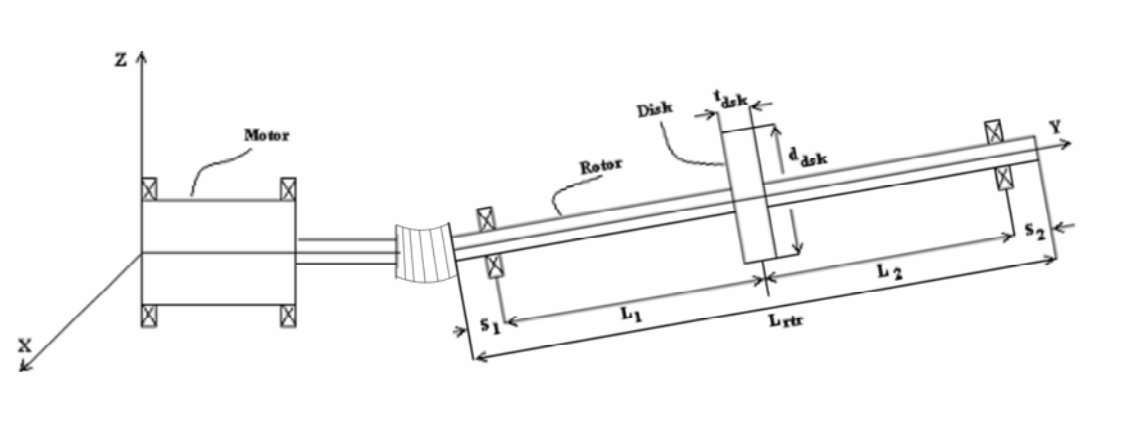

Figure 4.1 Misaligned motor-helical coupling-rotor system.

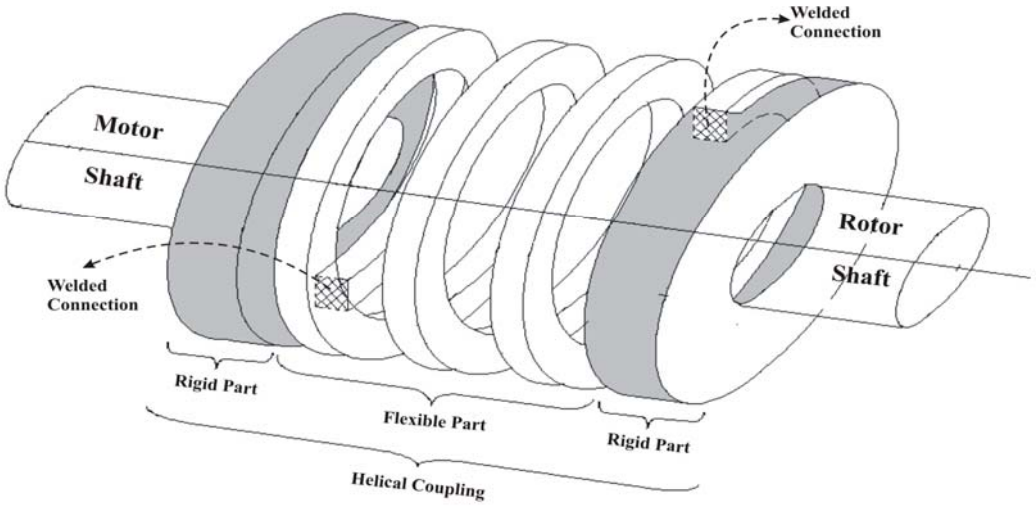

Figure 4.2 Model of the helical coupling.

Mechanical model proposed with above assumptions is shown in Figure 4.3, details of which are given as follows:

a) O_m and O_r are points where motor and rotor, respectively, are attached to the coupling.

b) α is the angular misalignment value which is measured between aligned and misaligned coupling axes (i.e. $\mathbf{n}_{r,0}$ and $\mathbf{n}_r$ respectively). Thus unit vector of rotor axis in misaligned configuration (n_r) is related to the aligned one ($n_{r,0}$) as:

$$n_r = \Lambda(\alpha) \cdot n_{r,0} \tag{4.1}$$

where $\Lambda(\bullet)$ is the rotation tensor (see Equation (8)).

c) n_m is the unit vector along the motor axis.

d) δ is the parallel misalignment which is defined as the vector from $O_{r,0}$ to O_r, i.e. $\delta = O_{r,0}O_r$.

e) I_m and I_r are the rotary inertias of motor and rotor, respectively, around their axes.

f) r_0 and r_L are the location vectors of centroid of boundary cross-sections of beam in aligned configuration with respect to points O_m and $O_{r,0}$, respectively.

g) If we assume that misaligned configuration in Figure 4.3 represents the initial configuration of the system (i.e. t=0), initial values of location vectors with respect to the coordinate system, origin of which is placed to the point O_m are given as

$$\varphi_0(0) = r_0 \tag{4.2}$$

$$\varphi_\ell(0) = L + \delta + r_\ell(0) \tag{4.3}$$

where $\varphi_s(t)$ is the location vector of the beam cross-section at arc-length s and time t. L is the coupling length in aligned configuration which is given as $L = |O_m O_{r,0}|$. $r_\ell(0)$ is the centroid of cross-section at initial configuration with respect to point O_r and it is related to r_L as

$$r_\ell(0) = \Lambda(\alpha) \cdot r_L \tag{4.4}$$

ℓ is the coupling length and subscript ℓ is used to refer to end of the beam or boundary of the beam at rotor side.

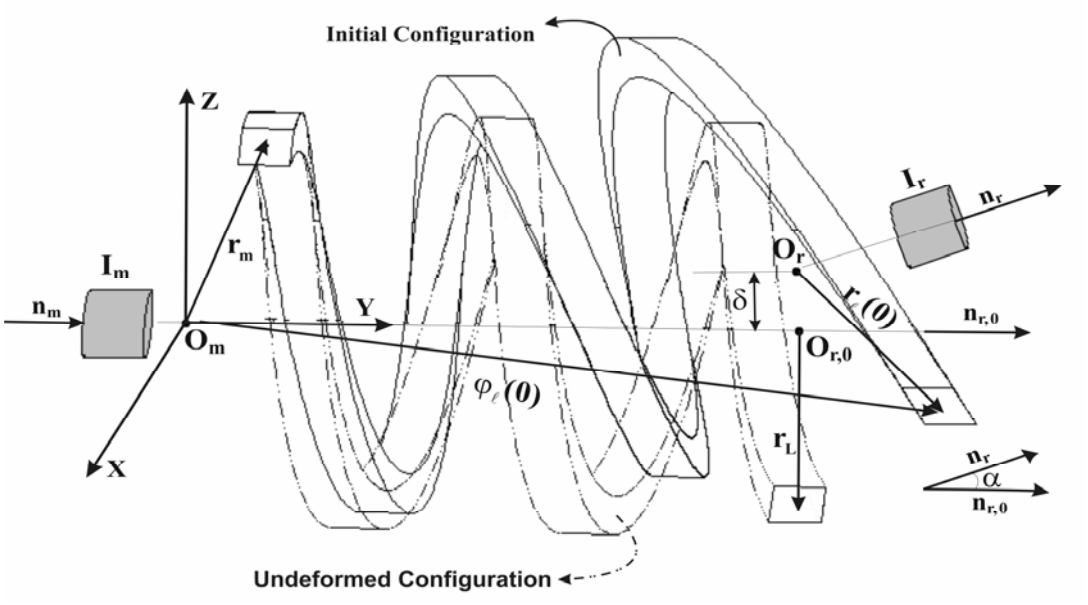

Figure 4.3 Computational model of motor-helical coupling-rotor system. See text for details.

4.2 Kinetic and Potential Energy Expressions

Total kinetic energy of sytem in Figure 4.1 consists of kinetic energies of motor, coupling and rotor. If one takes into account that kinetic energy of coupling is much smaller than that of motor and rotor it can be ignored. Then total kinetic energy, by noting the assumptions, can be written as

$$T = \frac{1}{2} I_m \dot{\theta}_m^2 + \frac{1}{2} I_r \dot{\theta}_r^2 \tag{4.5}$$

where I_m and I_r are the rotary inertias of motor and rotor, respectivelly. $\dot{\theta}_m$ and $\dot{\theta}_r$ are the corresponding angular speeds. Since motor and rotor shafts are assumed to be rigid, only helical beam contributes to the system potential energy, i.e.

$$\Pi = \frac{1}{2} \int_0^L (\gamma \cdot n + \omega \cdot m) ds \tag{4.6}$$

From Equation 4.5 and 4.6 Lagrangian of the system is obtained as:

$$L = T - \Pi = \frac{1}{2} I_m \dot{\theta}_m^2 + \frac{1}{2} I_r \dot{\theta}_r^2 - \frac{1}{2} \int_0^L (\varepsilon \cdot n + k \cdot m) ds \tag{4.7}$$

Since motor angular speed is stated explicitly, motor kinetic energy does not contribute to the virtual work equation (i.e. $\delta\theta_m = 0$). Then Lagrangian may be written as:

$$L = \frac{1}{2} I_r \dot{\theta}_r^2 - \frac{1}{2}\int_0^L (\varepsilon \cdot n + k \cdot m) ds \tag{4.8}$$

4.3 Boundary Conditions and Constraint

Since helical beam (or flexible part of coupling) follows the motion of rigid parts (as stated by assumptions) rotation vectors corresponding to boundary cross-sections of helical beam may be written as (Figure 4.3)

$$\theta_0(t) = \theta_m(t) \cdot n_m \tag{4.9}$$

$$\theta_\ell(t) = \theta_r(t) \cdot n_r \tag{4.10}$$

where $\theta_0(t)$ and $\theta_\ell(t)$ are the rotation vectors of boundary cross-sections. $\theta_m(t)$ and $\theta_r(t)$ are the rotation angles of motor and rotor, respectively. n_m and n_r are unit vectors along the motor and rotor axes, respectively. Since n_m and n_r are assumed to fixed in space, unit normal vectors of boundary cross-sections stay in the planes perpendicular to n_m and n_r.

Moreover misalignment values are assumed to be known then the location vectors of boundary cross-sections are related to the corresponding rotation vectors as (Figure 4.3)

$$\varphi_0(t) = \Lambda(\theta_0(t)) \cdot \varphi_0(t) \tag{4.11}$$

$$\varphi_\ell(t) = L + \delta + r_\ell(t) \tag{4.12}$$

where $r_\ell(t)$ is given as

$$r_\ell(t) = \Lambda(\theta_\ell(t)) \cdot r_\ell(0) \tag{4.13}$$

Since motor speed $\dot{\theta}_m(t)$ is specified (as stated with assumption (f) in section (3)), boundary conditions corresponding to s=0 (i.e. $\theta_0(t)$ and $\varphi_0(t)$) are also

specified by Equations 4.9 and 4.11. Rotor speed is not known *a priori*. Thus boundary conditions at s=ℓ, (i.e. $\theta_\ell(t)$ and $\varphi_\ell(t)$) can not be calculated from Equation 4.10 and 4.12. However one can use the reaction forces and moments together with constitutive equation in order to find another relation between $\theta_\ell(t)$ and $\varphi_\ell(t)$ as follows:

Motion of Jefcott rotor is imposed by the reaction forces and moments formed at the end of the beam (see Figure 4.4), i.e.

$$\left[r_\ell(t)\times\left(-F_\ell(t)\right)+\left(-M_\ell(t)\right)\right]\cdot n_r = I_r\ddot{\theta}_r(t) \tag{4.14}$$

where $F_\ell(t)$ and $M_\ell(t)$ are the reaction forces and moments, respectively, at s=ℓ. $\ddot{\theta}_r(t)$ is the angular acceleration of rotor. $F_\ell(t)$ and $M_\ell(t)$ are related to $\theta_\ell(t)$ and $\varphi_\ell(t)$ through constitutive equations as

$$F_\ell(t) = \Lambda(\theta_\ell(t))\cdot C\cdot\Lambda^T(\theta_\ell(t))\cdot\gamma(\theta_\ell(t),\varphi'_\ell) \tag{4.15}$$

$$M_\ell(t) = \Lambda(\theta_\ell(t))\cdot D\cdot\Lambda^T(\theta_\ell(t))\cdot\omega(\theta_\ell(t),\theta'_\ell(t)) \tag{4.16}$$

where $\gamma(\bullet)$ is axial and shear strain measures energy conjugate to $F_\ell(t)$, and $\omega(\bullet)$ is the bending strain measures energy conjugate to $M_\ell(t)$. C and D are the corresponding constitutive matrices. Explicit form of $\gamma(\bullet)$, $\omega(\bullet)$, C and D are presented in Section 2. As stated above, prime denotes the derivative with respect to arc-length s.

If one uses the Equations 4.14 to 4.16 to obtain relation between $\theta_\ell(t)$ and $\varphi_\ell(t)$, it finds highly nonlinear equation in the form

$$\mathfrak{I}\left(\theta_\ell(t),\theta'_\ell(t),\varphi_\ell(t),\varphi'_\ell(t)\right)+I_r\ddot{\theta}_r(t)=0 \tag{4.17}$$

where explicit form of $\mathfrak{I}(\bullet)$ is given in Appendix I. Equation 4.10 and 4.12 can be substituted into Equation 4.17 to find a boundary condition which depends on single variable. However obtained boundary condition will be difficult to handle. If we note that any boundary condition may also be treated as constraint, difficulty can be

overcome by employing Lagrange multiplier method. In other words Equation 4.17 is substituted into Equation 4.8 to form augmented Lagrangian (Bathe, 1996, page 270) as

$$L_{aug} = \frac{1}{2} I_r \dot{\theta}_r^2 n_r - \frac{1}{2} \int_0^L (\varepsilon \cdot n + k \cdot m) ds + \lambda(t) \cdot \hbar(t) \tag{4.18}$$

where $\lambda(t)$ is the scalar Lagrangian multiplier and $\hbar(t)$ is the constraint equation given as

$$\hbar(t) = \Im(\theta_\ell(t), \theta'_\ell(t), \varphi_\ell(t), \varphi'_\ell(t)) + I_r \ddot{\theta}_r(t) \tag{4.19}$$

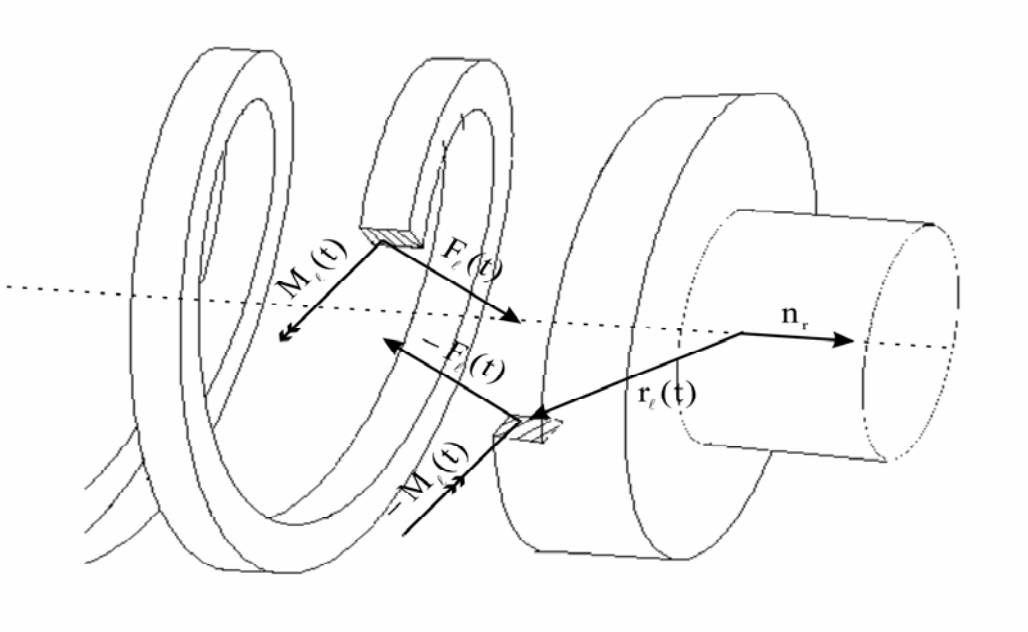

Figure 4.4 Rotor motion is caused by the torque which

4.4 Weak Form of Equation of Motion

The weak form of the equation of motion, by ignoring the friction and other non-conservative forces and moments, is

$$\delta \int_{t_2}^{t_2} L_{augm} dt = \delta \int_{t_2}^{t_2} (T - \Pi - \lambda(t) \cdot \hbar(t)) dt = 0 \tag{4.20}$$

If one makes use of the partial differentiation explicit form of weak form is found as

$$\delta L_{aug} = \delta\Pi + I_r\ddot{\theta}_r(t)\delta\theta_r + I_r\ddot{\lambda}(t)\delta\theta_r + \hbar(t)\delta\lambda(t) + \lambda(t)\delta\Im(\bullet) = 0 \qquad (4.21)$$

where $\delta\Pi$ is the virtual work of the beam and it is given in Equation (6). $\Im(\bullet)$ is defined in previous section and its explicit form and variation ($\delta\Im(\bullet)$) is presented in Appendix 2. Overdot denotes derivative with respect to time.

Because Equation 4.21 is highly nonlinear; one needs to employ an iterative procedure to obtain its solution. If Newton method is made use of for that purpose consistent linearization should be performed to obtain exact tangent operator and to ensure the quadratic convergence rate of the iterative procedure (Ibrahimbegovic & Mikad, 1998). Consistent linear approximation of Equation 4.21 may be obtained as:

$$L\left[\delta L^{(i)}_{aug,n+1}\right] = \delta L^{(i)}_{aug,n+1} + \left.\frac{d}{d\varepsilon}\right|_{\varepsilon=0}\left[\delta L^{(i)}_{aug,n+1,\varepsilon}\right] \qquad (4.22)$$

where (i) is the iteration counter, n+1 is the dicritized time step number. Since we employed spatial incremental rotation vector update procedure [21] linearization of a spatial tensor field is carried out with Lie derivative formulization given in Equation (17).

Consistent linearization of virtual work of beam (i.e. $L[\delta\Pi]$) is summarized in Section 2 and details of its linearization procedure can be found in Ibrahimbegovic & Mikad (1998). Since $\delta\Im(\bullet)$ depends on $\theta(t)$ and $\varphi(t)$, same procedure is used for its linearization. Explicit form of $L_\Delta[\delta\Im(\bullet)]$ are presented in Appendix 2.

In order to linearize the angular acceleration ($L[\ddot{\theta}]$) and second derivative of Lagrange multiplier ($L[\ddot{\lambda}]$), one first needs to obtain their values at the chosen instants of time interval of interest (Ibrahimbegovic & Mikad, 1998). If we take advantage of scalar nature of $\theta(t)$ and $\lambda(t)$, their time derivative may simply be approximated as:

$$\dot{\lambda}_{n+1} = \frac{\lambda_{n+1} - \lambda_n}{\Delta t} \qquad \ddot{\lambda}_{n+1} = \frac{\dot{\lambda}_{n+1} - \dot{\lambda}_n}{\Delta t} = \frac{\lambda_{n+1} - \lambda_n}{(\Delta t)^2} - \frac{\dot{\lambda}_n}{\Delta t} \tag{4.23a,b}$$

$$\dot{\theta}_{r,n+1} = \frac{\theta_{r,n+1} - \theta_{r,n}}{\Delta t} \quad \ddot{\theta}_{r,n+1} = \frac{\dot{\theta}_{r,n+1} - \dot{\theta}_{r,n}}{\Delta t} = \frac{\theta_{r,n+1} - \theta_{r,n}}{(\Delta t)^2} - \frac{\dot{\theta}_{r,n}}{\Delta t} \tag{4.24a,b}$$

where $\Delta t = t_{n+1} - t_n$ is a typical time step. If values of $\theta(t_n)$ and $\dot{\theta}(t_n)$ as well as $\lambda(t_n)$ and $\dot{\lambda}(t_n)$ are assumed to be known then linearized forms of $\ddot{\theta}(t)$ and $\ddot{\lambda}(t)$ may be found as

$$\left.\frac{d}{d\varepsilon}\right|_{\varepsilon=0} \left[\ddot{\theta}^{(i)}_{r,n+1,\varepsilon}\right] = \frac{\Delta\theta^{(i)}_{r,n+1}}{(\Delta t)^2} \tag{4.25}$$

$$\left.\frac{d}{d\varepsilon}\right|_{\varepsilon=0} \left[\ddot{\lambda}^{(i)}_{n+1,\varepsilon}\right] = \frac{\Delta\lambda^{(i)}_{n+1}}{(\Delta t)^2} \tag{4.26}$$

Explicit form of δL_{aug} and $L[\delta L_{aug}]$ are presented in Appendix 2. Technical computing program MATLAB is used for computer implementation of proposed scheme and its details are presented in Appendix 6.

4.5 Remarks on the Numerical Implementation

The finite element method is implemented to solve the linearized virtual work equation given in Equation 4.21. The element configuration is approximated with an assembly of 4 node elements with

$$\mathbf{x}^h\big|_{L^e} = \sum_{I=1}^{4} N_I(\zeta)\cdot \mathbf{x}_I \qquad \begin{aligned} \mathbf{N_1} &= -\tfrac{9}{16}\left(\mathbf{1}-\zeta\right)\left(\tfrac{1}{3}+\zeta\right)\left(\tfrac{1}{3}-\zeta\right) \\ N_2 &= \tfrac{27}{16}\left(\mathbf{1}+\zeta\right)\left(1-\zeta\right)\left(\tfrac{1}{3}-\zeta\right) \\ N_3 &= \tfrac{27}{16}\left(\mathbf{1}+\zeta\right)\left(1-\zeta\right)\left(\tfrac{1}{3}+\zeta\right) \\ \mathbf{N_4} &= -\tfrac{9}{16}\left(\tfrac{1}{3}+\zeta\right)\left(\tfrac{1}{3}-\zeta\right)\left(\mathbf{1}+\zeta\right) \end{aligned} \tag{4.27}$$

where $N_I(\zeta)$ are the standard linear shape functions, and $\mathbf{x_I}$ are nodal coordinates. The dependent variables φ and θ, and their variations are interpolated in isoparametric manner (Ibrahimbegovic & Mikad, 1998); i.e.

$$\boldsymbol{\theta}^h\big|_{L^e} = \sum_{I=1}^{4} N_I(\zeta)\cdot \boldsymbol{\theta}_I \qquad \boldsymbol{\varphi}^h\big|_{L^e} = \sum_{I=1}^{4} N_I(\zeta)\cdot \boldsymbol{\varphi}_I \tag{4.28}$$

$$\delta\boldsymbol{\theta}^{\mathbf{h}}\Big|_{L^e} = \sum_{I=1}^{4} N_I(\zeta)\cdot\delta\boldsymbol{\theta}_{\mathbf{I}} \qquad \delta\boldsymbol{\varphi}^{\mathbf{h}}\Big|_{L^e} = \sum_{I=1}^{4} N_I(\zeta)\cdot\delta\boldsymbol{\varphi}_{\mathbf{I}}$$

$$\Delta\boldsymbol{\theta}^{\mathbf{h}}\Big|_{L^e} = \sum_{I=1}^{4} N_I(\zeta)\cdot\Delta\boldsymbol{\theta}_{\mathbf{I}} \qquad \Delta\boldsymbol{\varphi}^{\mathbf{h}}\Big|_{L^e} = \sum_{I=1}^{4} N_I(\zeta)\cdot\Delta\boldsymbol{\varphi}_{\mathbf{I}}$$

The 3-point Gauss integration scheme is used to integrate resultant equations. This method produces the element stiffness matrix of the correct rank and at the same time alleviates the locking phenomena (Bathe, 1996).

As mentioned above, rotor is constrained to move only around its axis. Thus, if one discretizes the helical beam starting from motor end through rotor end with n_{elm} number of finite elements, the interpolations of the last element reduces to, noting Equations 4.14 and 4.15

$$\boldsymbol{\varphi}_{n_{elm}} = \sum_{I=1}^{3} N_I(\zeta)\cdot\delta\boldsymbol{\varphi}_I + N_4(\zeta)\cdot\left(\ell + \boldsymbol{\delta} + \boldsymbol{\Lambda}(\boldsymbol{\theta}_4^{n_{elm}})\cdot\boldsymbol{\Lambda}(\boldsymbol{\alpha})\cdot\mathbf{r}_L\right) \tag{4.29a}$$

$$\delta\boldsymbol{\varphi}_L = \sum_{\mathbf{I=1}}^{\mathbf{3}} N_I(\zeta)\cdot\delta\boldsymbol{\varphi}_{\mathbf{I}} + N_4(\boldsymbol{\zeta})\cdot\boldsymbol{\Xi}(\boldsymbol{\Lambda}(\boldsymbol{\alpha})\cdot\mathbf{r}_L)\cdot\delta\theta_4^{n_{elm}}\cdot\mathbf{n}_R \tag{4.29b}$$

$$\Delta\boldsymbol{\varphi}_{n_{elm}} = \sum_{\mathbf{I=1}}^{\mathbf{3}} N_I(\zeta)\cdot\Delta\boldsymbol{\varphi}_{\mathbf{I}} + N_4(\boldsymbol{\zeta})\cdot\boldsymbol{\Xi}(\boldsymbol{\Lambda}(\boldsymbol{\alpha})\cdot\mathbf{r}_L)\cdot\Delta\theta_4^{n_{elm}}\cdot\mathbf{n}_R \tag{4.29c}$$

where $\theta_4^{n_{elm}}$ is the angular position of the rotor corresponding to 4th node of the last element with variations $\delta\theta_4^{n_{elm}}$ and $\Delta\theta_4^{n_{elm}}$.

CHAPTER FIVE
RESULTS

5.1 Introduction

Helical coupling used in simulations is a (right helix) commercial flexible coupling made up of 7075-T6 Aluminum alloy. Geometric and material properties of helical coupling are presented in Appendix 4. Simulations are performed for pure angular and parallel misalignment cases. Angular misalignment is introduced around positive X-axis. Parallel misalignment is induced along positive Z-axis (see Figure 4.4). In previous studies effect of rotary inertia on rotor speed and reaction loads are not taken into account. In order to study inertia effect, rotor-disk system having I_r= $6.53x10^{-4}$ Kg-m^2 mass moment of inertia around its rotational axis is chosen as reference and simulations are performed for values of $0.1I_r$, I_r and $10I_r$. Hypothetical rotor-disk system and its parameter values are presented in Appendix 5. Motor speed is assumed to be constant and set to 5000 RPM (83.33 Hz) during simulations.

5.2 Aligned System

Figure 5.1 shows the calculated angular velocity variation of rotor (ω_R) for aligned system (δ=0.0 mm $\alpha=0^o$). As can be seen from Figure 5.1 proposed scheme is capable of predicting the constant angular velocity of rotor for aligned system.

5.3 Angular Misalignment

First set of simulations is performed for pure angular misalignment (i.e. $\alpha=1^o$, δ=0.0 mm). Figure 5.2a and Figure 5.3a show the angular velocity and acceleration variations, respectively, of driven shaft for inertia values of $0.1I_r$, I_r and $10I_r$ (see above). Frequency spectrums are presented in Figure 5.2b and Figure 5.3b. In previous studies it is assumed that angularly misaligned coupling behaves exactly as universal joint. Thus universal joint velocity and acceleration variations are also added to figures for comparison. It is clear from figures that variations are dependent not only misalignment but also inertia value. Since larger inertia results in driven

shaft speed to converge to that of driven shaft, effect of angular misalignment on driven shaft's speed diminishes with increasing inertia. Frequency spectrums indicate that angular velocity and acceleration have three frequency components, two of which are common to all inertia values (i.e. 1X and 2X of motor speed). This suggests that these frequencies are related to coupling geometry. Third frequency component is not constant and changes with changing inertia. It has the value of 5.21, 10.42 and 36.46 HZ for inertia values of $0.1I_r$, I_r and $10I_r$, respectively. For all cases 1X motor speed is dominant frequency. Comparison of universal joint velocity and acceleration with present study validates our criticism of associating misaligned behavior with universal joint (i.e. Cardan joint).

Calculated reaction loads generated by angularly misaligned coupling on driven shaft are presented in Figure 5.4a through Figure 5.8a. Frequency spectrums are shown in Figure 5.4b through Figure 5.8b. Reaction loads vary around constant values which are corresponding to initial deformation of coupling. In previous studies, reaction loads are calculated *a priori* by associating coupling behavior with ideal spring element and/or universal joint. Thus inertia effect was not taken into account. However, as can be observed from figures, reaction loads are not only dependent on misalignment value but also inertia of rotor. As the case for angular velocity and acceleration, reaction loads have common frequency components for all inertia values, which can be associated with geometry of coupling. Reaction loads which act along the transverse direction have common frequency components of 1X, 2X and 3X of motor speed (i.e. 83.33 HZ) for all inertia values and reaction force F_y acting along the axial direction has common frequency components of 1X and 2X of motor speed. Reaction load variations in common frequencies do not change with changing inertia, i.e. independent of inertia. Effect of inertia on reaction loads are observable for lighter cases since additional frequency components are appeared for small inertia values. Effect of inertia becomes negligible for large values and coupling geometry dominates the system response.

In literature, 1X vibration component along axial direction is given as the characteristic of angular misalignment. It can be seen from Figure 5.5b that axial

load F_y has the dominant frequency component of 1X. Moreover, 2X component along transverse direction are associated with misalignment. Figure 5.4b and Figure 5.6b to 5.8b show that this is the dominant frequency of reaction loads which causes the vibration along transverse direction (i.e. F_x-M_z and F_z-M_x). Thus it can be concluded that proposed scheme are able to predict the associated frequency components of angular misalignment.

In order to demonstrate validity of conclusion given above, response of the hypothetical rotor-bearing system is obtained with commercial FEM program ANSYS. Hypothetical system parameters and its ANSYS model together with computer code are presented in Appendix 5. Xu & Marangoni (1994a, 1994b) concluded that misalignment could be hidden if 2X of motor speed is not close enough to one of the system natural frequencies. Thus parameters of hypothetical system are chosen such that one of the system natural frequencies is close to 2X of motor speed. It should be pointed out that reaction loads are calculated for three different inertia values. For this reason, simulations are performed for three different systems, of which rotary inertias are equal to the mentioned inertia values. Parameters of hypothetical systems are presented in Appendix.

Systems having inertia values of $0.1I_r$ and I_r have 2X of motor speed (i.e. 166.667 Hz) as their first natural frequency. Displacements and frequency spectrums obtained with ANSYS along the transverse directions (i.e. along X and Z axes) are presented in Figure 5.9 and 5.10 for system with 0.1Ir inertia, and in Figure 5.11 and 5.12 for system with Ir inertia. As expected, 2X component is the dominant frequency of vibration response. It can be seen from frequency spectrums that common frequency components of 1X and 3X of motor speed are also present. As mentioned above, lighter inertia results in additional frequency components in reaction loads. These frequencies are also observed in vibration spectrums. Since 2X of motor speed is close (not equal) to one of the system natural frequencies, vibration responses exhibit the characteristic of beating phenomena. This behavior is also observed by Xu & Marangoni, (1994b). Hypothetical system with largest inertia ($10I_r$) has the 2X of motor speed as second natural frequency. The first one is 29.96 HZ. Displacement

and frequency spectrums presented in Figure 5.13 and 5.14 show that system first natural frequency dominates the system response. This result was not expected. It is also interesting that misalignment excited higher natural frequencies of the system. This behavior is not observed for other inertia values.

Xu & Marangoni, (1994b) measured the system response connected with helical coupling in case of angular misalignment. Their results obtained for aligned system show that system has initial fault which is manifested in frequency spectrum with 1X, 2X and 3X of motor speed. Their results for aligned system are reproduced in Figure 5.14a. As can be seen from Figure 5.14a, 2X of motor speed shows the largest change and 3X response is larger than the 1X response. Figure 5.14b shows the response of angularly misaligned system of Xu & Marangoni, (1994b). Since system response increase in all frequencies which are observed in aligned system, it can be concluded that reaction loads generated by misaligned coupling should have frequency components of 1X, 2X and 3X of motor speed. In misaligned system, 2X component shows the largest change and dominates the response. Thus reaction loads should have the dominant frequency of 2X of motor speed. Order of response in 1X and 3X components for misaligned system is reversed, i.e. 1X response is higher that 3X response for misaligned system. It can be seen from Figure 5.4 and Figures 5.6 to 5.8, frequency components of predicted reaction loads show the trend mentioned above. Thus it is concluded that results of Xu & Marangoni, (1994b) presented in Figure 5.15 indicates the validity of proposed scheme.

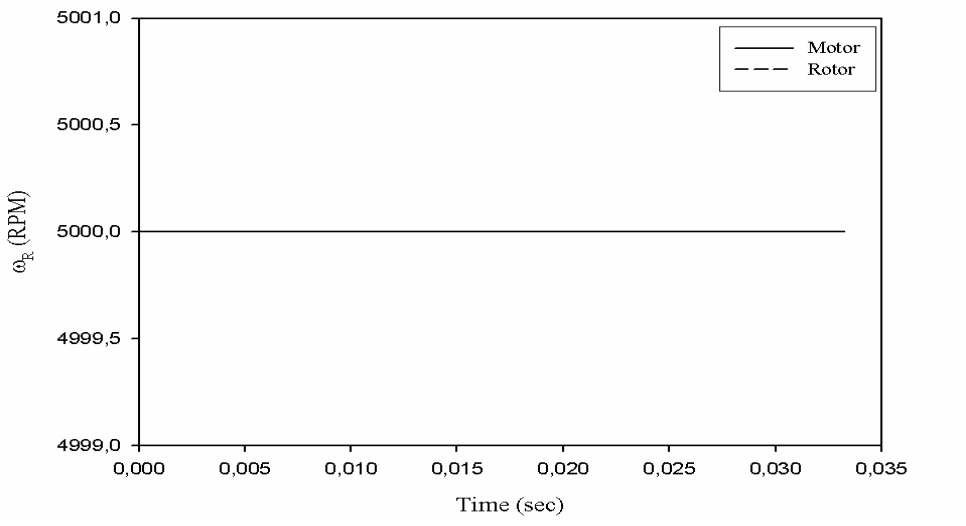

Figure 5.1 Angular velocity (ω_R) variation of rotor for aligned case (δ=0.0 mm α=0^o).

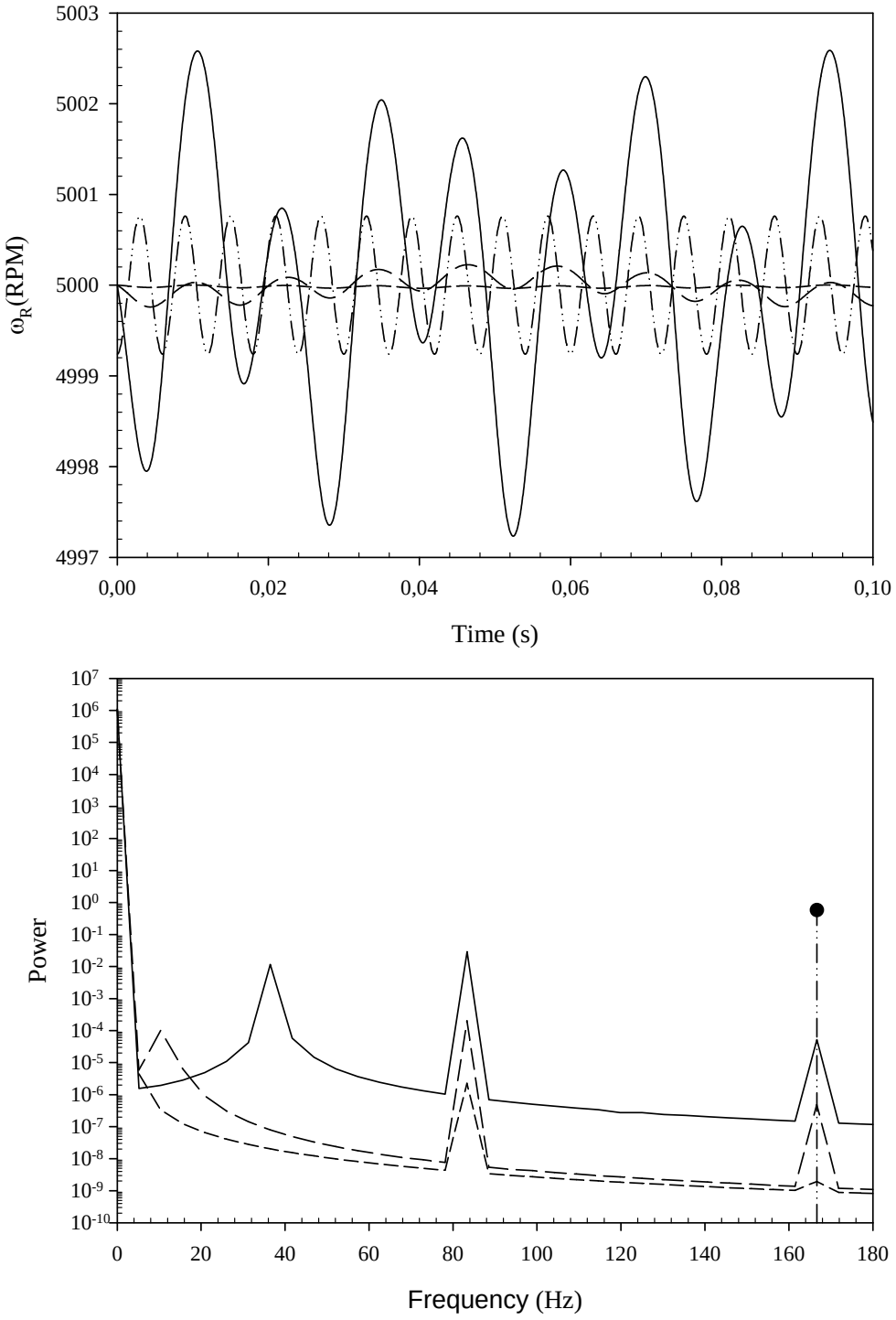

Figure 5.2 (a) Angular velocity variations of rotor and (b) its power spectrum for pure angular misalignment (δ=0.0 mm, α=1^o). (———— $0.1I_R$, — — — — I_R, – – – – – – $10I_R$, —··—··— Universal Joint Velocity). Simulations are performed with Technical computing program MATLAB® and results are plotted with drawing and data analysis software SigmaPlot®.

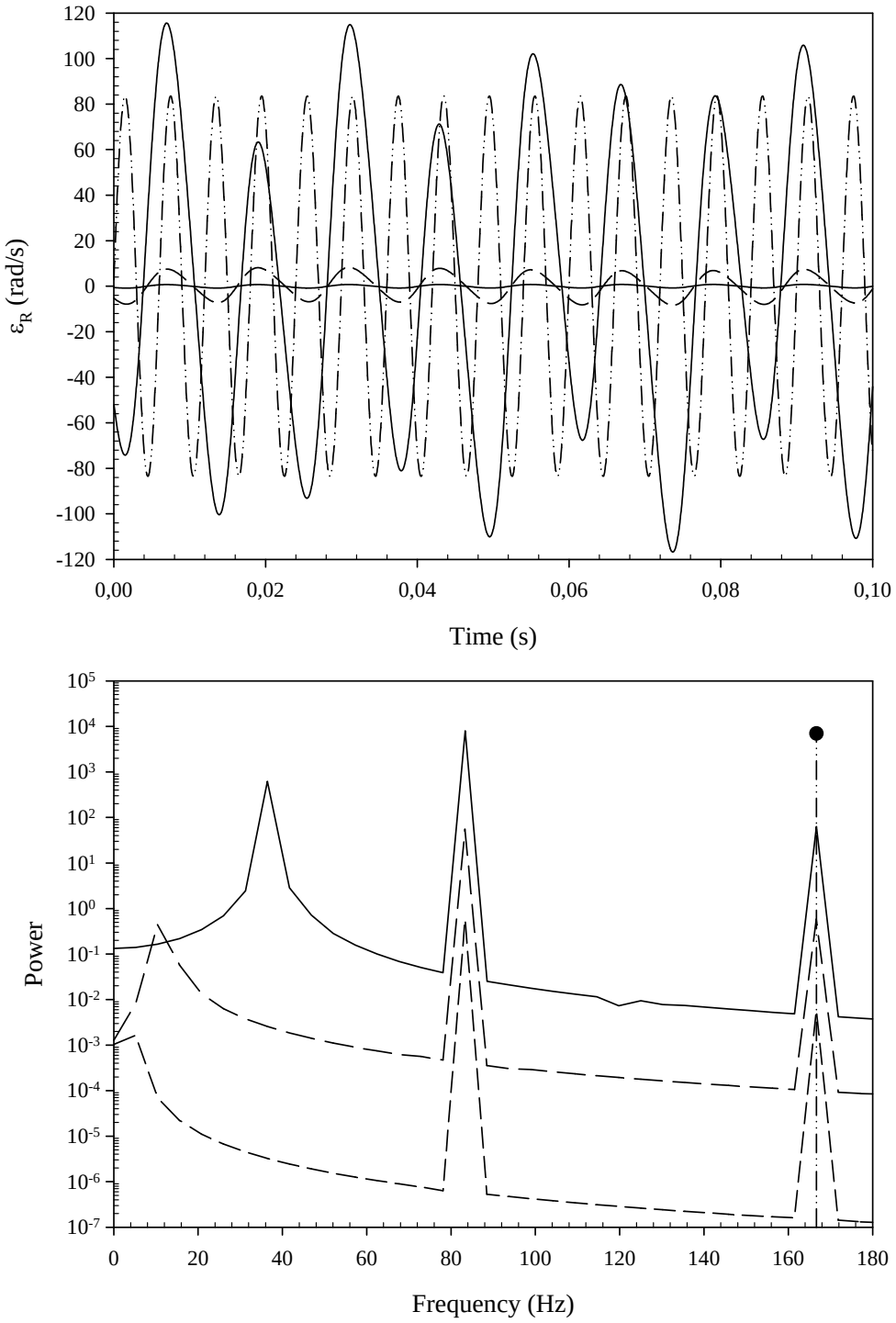

Figure 5.3 (a) Angular acceleration variations of rotor and (b) its power spectrum for pure angular misalignment (δ=0.0 mm, α=1^o). (———— 0.1I_R, — — — — I_R, – – – – – –10I_R, —·—·—·— Universal Joint Acceleration).Simulations are performed with Technical computing program MATLAB® and results are plotted with drawing and data analysis software SigmaPlot®.

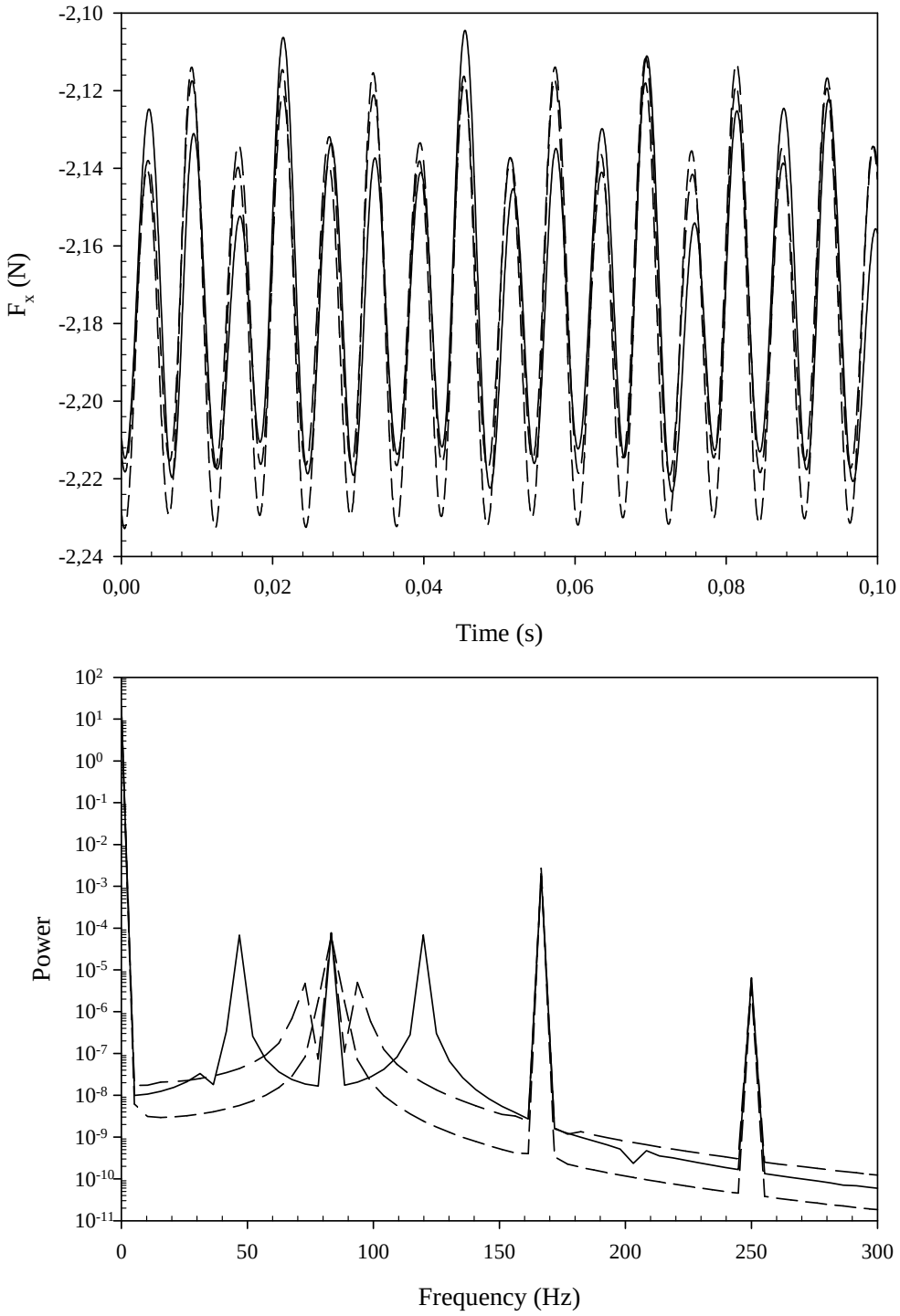

Figure 5.4 (a) Reaction force variation along X-axis (F_x) and (b) its power spectrum for pure angular misalignment (δ=0.0 mm, α=1^o). (———— $0.1I_R$, — — — — I_R, – – – – – – $10I_R$). Simulations are performed with Technical computing program MATLAB® and results are plotted with drawing and data analysis software SigmaPlot®.

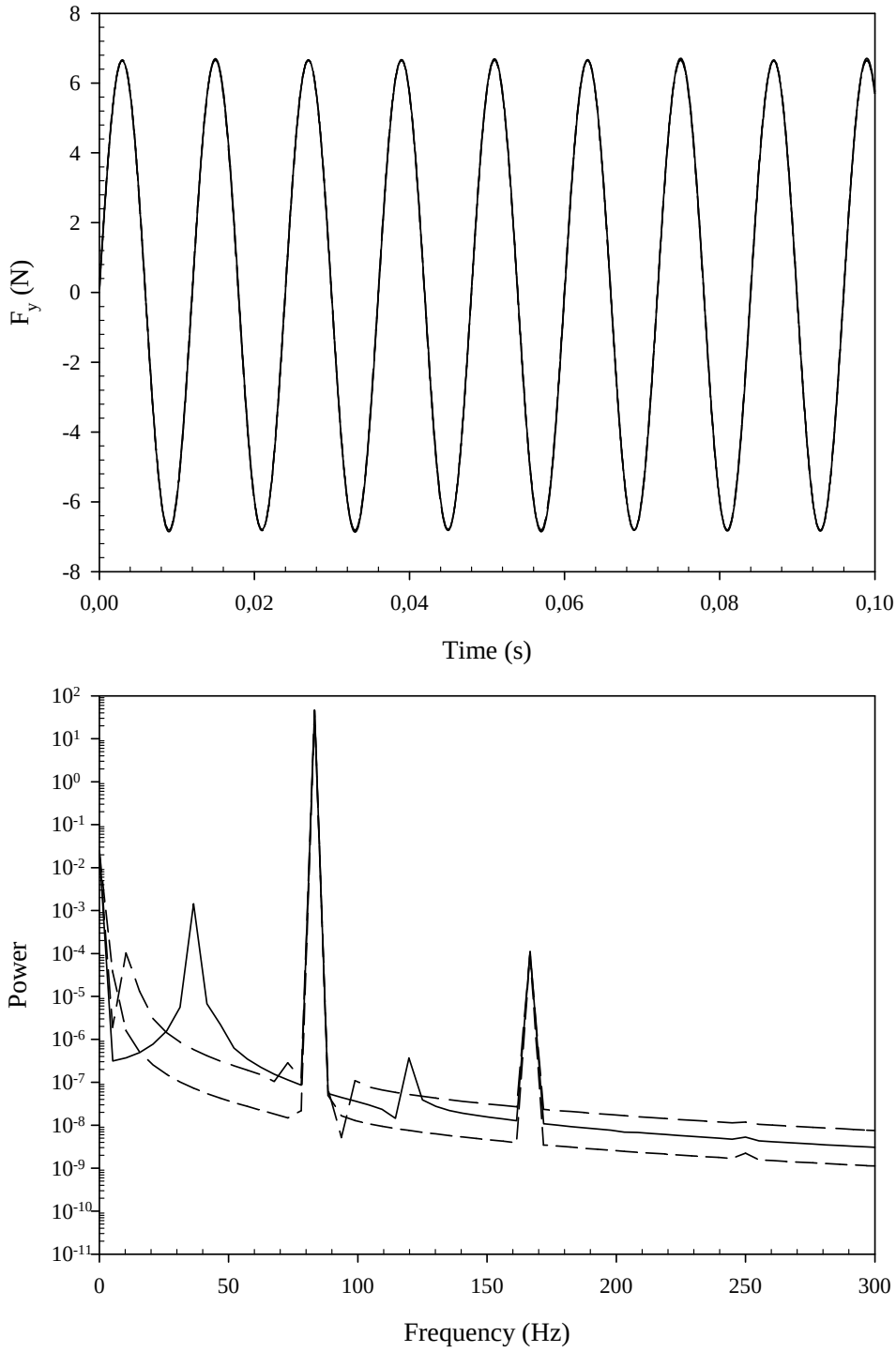

Figure 5.5 (a) Reaction force variation along Y-axis (Fy) and (b) its power spectrum for pure angular misalignment (δ=0.0 mm, α=1^o). (———— $0.1I_R$, — — — — I_R, – – – – – – $10I_R$). Simulations are performed with Technical computing program MATLAB® and results are plotted with drawing and data analysis software SigmaPlot®.

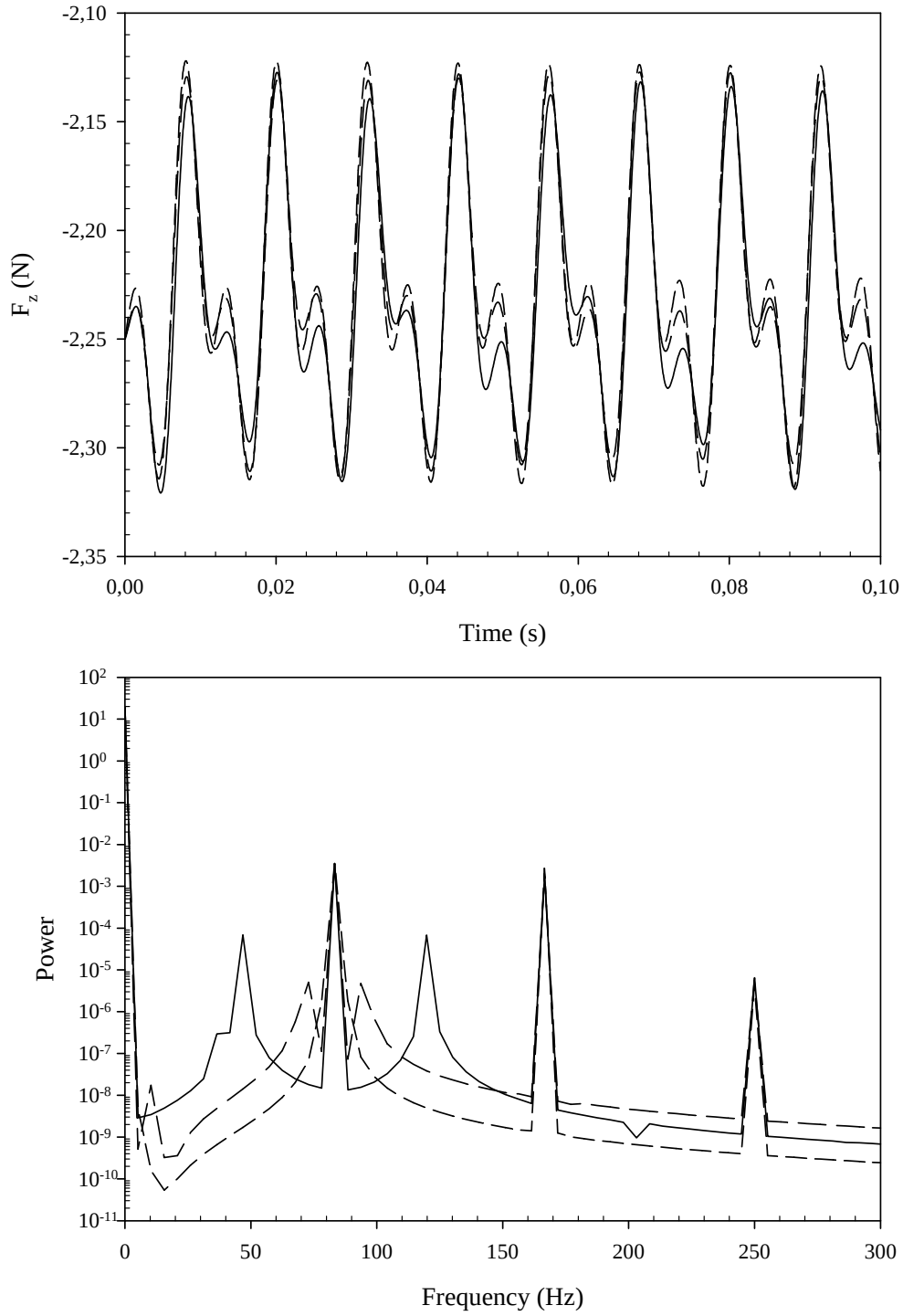

Figure 5.6 (a) Reaction force variation along Z-axis (Fz) and (b) its power spectrum for pure angular misalignment (δ=0.0 mm, α=1^o). (———— 0.1I_R, — — — — I_R, – – – – – 10I_R). Simulations are performed with Technical computing program MATLAB® and results are plotted with drawing and data analysis software SigmaPlot®.

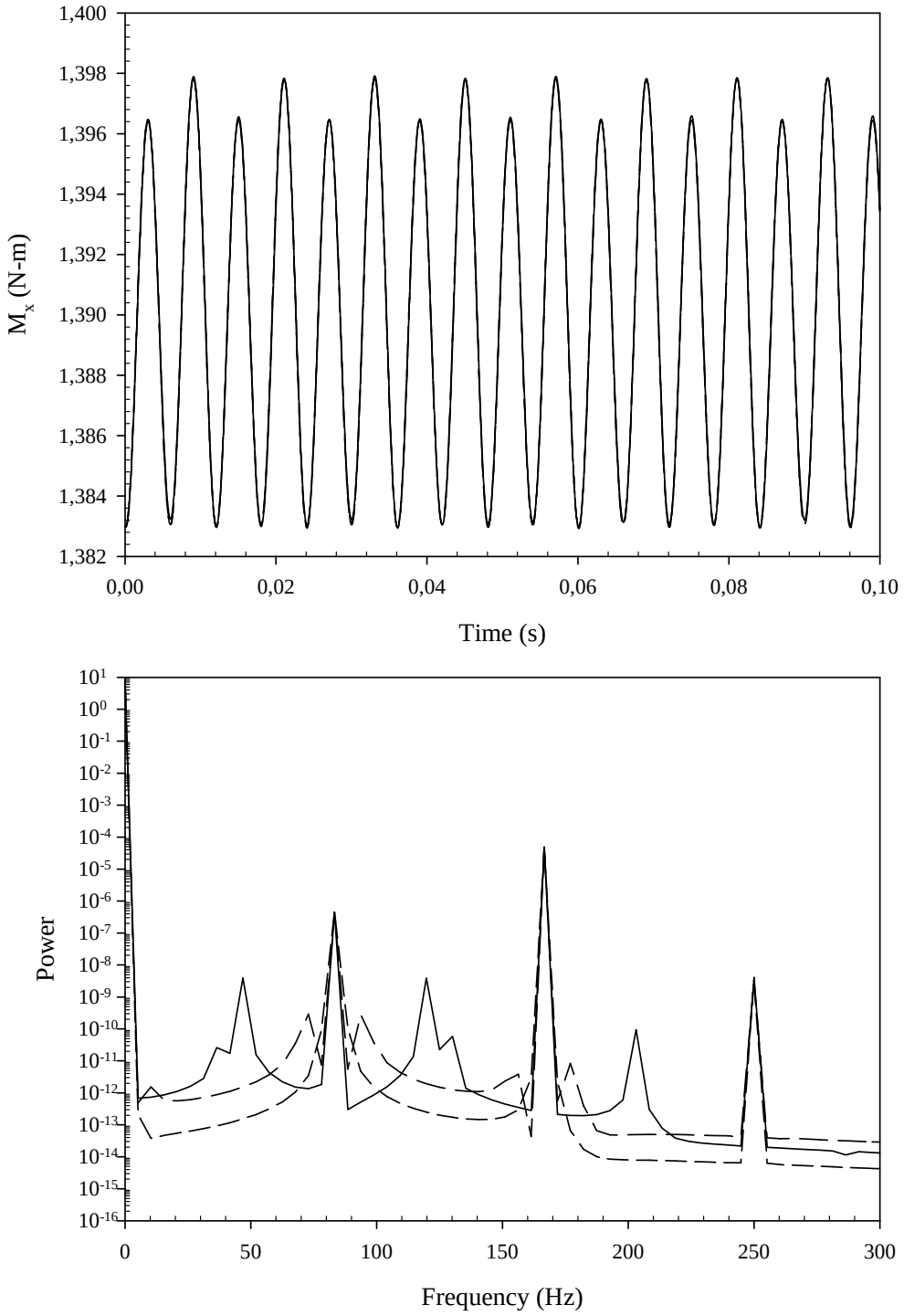

Figure 5.7 (a) Reaction moment variation around X-axis (M_x) and (b) its power spectrum for pure angular misalignment (δ=0.0 mm, α=1^o). (———— $0.1I_R$, — — — — I_R, – – – – – – $10I_R$). Simulations are performed with Technical computing program MATLAB® and results are plotted with drawing and data analysis software SigmaPlot®.

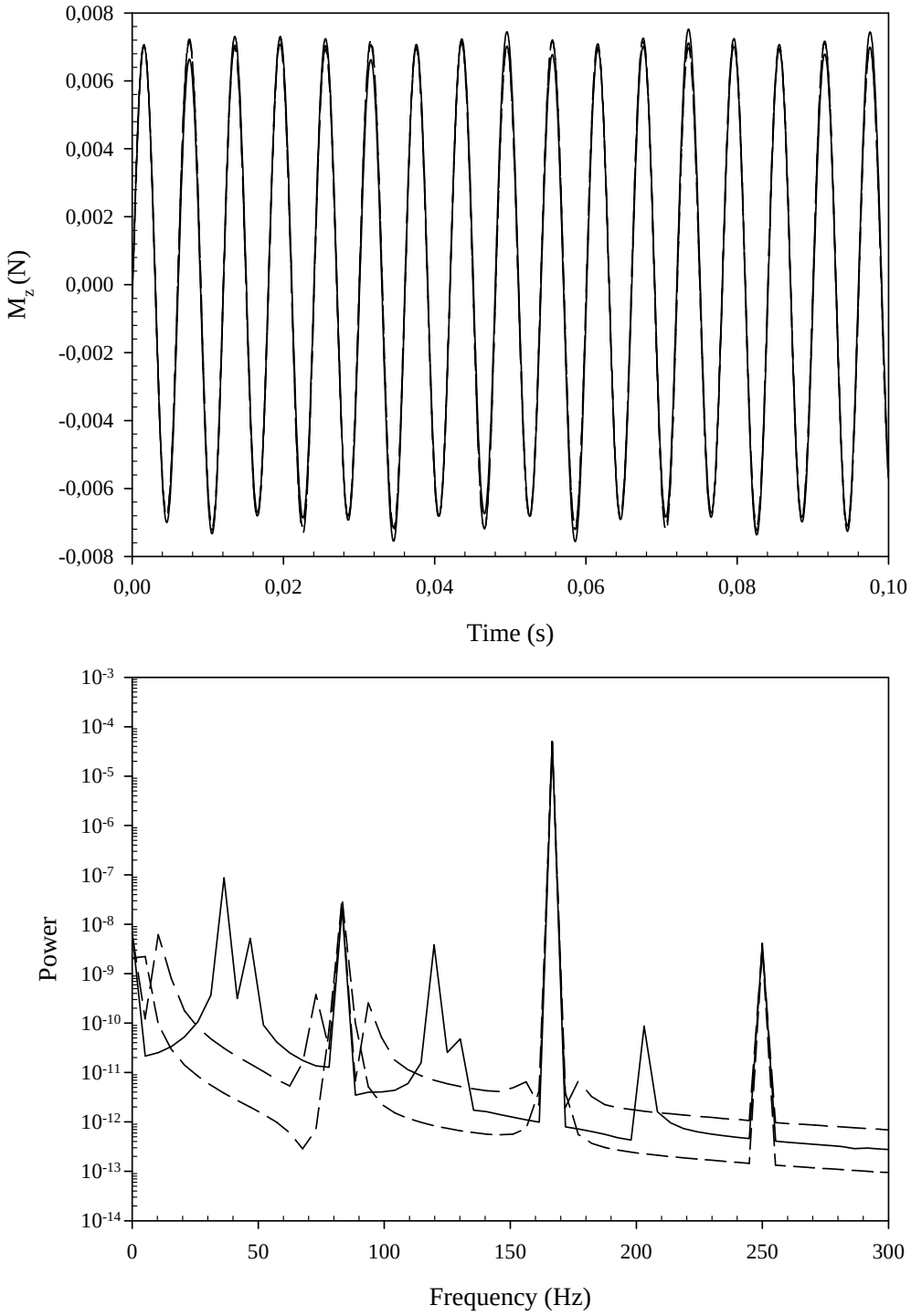

Figure 5.8 (a) Reaction moment variation around Z-axis (M_z) and (b) its power spectrum for pure angular misalignment (δ=0.0 mm, α=1^o). (———— $0.1I_R$, — — — — I_R, – – – – – – $10I_R$). Simulations are performed with Technical computing program MATLAB® and results are plotted with drawing and data analysis software SigmaPlot®.

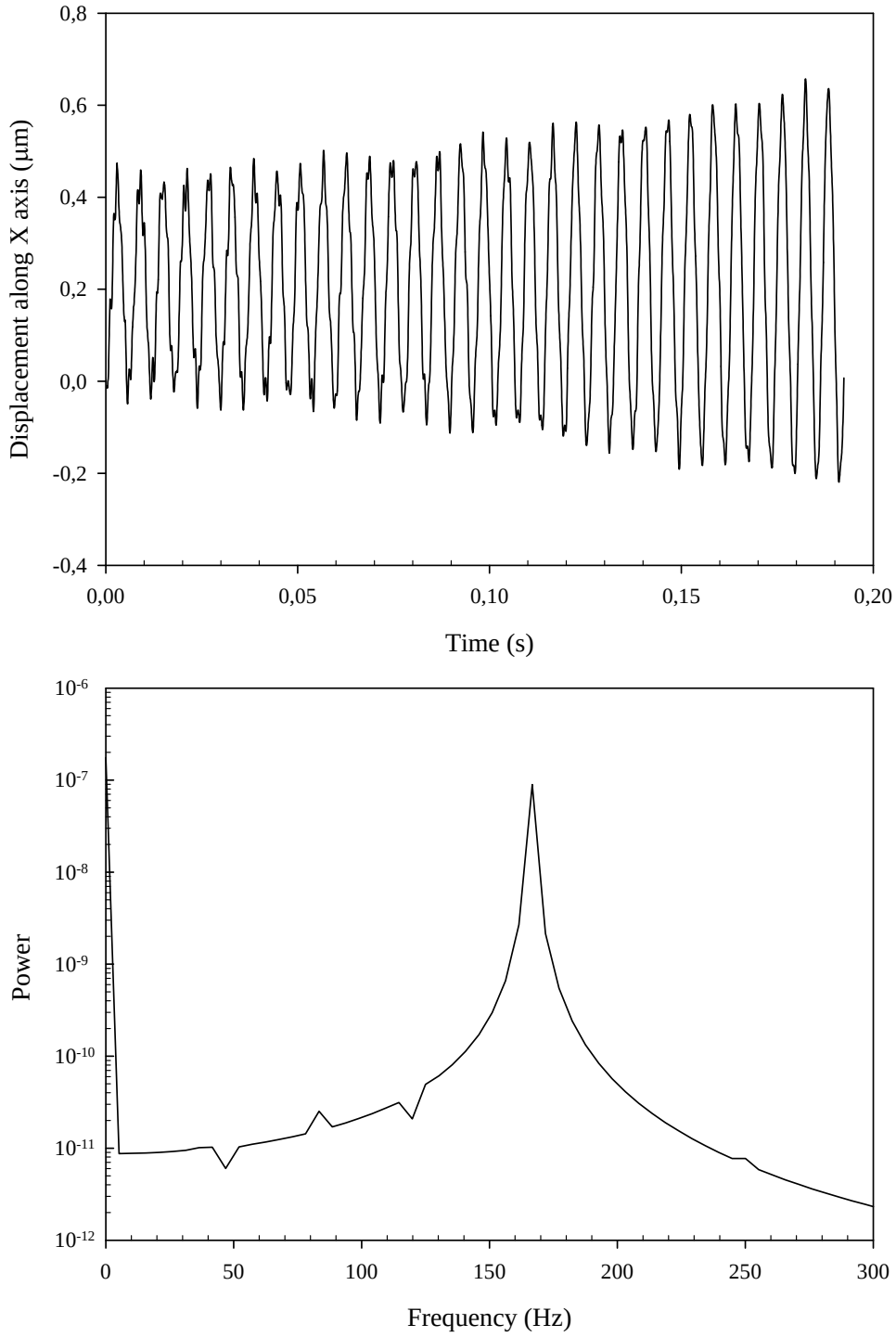

Figure 5.9 Hypothetical system response along X axis for pure angular misalignment (δ=0.0 mm, α=1^o).. Inertia is 0.1I_r. See Appendix 5 for system parameters. a) Displacement b) Frequency spectrum. Simulations are performed with commercial FEM program ANSYS® transient dynamic module and results are plotted with drawing and data analysis software SigmaPlot®.

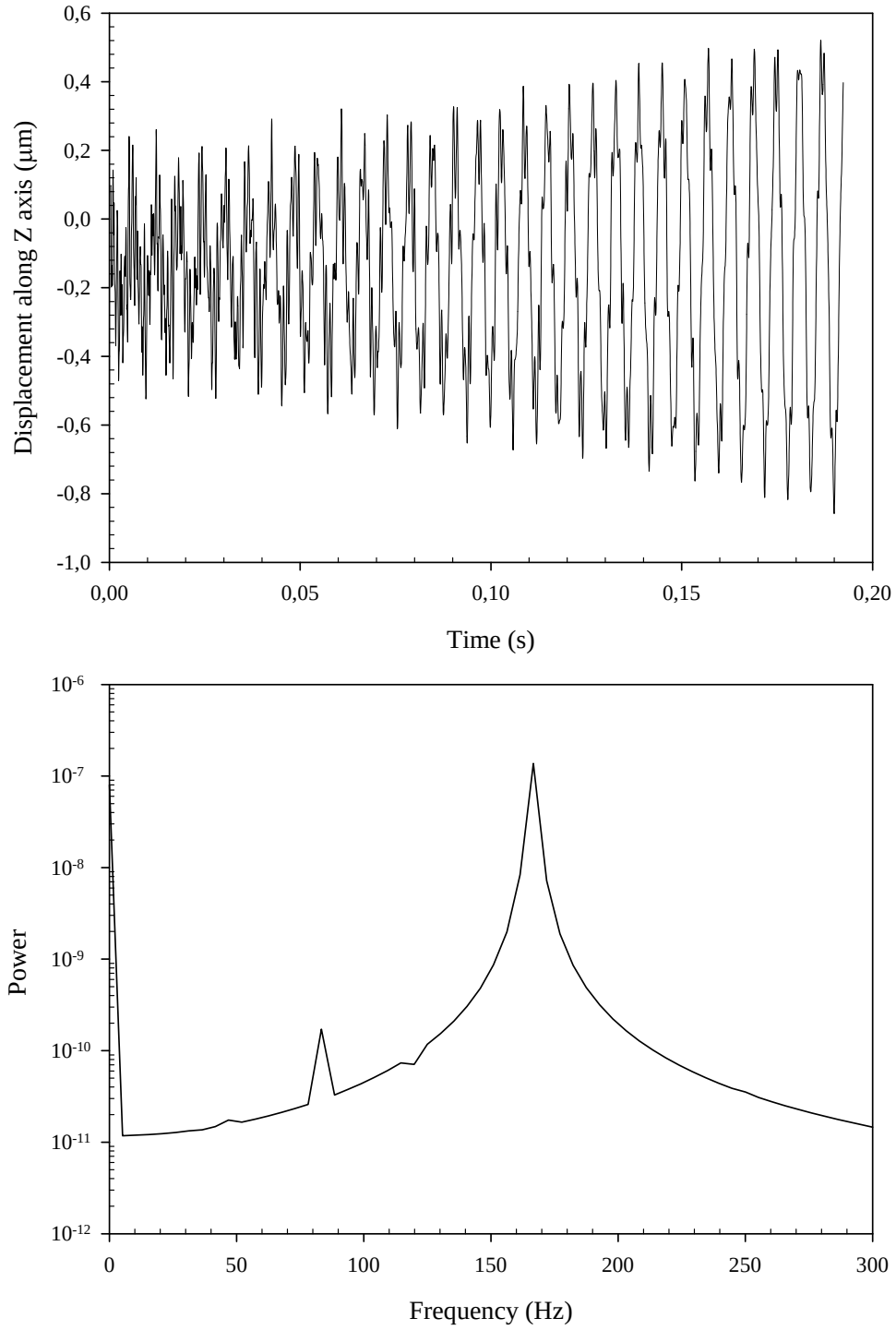

Figure 5.10 Hypothetical system response along Z axis for pure angular misalignment (δ=0.0 mm, α=1^o). Inertia is 0.1I_r. See Appendix 5 for system parameters. a) Displacement b) Frequency spectrum. Simulations are performed with commercial FEM program ANSYS® transient dynamic module and results are plotted with drawing and data analysis software SigmaPlot®.

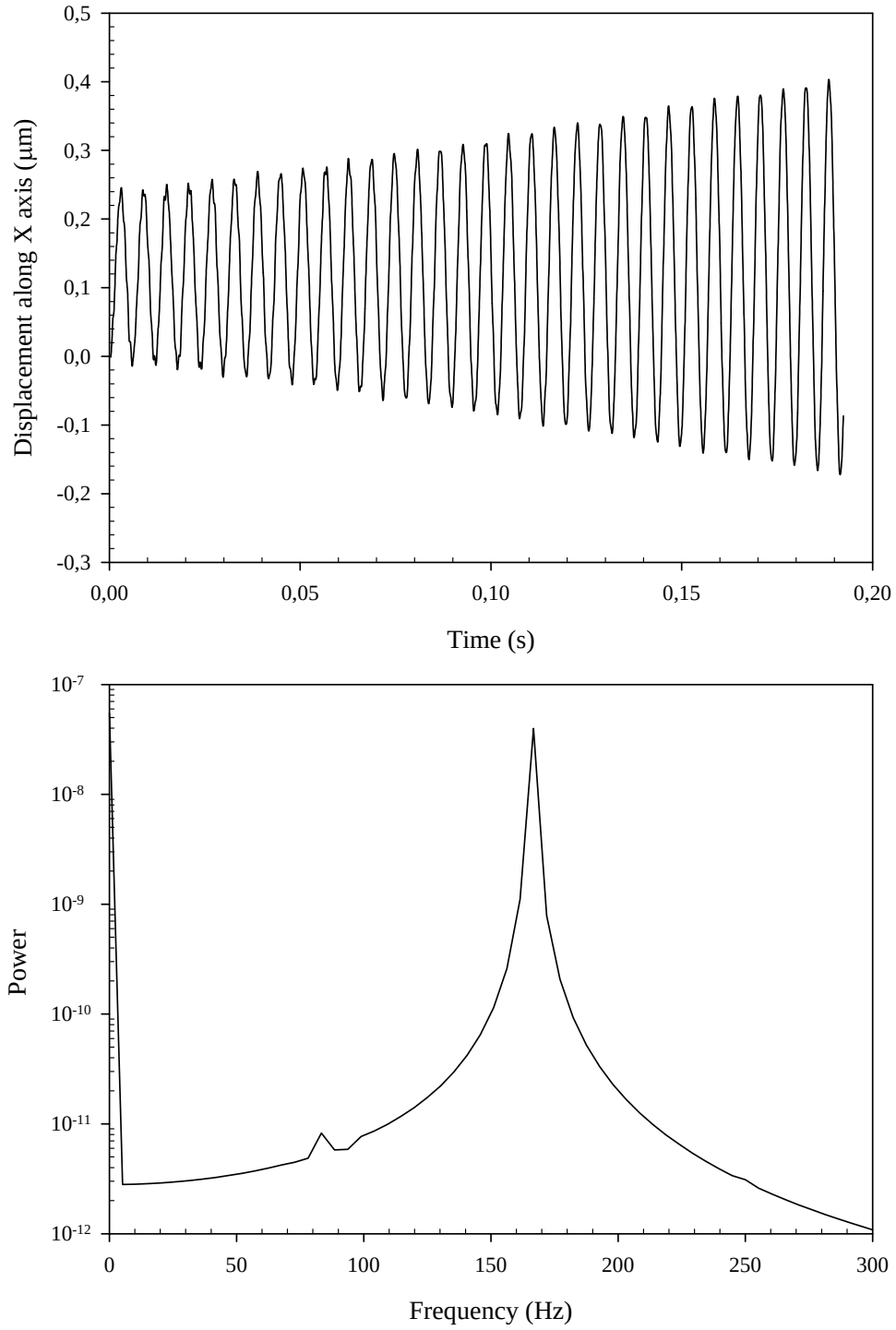

Figure 5.11 Hypothetical system response along X axis for pure angular misalignment (δ=0.0 mm, α=1^o). Inertia is I_r. See Appendix 5 for system parameters. a) Displacement b) Frequency spectrum. Simulations are performed with commercial FEM program ANSYS® transient dynamic module and results are plotted with drawing and data analysis software SigmaPlot®.

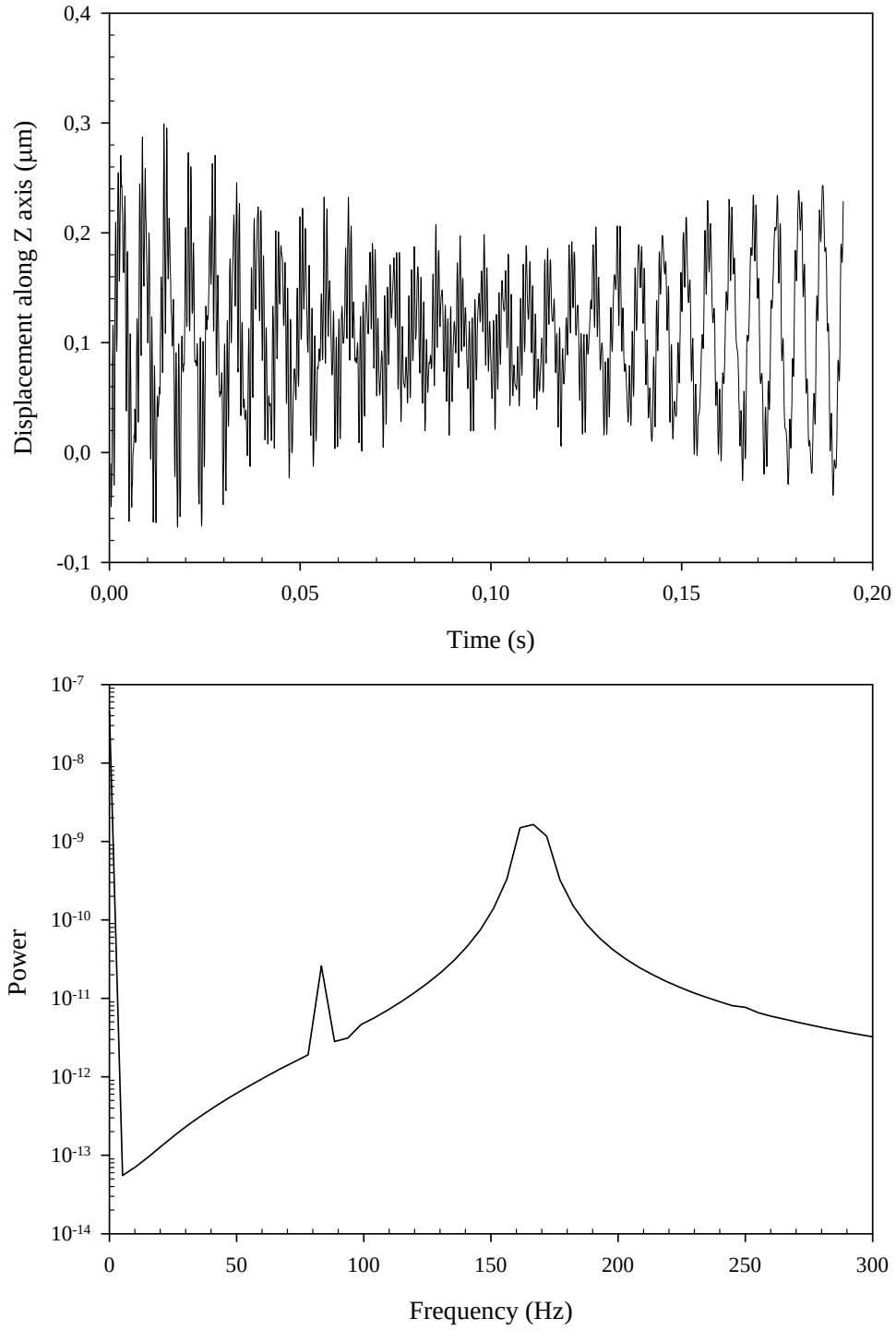

Figure 5.12 Hypothetical system response along Z axis for pure angular misalignment (δ=0.0 mm, α=1^o). Inertia is I_r. See Appendix 5 for system parameters. a) Displacement b) Frequency spectrum. Simulations are performed with commercial FEM program ANSYS® transient dynamic module and results are plotted with drawing and data analysis software SigmaPlot®.

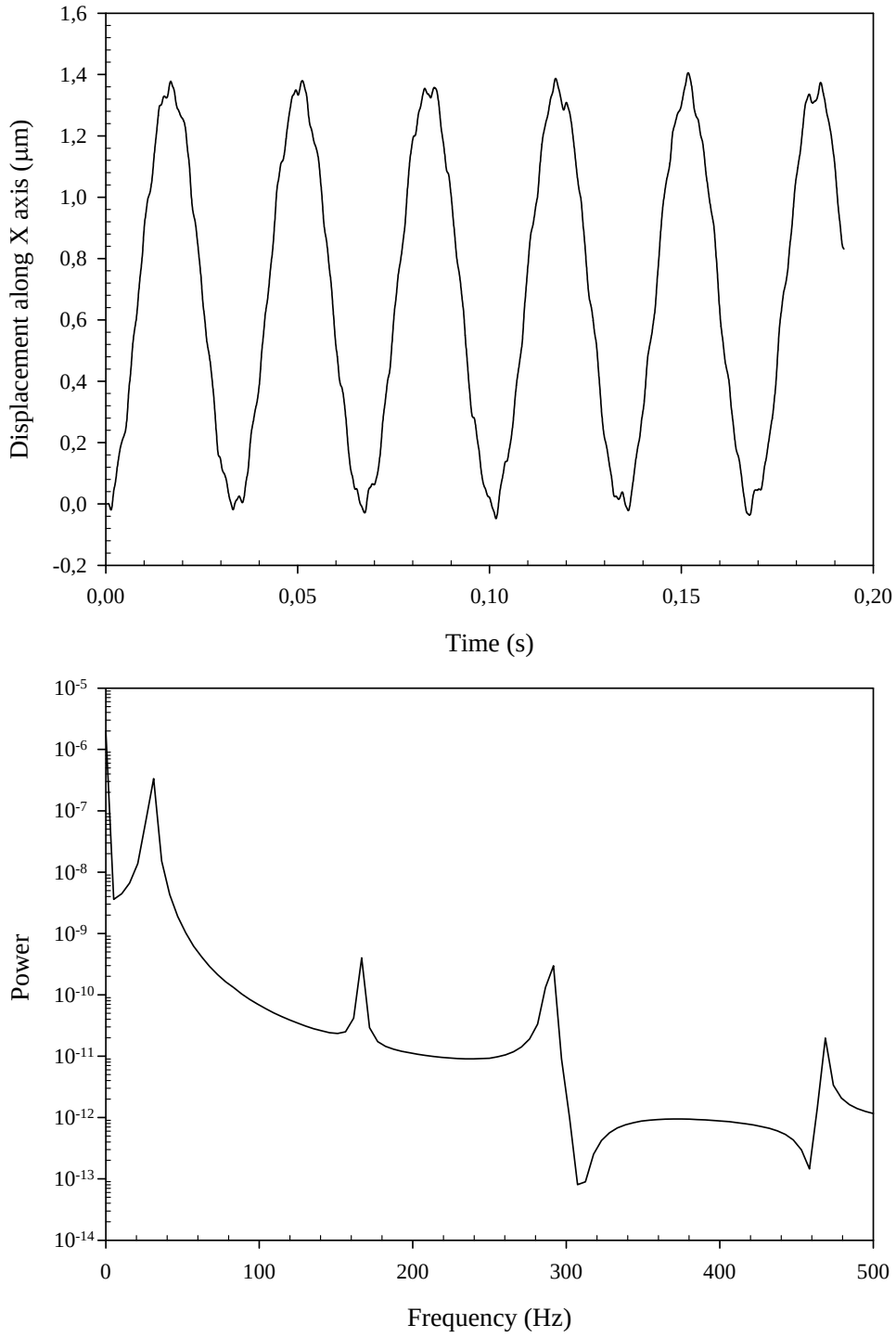

Figure 5.13 Hypothetical system response along X axis for pure angular misalignment (δ=0.0 mm, α=1^o). Inertia is 10I_r. See Appendix 5 for system parameters. a) Displacement b) Frequency spectrum. Simulations are performed with commercial FEM program ANSYS® transient dynamic module and results are plotted with drawing and data analysis software SigmaPlot®.

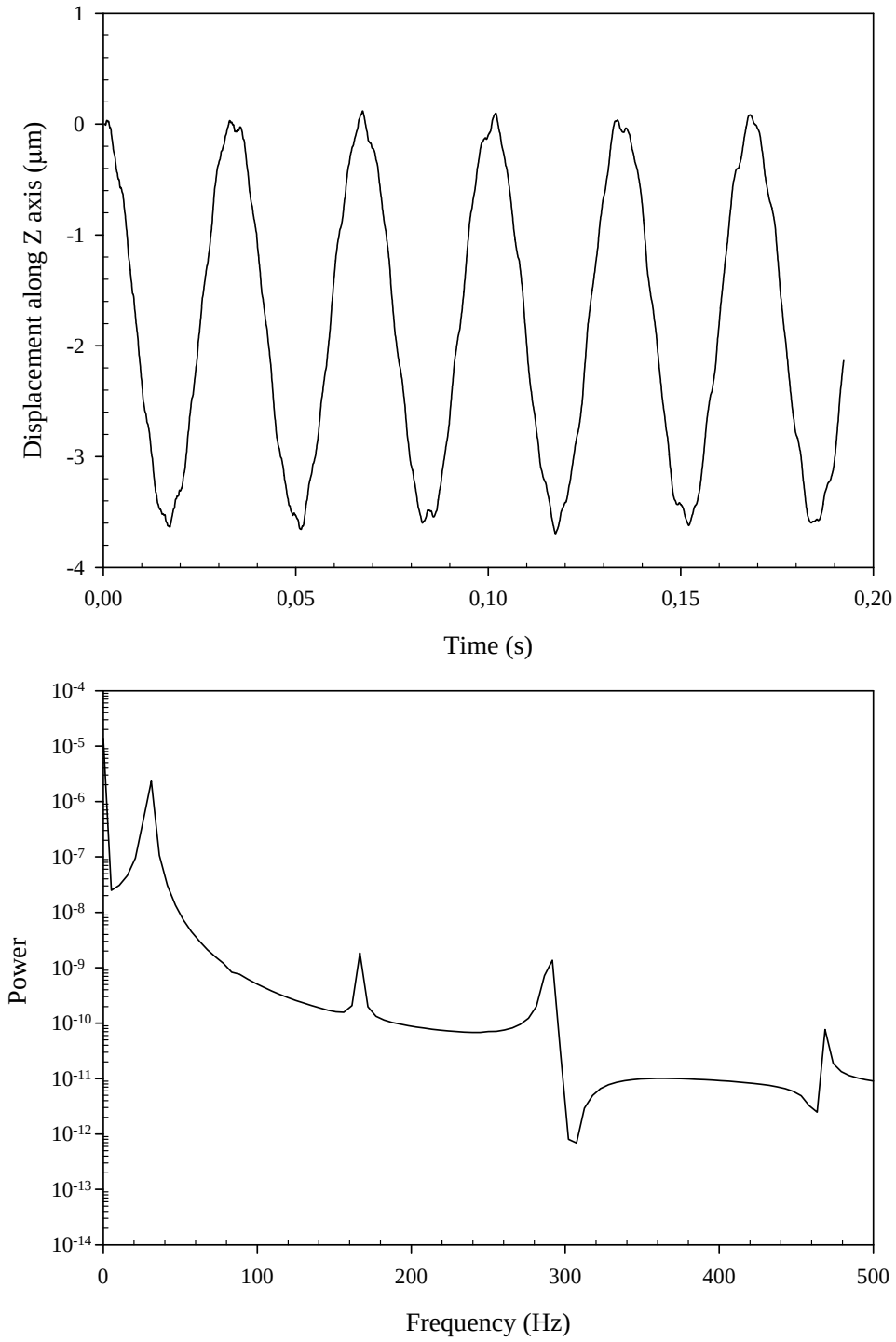

Figure 5.14 Hypothetical system response along Z axis for pure angular misalignment (δ=0.0 mm, $\alpha=1^o$). Inertia is $10I_r$. See Appendix 5 for system parameters. a) Displacement b) Frequency spectrum. Simulations are performed with commercial FEM program ANSYS® transient dynamic module and results are plotted with drawing and data analysis software SigmaPlot®.

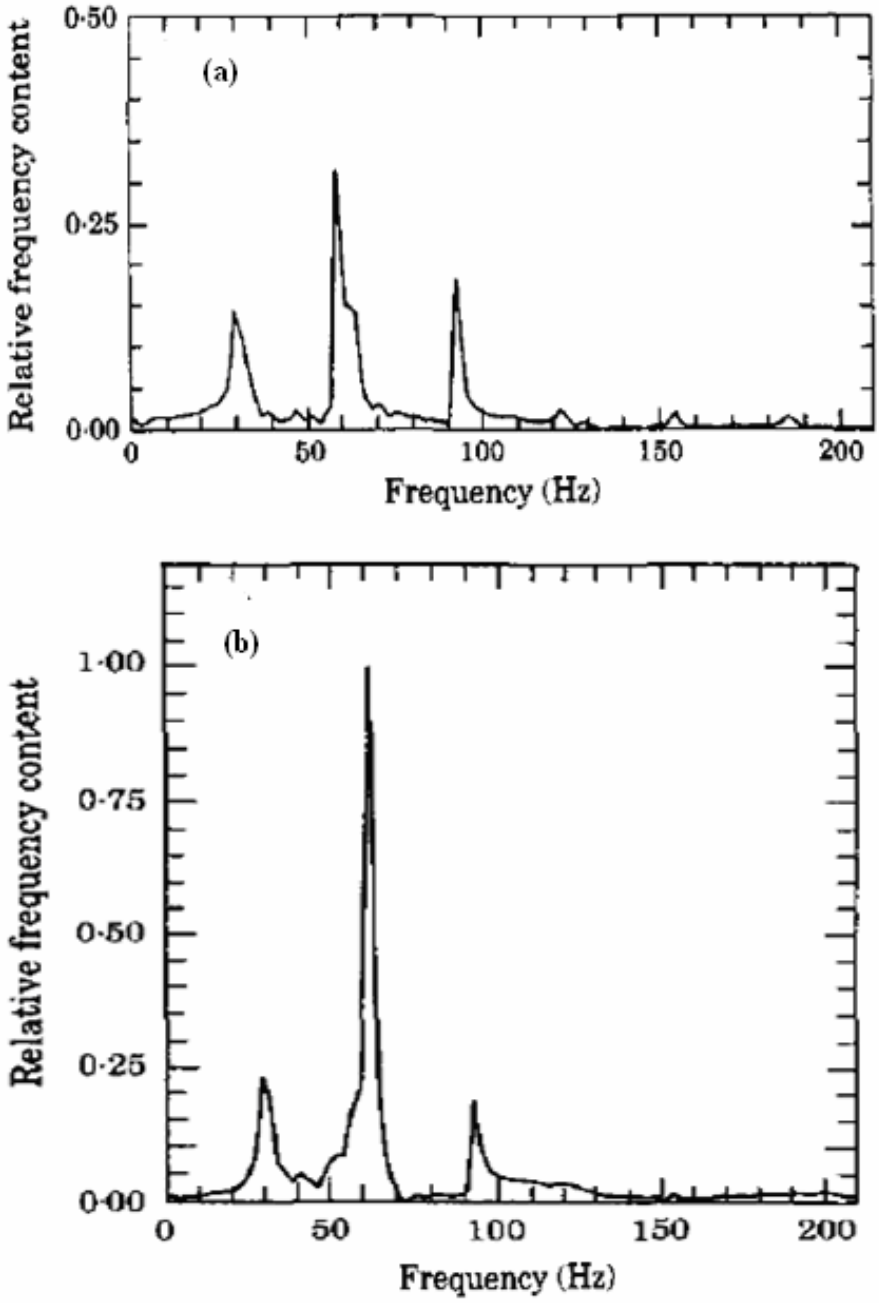

Figure 5.15 Frequency spectrum of (a) aligned (b) misaligned system. Reproduced from Xu and Marangoni, (1994b). Motor rotation speeds are 30.36 Hz and 30.33 Hz, respectively. Misalignment angle is α=0.25^{o}. One of the system natural frequencies is 30 Hz. Relative frequency content is defined as the FFT coefficient divided by the maximum FFT coefficient.

5.4 Parallel Misalignment

Calculations for parallel misalignment is performed for misalignment value of δ=0.25 mm and $\alpha=0^{o}$. Figure 5.16a and Figure 5.17a show the angular velocity and acceleration variations, respectively, of driven shaft for inertia values of $0.1I_r$, I_r and $10I_r$. Figure 5.16b and Figure 5.17b present the frequency spectrums of velocity and acceleration, respectively. As oppose to the angular misalignment, current authors did not come across any information for velocity and acceleration variations in case of parallel misalignment. It can be seen from Figures 5.16 and Figure 5.17 that driven shaft rotation speed thus acceleration also varies for parallel misalignment. It is interesting that angular velocity and acceleration variations exhibit the same pattern as the case for angular misalignment, i.e. large inertia values cause velocity variation diminish and converge to the motor speed. Effect of coupling geometry can be observed with appearance of 1X and 2X components in frequency spectrums for all inertia values. It is also clear from frequency spectrums that third frequency which has the values of 5.21, 10.42 and 36.46 Hz for inertia values of $0.1I_r$, I_r and $10I_r$, respectively is directly dependent on inertia since not only its value but also its power in frequency spectrum decreases with increasing inertia.

Calculated reaction loads generated by deformed coupling in case of parallel misalignment are presented in Figure 5.18a through Figure 5.22a. Frequency spectrums are shown in Figure 5.18b through Figure 5.22b. Initial deformation causes reaction loads to vary around non-zero mean values. Since parallel misalignment is induced along Z-axis mean value of F_z is much higher than that of F_x and F_y. As the case form angular misalignment, reaction loads are dependent on coupling geometry and inertia. Effect of coupling geometry can be observed in power spectrums with appearance of frequency components which are common to all inertia values. Since powers of common frequency components do not change with changing inertia, it can be concluded that variations in these frequencies are solely result of the coupling geometry. Effect of inertia can be observed in frequency spectrums with the appearance of additional frequency components, of which values change with respect to inertia. Since variations of reaction loads in frequencies

resulted from inertial effect diminish with increasing inertia, it can be said that geometry of coupling dominates the system response for large inertia values. Similar to angular misalignment, reaction loads which act along transverse direction (i.e. F_y, M_x and M_z) have common frequency components of 1X, 2X and 3X of motor speed. Reaction load Fx has the common frequency components of 1X and 2X of motor speed. F_x recovers the 1X component for large inertia values. Axial force (F_y) has the common frequency components of 1X and 2X of motor speed.

As mentioned above, 2X component observed along transverse direction is given as the indication of misalignment. It can be seen from Figure 5.18 and Figures 5.20 to 5.22 that twice the motor speed (i.e. 2X component) is the dominant frequency of reaction loads which act along transverse direction. Thus proposed scheme was able to predict frequency component which is associated with parallel misalignment. As the case for angular misalignment, reaction loads are introduced to the above mentioned hypothetical systems and their response in case of parallel misalignment are calculated with commercial finite element program ANSYS. As can be seen from Figure 5.23 through 5.26, 2X component in vibration spectrums obtained for the systems having inertia values of 0.1Ir and Ir dominates the system responses. This result is expected since first natural frequency of system is close to twice the motor speed (i.e. 166.67 Hz). As oppose to the case for angular misalignment, 1X and 3X components are not present in frequency spectrums. However frequency components resulted from smallest inertia value (i.e. 0.1Ir) can be seen in Figures 5.23 and 5.24. System having inertia value of 10Ir has first natural frequency of 29.71Hz. Even if reaction loads for this system have dominant frequency of twice the motor speed, first natural frequency dominates the vibration spectrum obtained along Z-axis (Figure 5.28b). Although dominant frequency for vibration response along X-axis (Figure 5.27b) is, as expected, twice the motor speed first natural frequency can also be seen clearly.

Ganeriwala, Patel & Hartung studied misalignment effect for different coupling types, one of which is helical coupling. They measured vibration data along axial and transverse directions from the sensors which are placed on motor and bearing

housing. Their results obtained for helical coupling in case of parallel misalignment are reproduced in Figure 5.29 for qualitative comparison with present study. Since measurements are taken from bearing housing, reaction forces formed due to parallel misalignment on the point where hypothetical system supposedly have bearing is calculated and qualitative comparison is made based on these forces. Figures 5.30a and 5.31a show the calculated reaction forces which act along the transverse direction. Frequency spectrums are presented in Figures 5.30b and 5.31b. As can be seen form Figures 5.29, 5.30b and 5.31b present study was able to predict the measured frequency components (i.e. 1X and 2X of motor speed) and their orders in magnitude (i.e. power of 2X component is larger than that of 1X component).

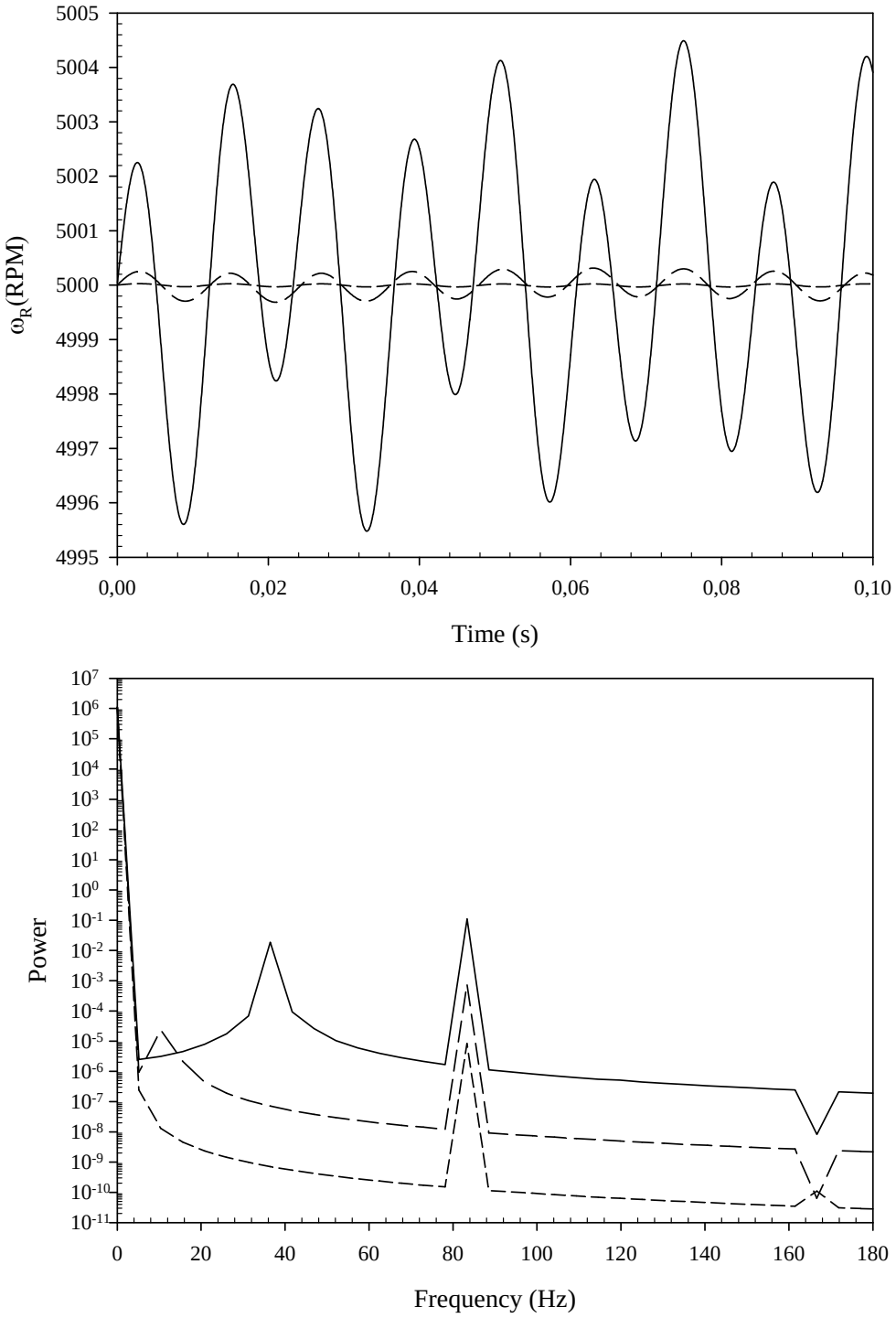

Figure 5.16 (a) Angular velocity variations of rotor and (b) its power spectrum for pure paralel misalignment (δ=0.25 mm, α=0^o). (———— 0.1I_R, — — — — I_R, – – – – – – 10I_R). Simulations are performed with Technical computing program MATLAB® and results are plotted with drawing and data analysis software SigmaPlot®.

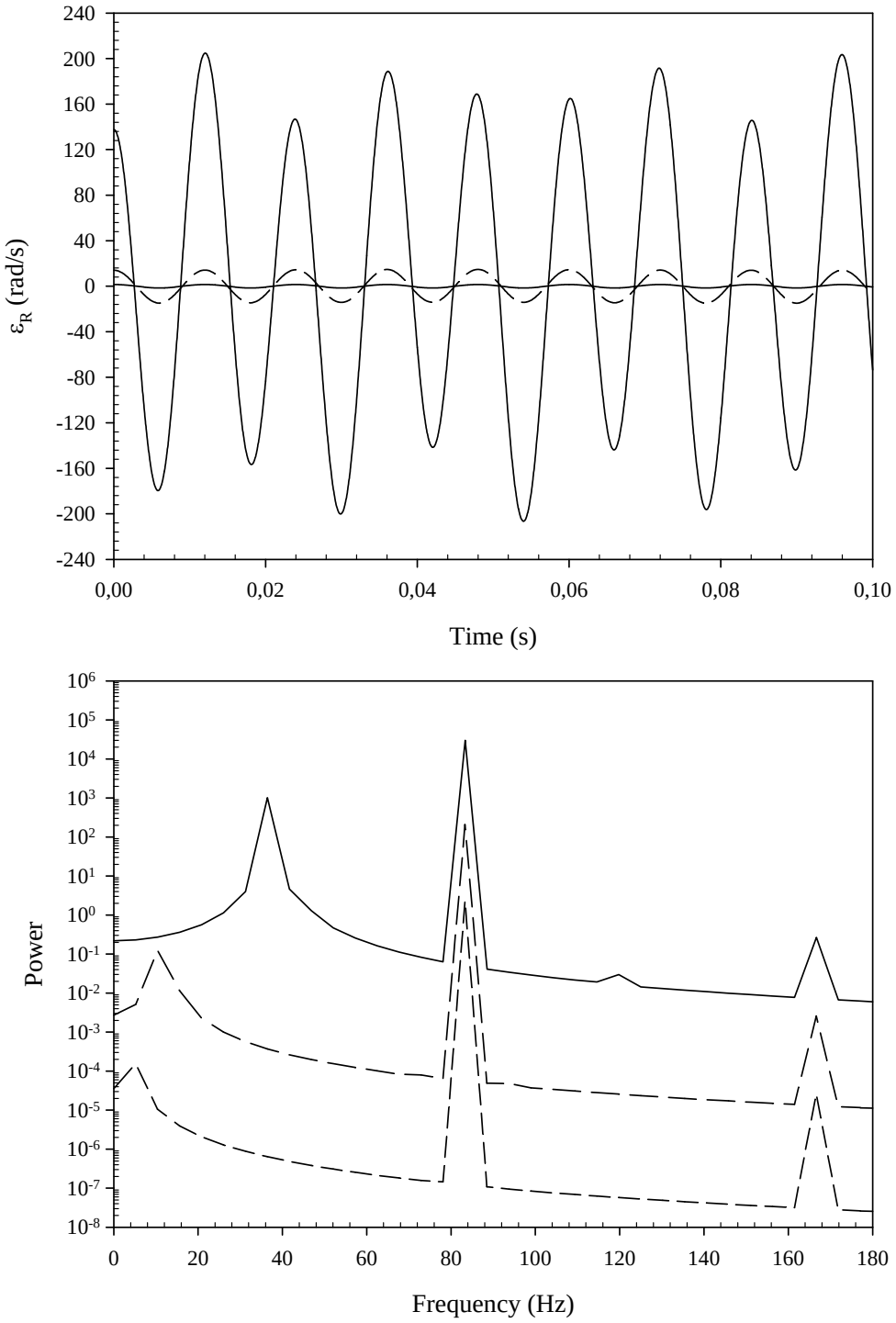

Figure 5.17 (a) Angular acceleration variations of rotor and (b) its power spectrum for pure parallel misalignment (δ=0.25 mm, α=0^o). (———— 0.1I_R, — — — — I_R, – – – – – – 10I_R,). Simulations are performed with Technical computing program MATLAB® and results are plotted with drawing and data analysis software SigmaPlot®.

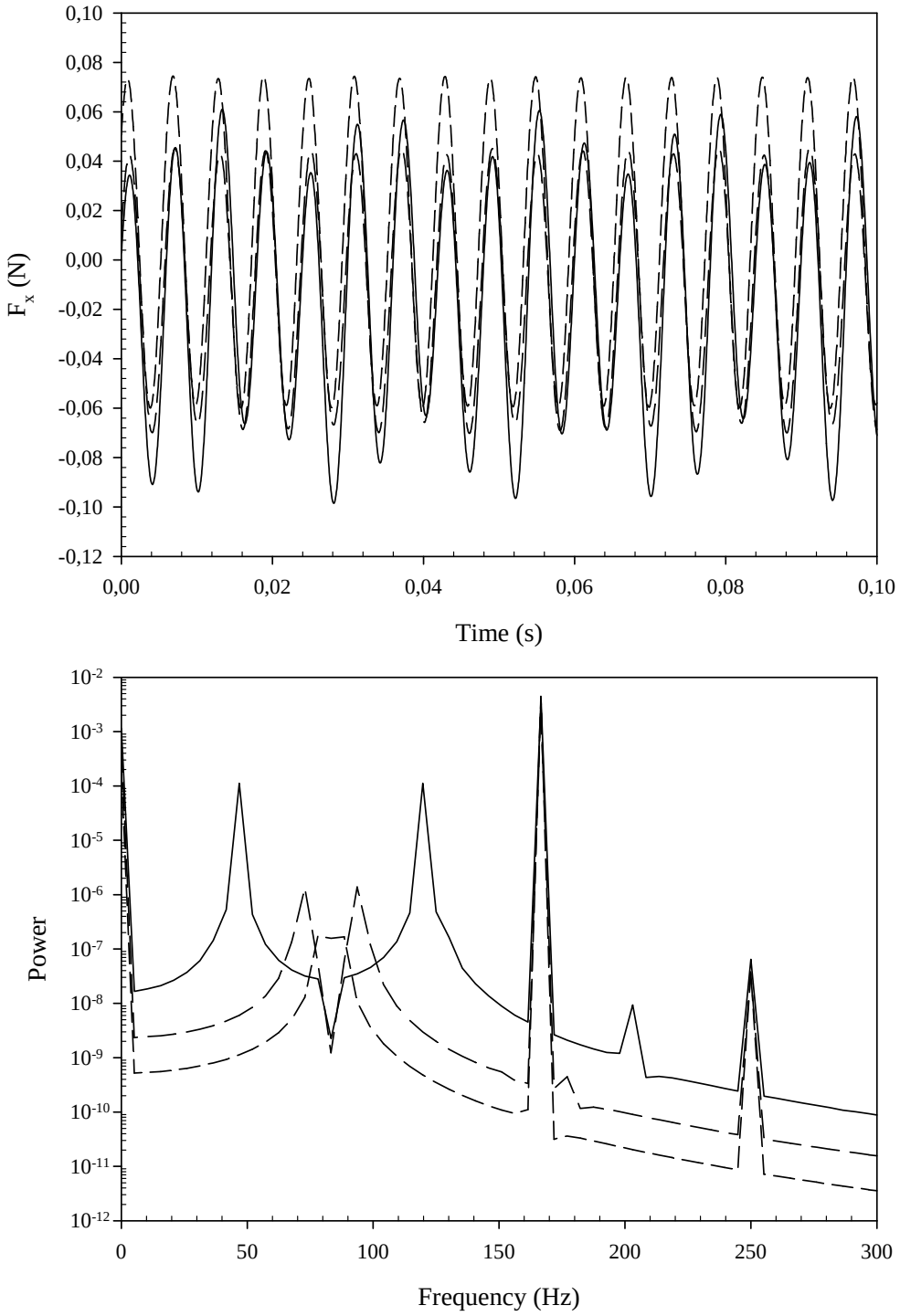

Figure 5.18 (a) Reaction force variation along X-axis (F_x) and (b) its power spectrum for pure parallel misalignment (δ=0.25 mm, $\alpha=0^o$). (———— $0.1I_r$, — — — — I_r, – – – – – – $10I_r$). Simulations are performed with Technical computing program MATLAB® and results are plotted with drawing and data analysis software SigmaPlot®.

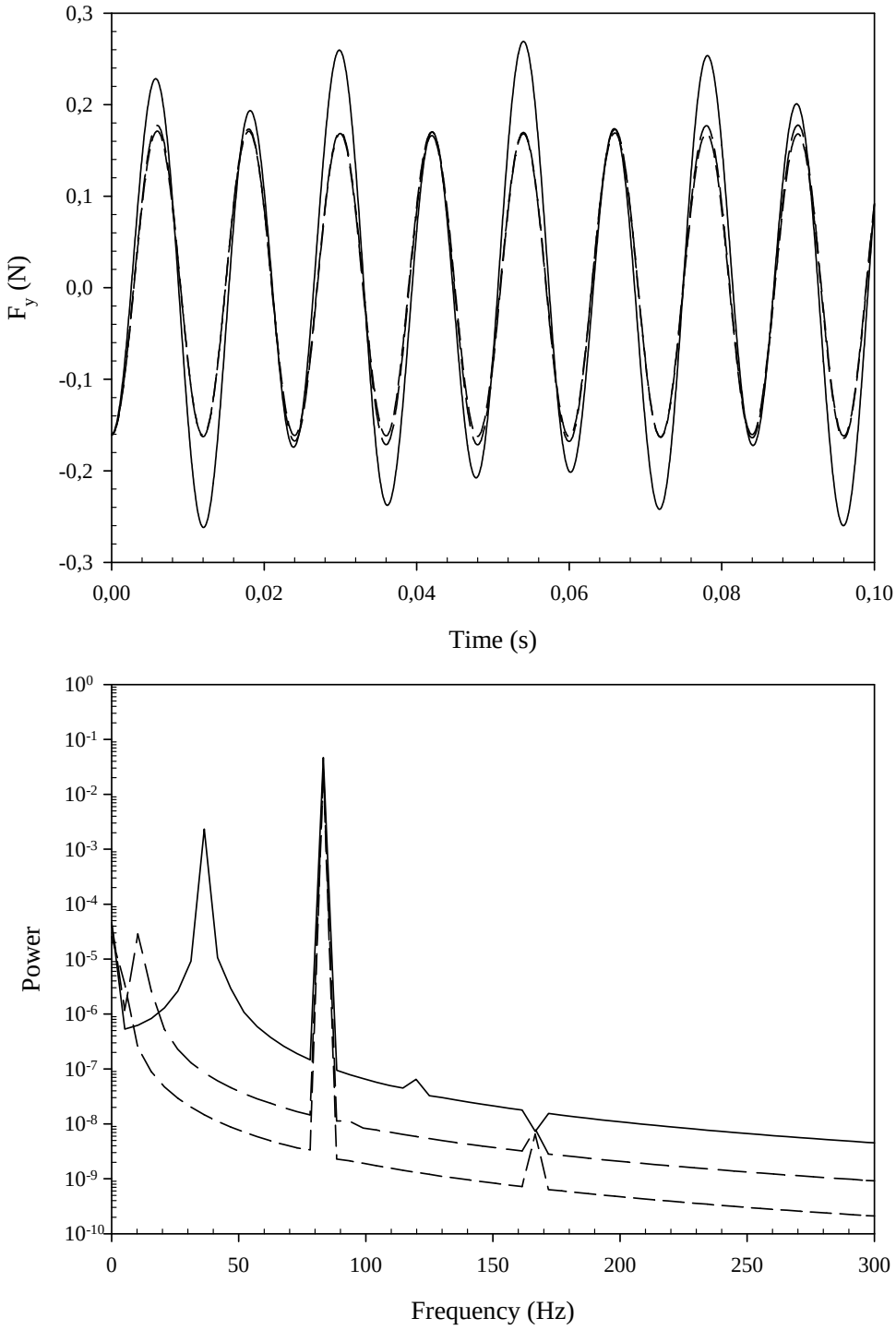

Figure 5.19 (a) Reaction force variation along Y-axis (F_y) and (b) its power spectrum for pure parallel misalignment (δ=0.25 mm, $\alpha=0^o$). (———— $0.1I_r$, — — — — I_r, – – – – – – $10I_r$). Simulations are performed with Technical computing program MATLAB® and results are plotted with drawing and data analysis software SigmaPlot®.

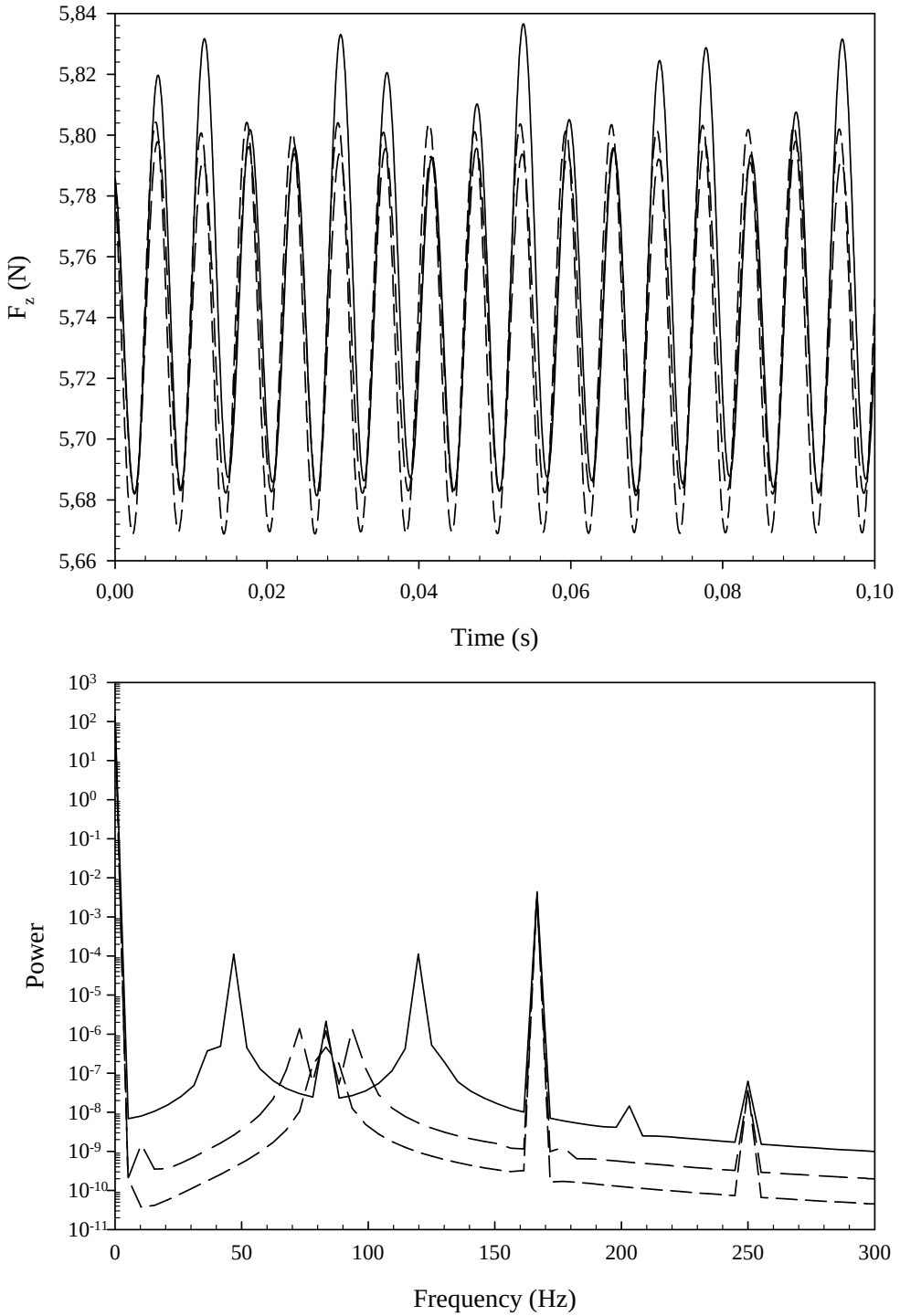

Figure 5.20 (a) Reaction force variation along Z-axis (F_z) and (b) its power spectrum for pure parallel misalignment (δ=0.25 mm, α=0^o). (———— $0.1I_R$, — — — — I_R, – – – – – – $10I_R$). Simulations are performed with Technical computing program MATLAB® and results are plotted with drawing and data analysis software SigmaPlot®.

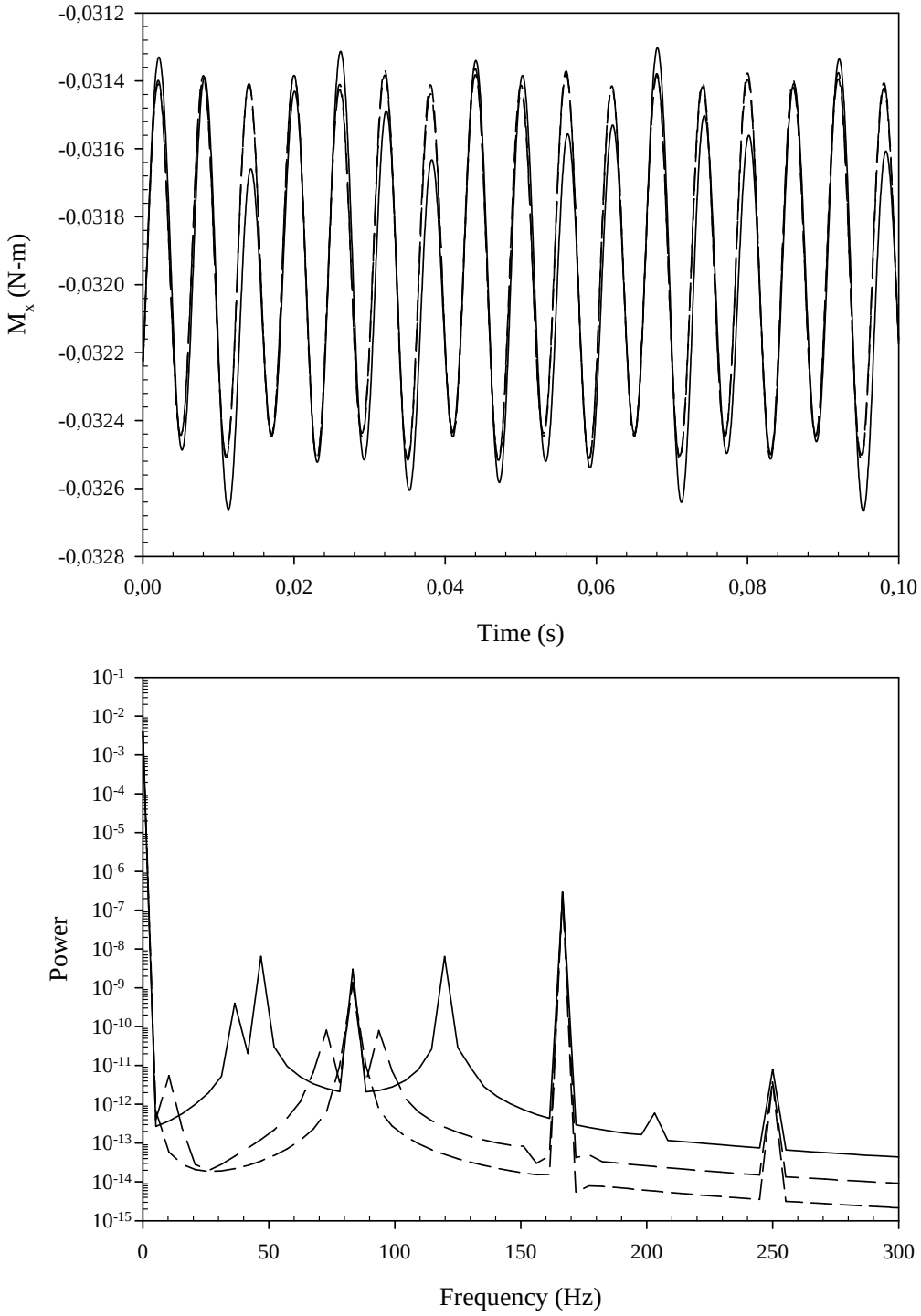

Figure 5.21 (a) Reaction moment variation around X-axis (M_x) and (b) its power spectrum for pure parallel misalignment (δ=0.25 mm, α=0^o). (———— $0.1I_r$, — — — — I_r, – – – – – – $10I_r$). Simulations are performed with Technical computing program MATLAB® and results are plotted with drawing and data analysis software SigmaPlot®.

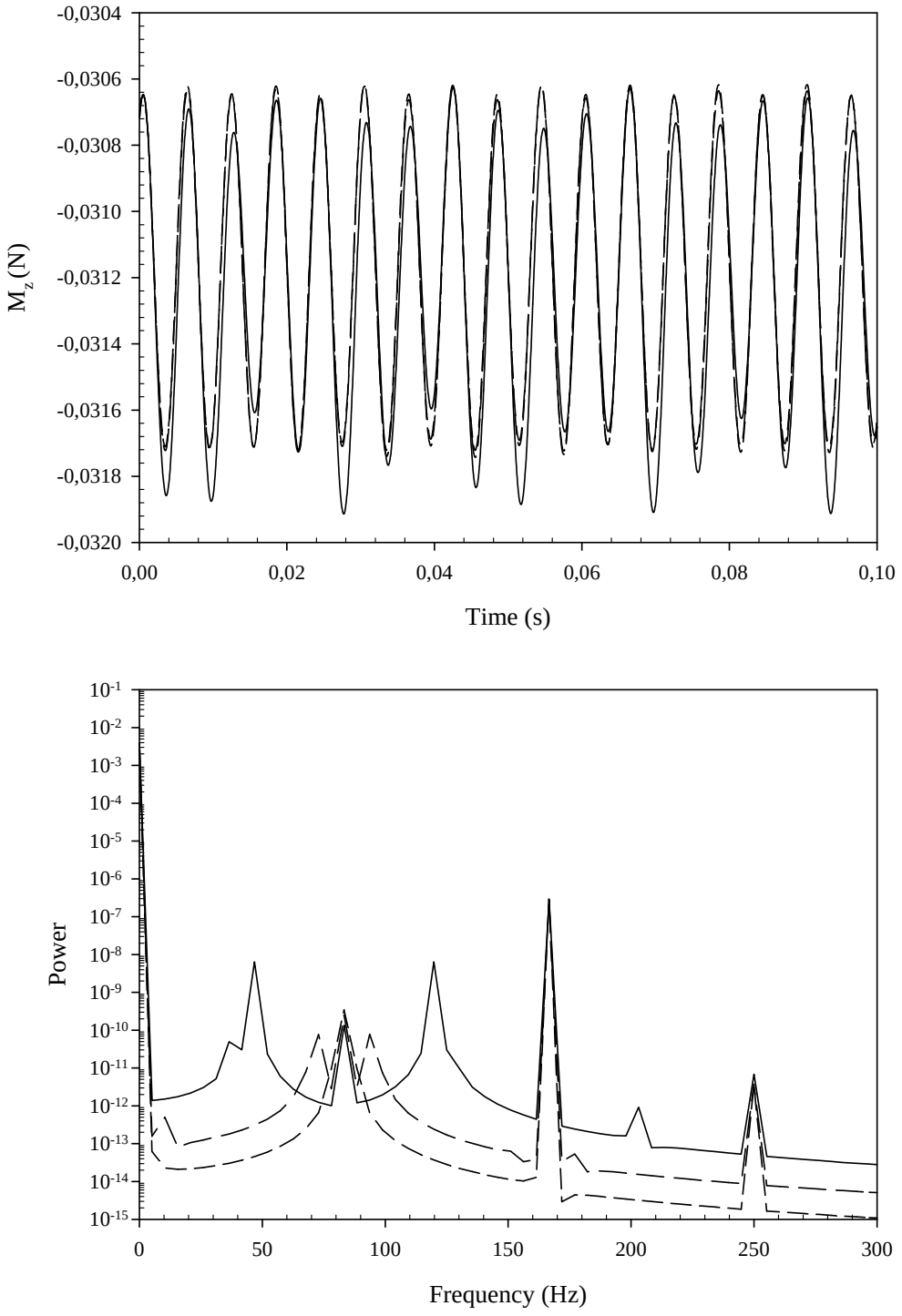

Figure 5.22 (a) Reaction moment variation around Z-axis (M_z) and (b) its power spectrum for pure parallel misalignment (δ=0.25 mm, α=0^o). (———— 0.1I_r, — — — — I_r, – – – – – – 10I_r). Simulations are performed with Technical computing program MATLAB® and results are plotted with drawing and data analysis software SigmaPlot®.

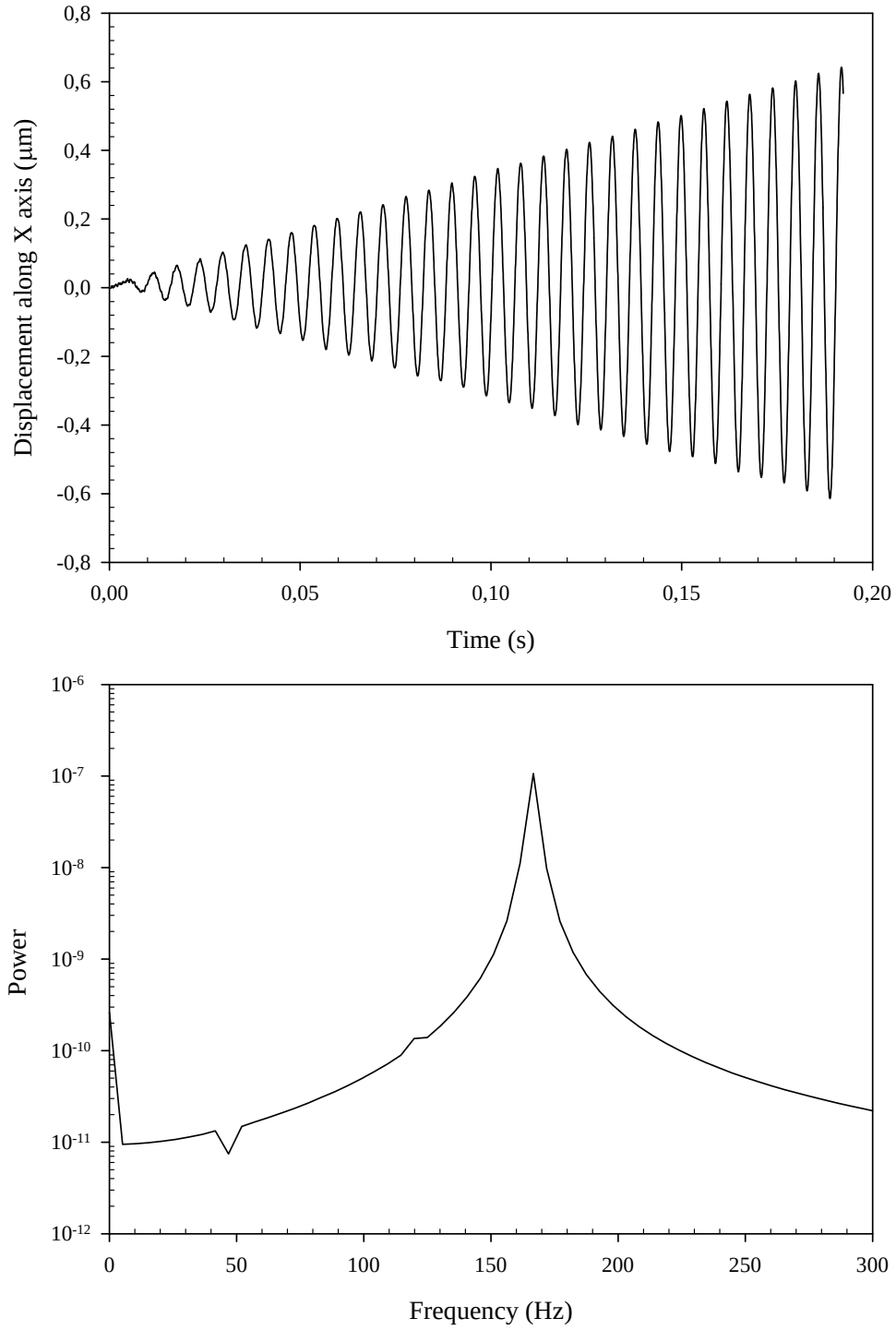

Figure 5.23 Hypothetical system response along X axis for pure parallel misalignment (δ=0.25 mm, α=0^o).. Inertia is 0.1I_r. See Appendix 5 for system parameters. a) Displacement b) Frequency spectrum. Simulations are performed with commercial FEM program ANSYS® transient dynamic module and results are plotted with drawing and data analysis software SigmaPlot®.

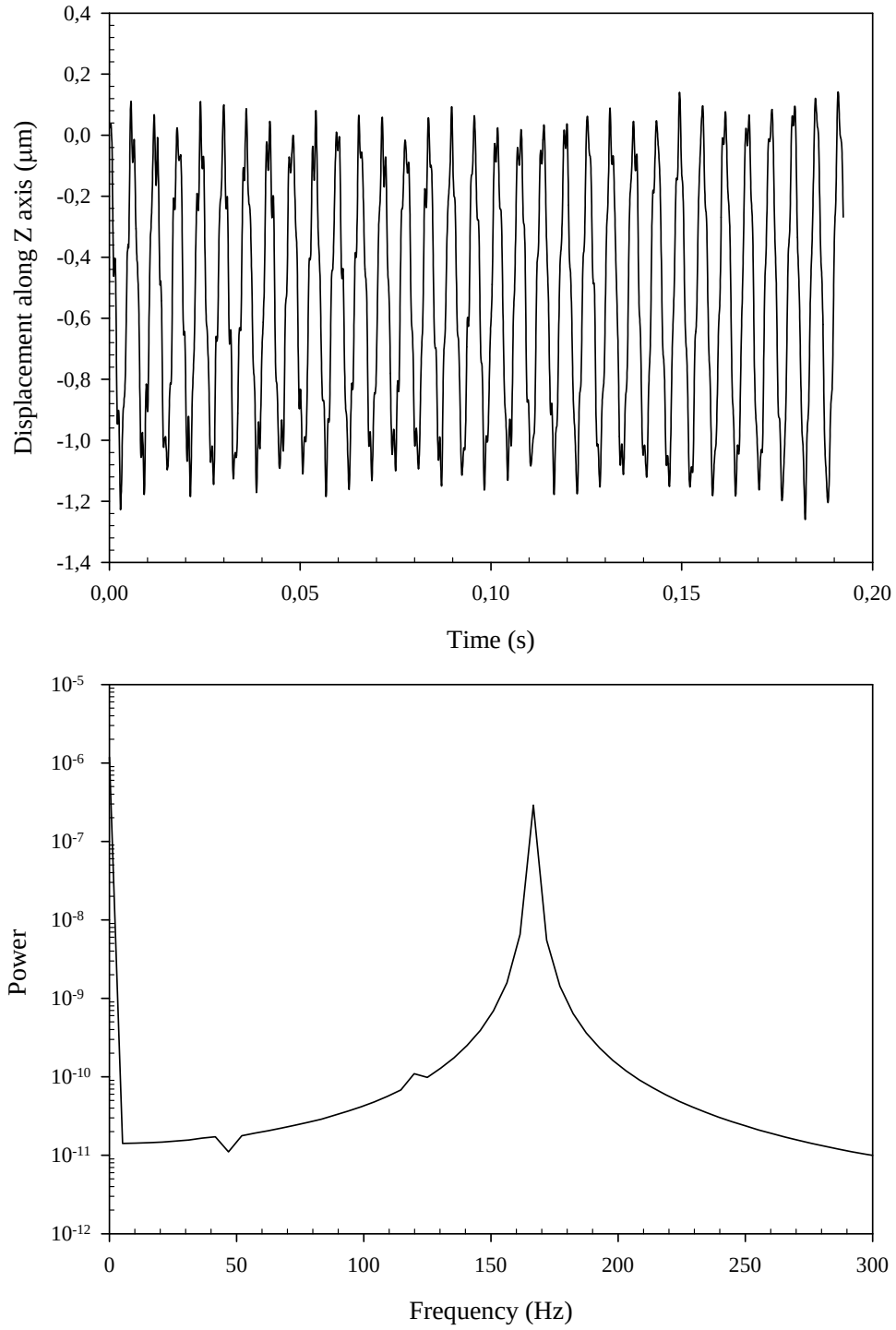

Figure 5.24 Hypothetical system response along Z axis for pure parallel misalignment (δ=0.25 mm, α=0^o). Inertia is 0.1I_r. See Appendix 5 for system parameters. a) Displacement b) Frequency spectrum. Simulations are performed with commercial FEM program ANSYS® transient dynamic module and results are plotted with drawing and data analysis software SigmaPlot®.

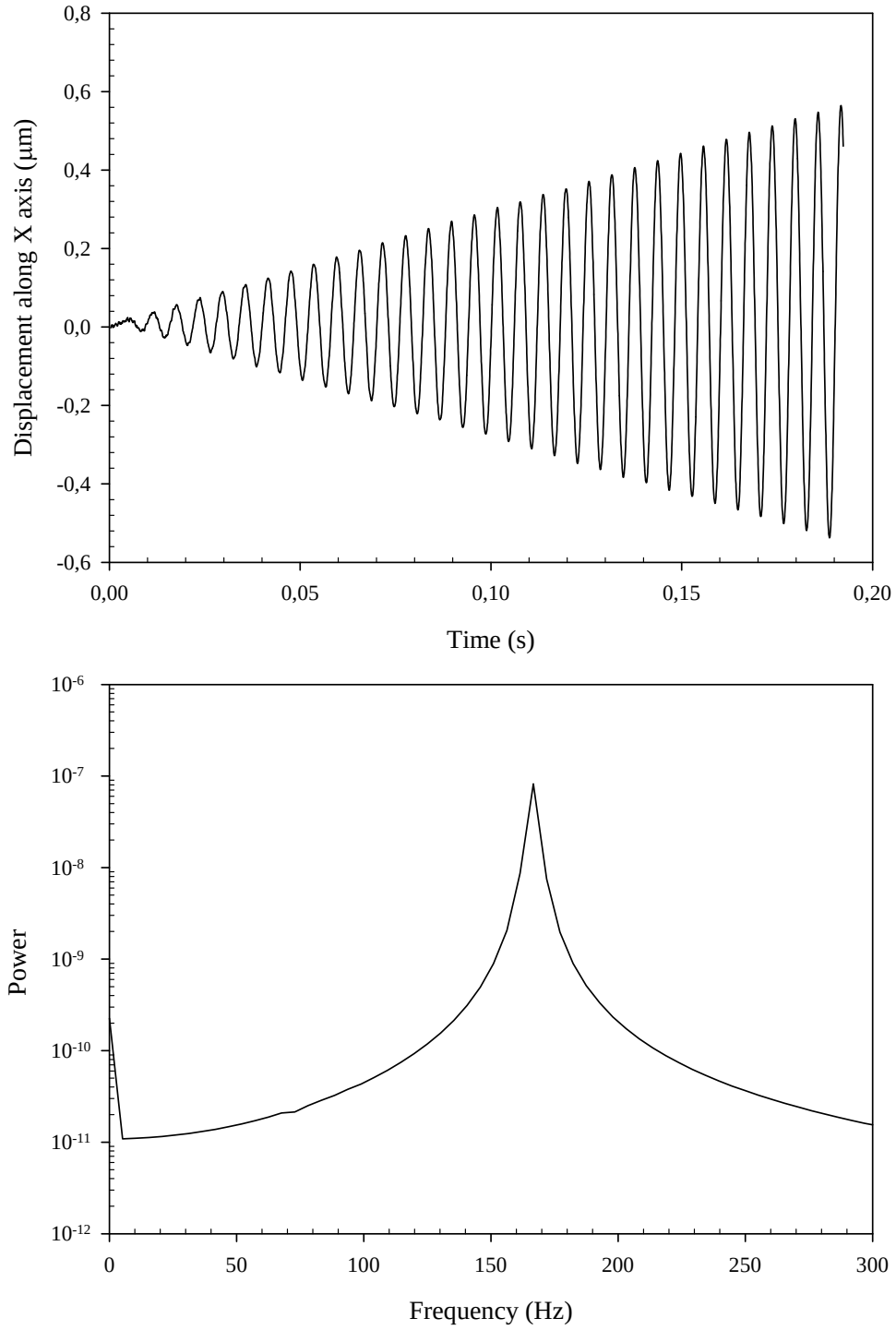

Figure 5.25 Hypothetical system response along X axis for pure parallel misalignment (δ=0.25 mm, $\alpha=0^o$). Inertia is I_r. See Appendix for system parameters. a) Displacement b) Frequency spectrum. Simulations are performed with commercial FEM program ANSYS® transient dynamic module and results are plotted with drawing and data analysis software SigmaPlot®.

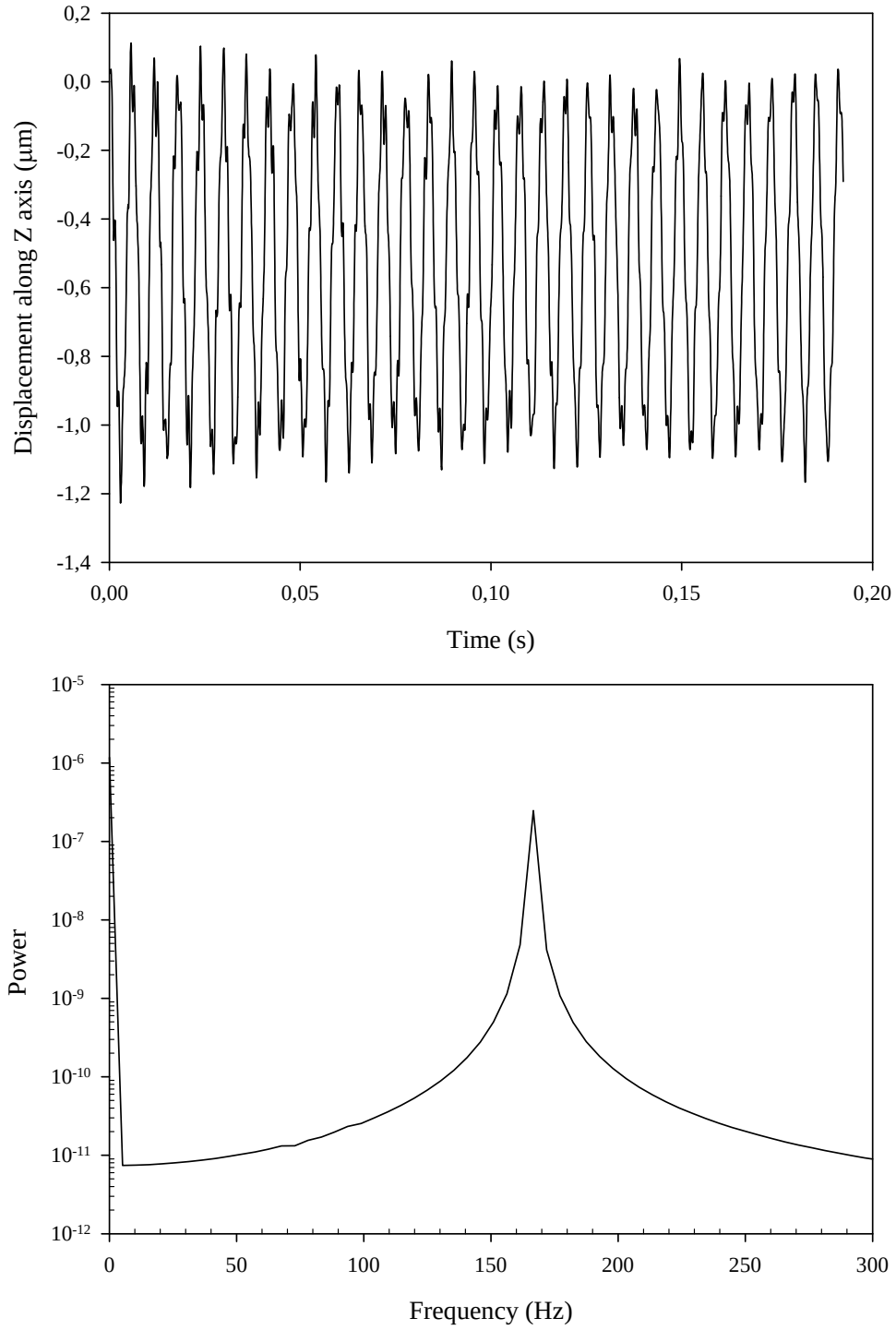

Figure 5.26 Hypothetical system response along Z axis for pure parallel misalignment (δ=0.25 mm, $\alpha=0^o$). Inertia is I_r. See Appendix 5 for system parameters. a) Displacement b) Frequency spectrum. Simulations are performed with commercial FEM program ANSYS® transient dynamic module and results are plotted with drawing and data analysis software SigmaPlot®.

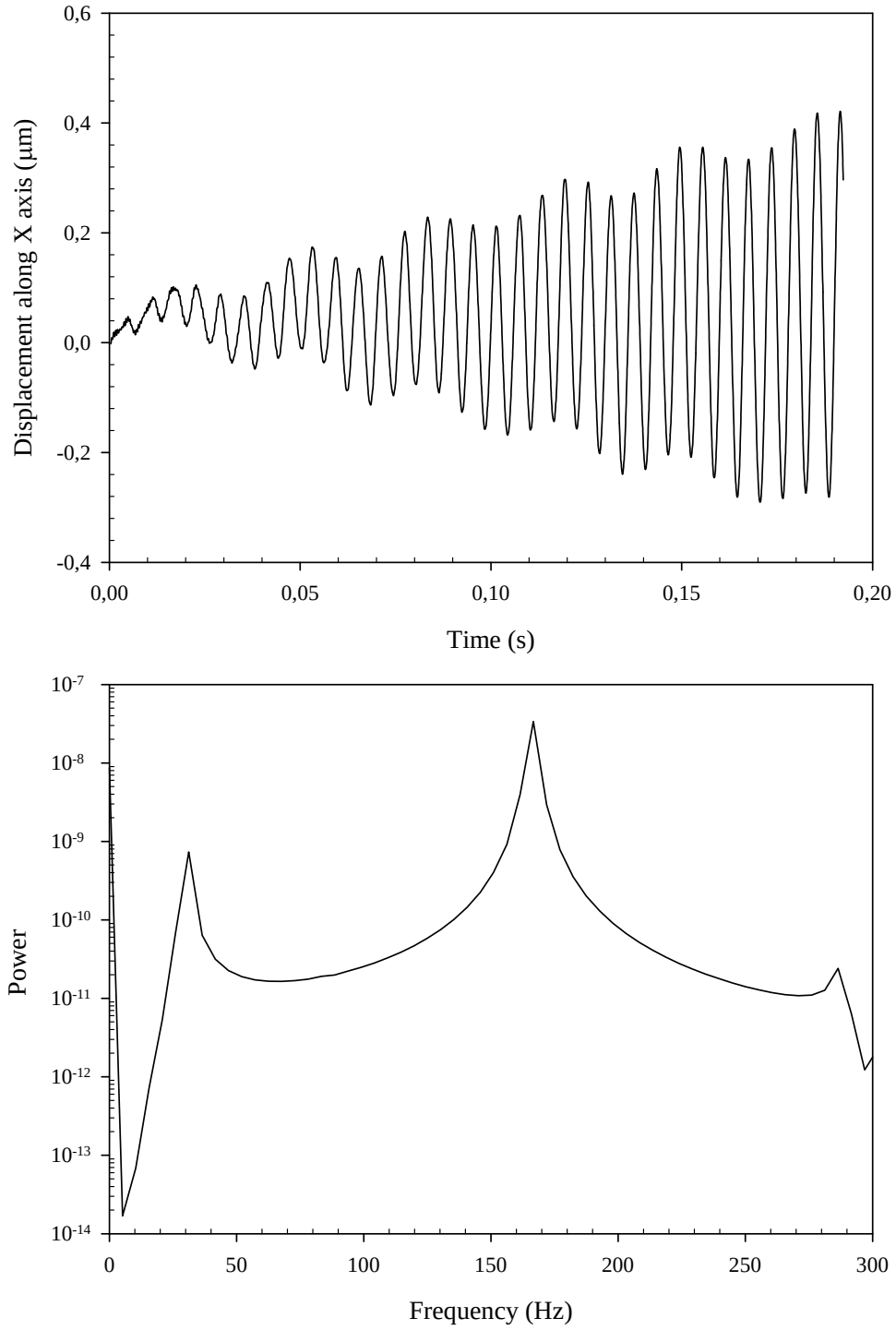

Figure 5.27 Hypothetical system response along X axis for pure parallel misalignment (δ=0.25 mm, α=0^o). Inertia is 10I_r. See Appendix 5 for system parameters. a) Displacement b) Frequency spectrum. Simulations are performed with commercial FEM program ANSYS® transient dynamic module and results are plotted with drawing and data analysis software SigmaPlot®.

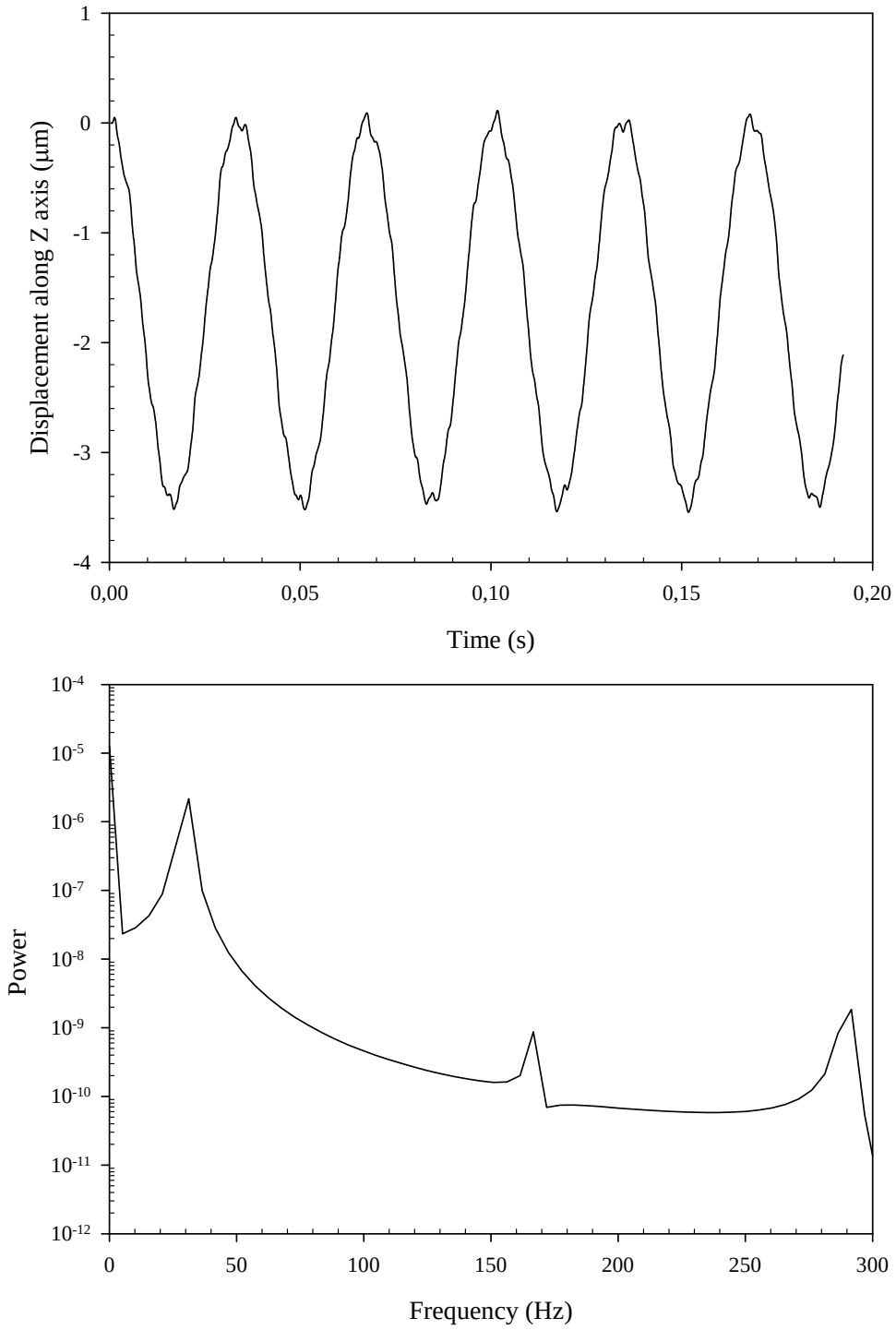

Figure 5.28 Hypothetical system response along Z axis for pure parallel misalignment (δ=0.25 mm, $\alpha=0^o$). Inertia is $10I_r$. See Appendix 5 for system parameters. a) Displacement b) Frequency spectrum. Simulations are performed with commercial FEM program ANSYS® transient dynamic module and results are plotted with drawing and data analysis software SigmaPlot®.

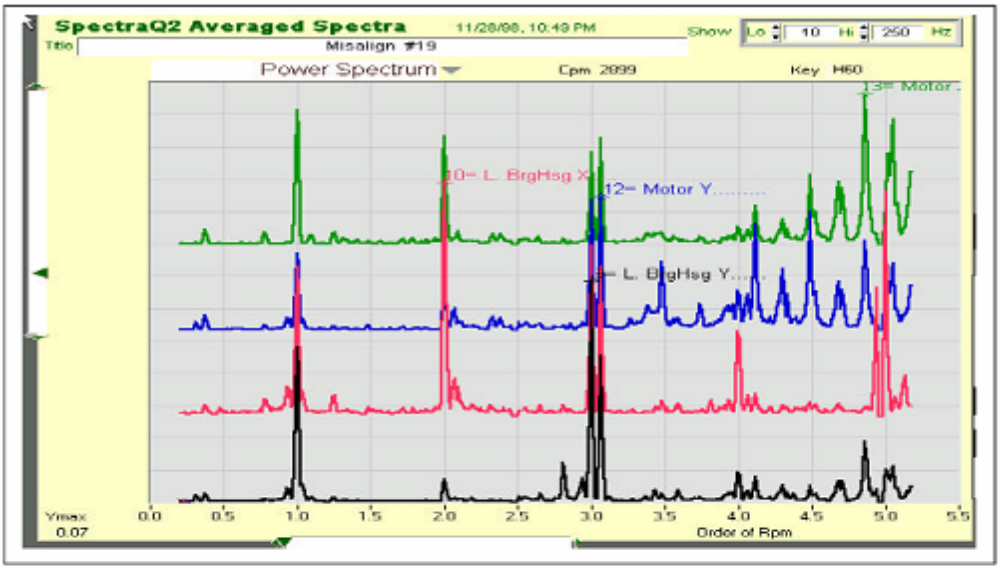

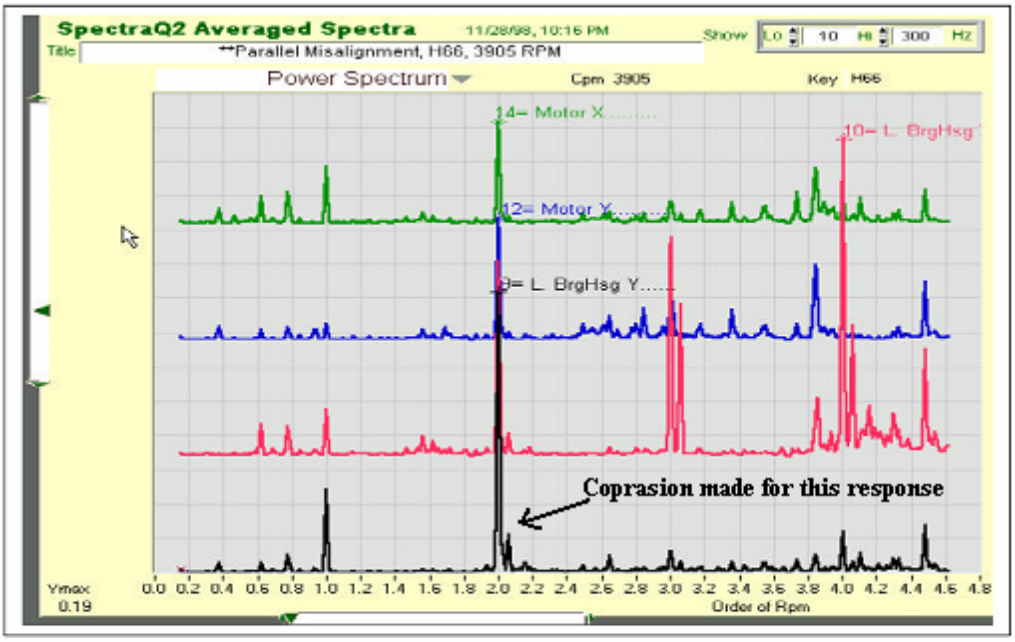

Figure 2. Comparisons of Vibration Spectra of the Left Bearing Housing and the Motor in vertical and axial directions of the Misaligned MFS with Helical Coupling at Two Different Speeds. The graphs illustrate the effect of speed on the spectra. At higher speed amplitude increases and the peak shows at 2X. The frequency scale is displayed as Order of RPM. Graphs are shifted vertically to clarify the differences. The vertical scale is 0.2 G's per block.

Figure 5.29 Frequency spectrum of Ganeriwala, Patel & Hartung

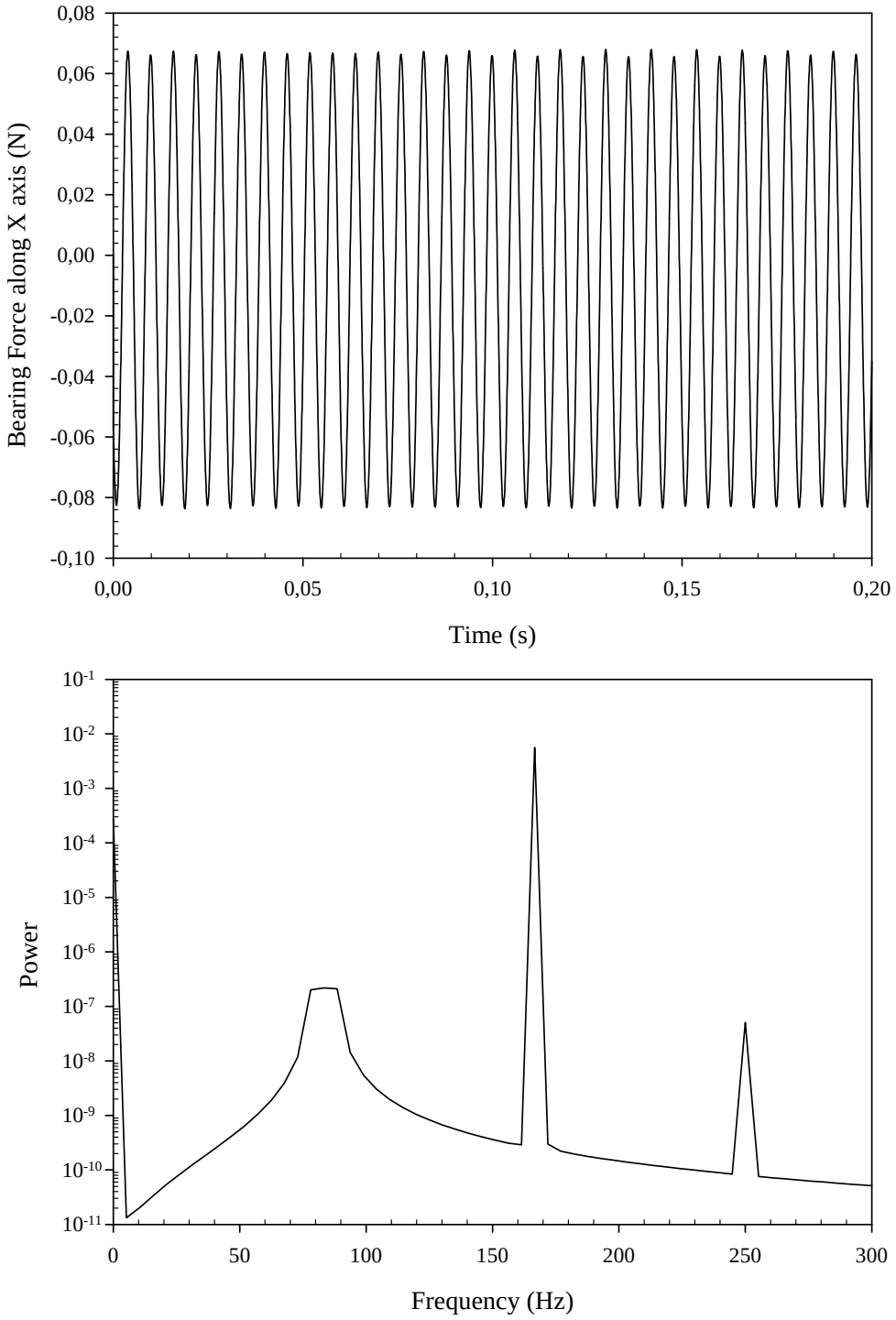

Figure 5.30 (a) Bearing reaction force along Z-axis for hypothetical system having inertia values of $10I_r$ (b) its power spectrum. Simulations are performed with commercial FEM program ANSYS® transient dynamic module and results are plotted with drawing and data analysis software SigmaPlot®.

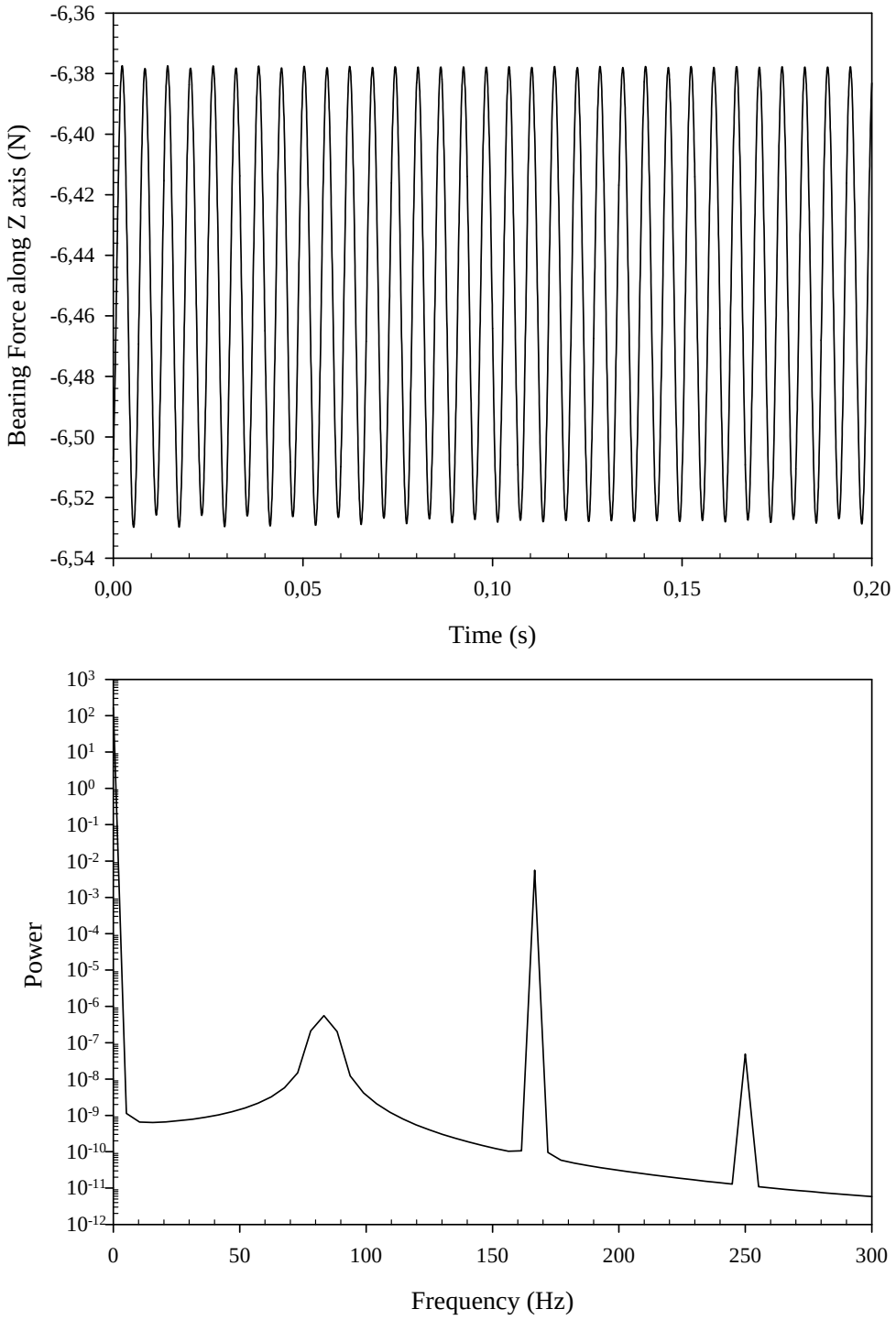

Figure 5.31 (a) Bearing reaction force along Z-axis for hypothetical system having inertia values of $10I_r$ (b) its power spectrum. Simulations are performed with commercial FEM program ANSYS® transient dynamic module and results are plotted with drawing and data analysis software SigmaPlot®.

CHAPTER SIX
CONCLUSION

Helical coupling is modeled with geometrically exact beam theory in order to investigate its behavior in case of misalignment. New scheme based on using constitutive equations as constraint was developed. Since geometrically exact beam theory is capable of modeling finite rotations and finite strains, proposed scheme was able to calculate the misaligned coupling behavior without any *a priori* assumptions. Comparison with previous results showed that proposed scheme was able to predict the frequency components associated with misalignment. Moreover calculated reaction loads' frequency components matched frequency components of vibration spectrums obtained experimentally from motor-helical coupling-rotor systems. Thus it is concluded that proposed scheme could model the rotating coupling accurately.

In previous studies, it was assumed that angularly misaligned coupling behaves exactly as universal joint. Thus driven shaft speed varies with frequency of twice the motor speed. Our results showed that driven shaft speed varies not only for the case of angular misalignment but also for the case of misalignment. Results indicated that driven shaft velocity was dependent of inertia value and geometry of coupling. Velocity variation diminished with increasing inertia and converged to driving shaft speed. Lighter inertia caused rotor speed to vary largely and resulted in observable frequency component in speed variation. Results obtained for angularly misaligned coupling contradicted universal joint assumption.

As the case for velocity variation, results showed that reaction loads generated by misaligned coupling on system depended on inertia value and coupling geometry. Calculation indicated that reaction load components resulted from coupling geometry do not change for changing inertia. However reaction load components due to inertia effect decrease with increasing inertia.

As mentioned above complexity of modeling misaligned system is the main obstacle to draw the necessary academic attentions. However proposed method could

give new perspective to the researchers who study this phenomenon. Since proposed method does not require any a priori assumptions for the rotating coupling behavior, response of the misaligned system could be calculated more accurately.

REFERENCES

Bathe, K. J. (1996). *Finite Element Procedures*. Prentice-Hall, Inc.

Dewel, D. L. & Mitchell, L. D. (1984). Detection of a misaligned disk coupling using spectrum analysis. *American Society of Mechanical Engineers Journal of Vibration, Acoustics, Stress, and Reliability in Design* 106, 9-15.

Dominick, J. & Larocque, T. (1999). Vibration monitoring at Weirton Steel. Retrieved December, 12 2006, from *www.ctconline.com/pdf/WEIRTON.PDF***.**

Ganeriwala, S., Patel, S. & Hartung, H. A. (1999). Truth behind misalignment vibration spectra of rotating machinery. *Proceedings of the International Modal Analysis Conference – IMAC, v 2*, 2078-2085.

Goldstein, H. (1980) *Classical Mechanics* (2nd ed.). Addison-Wesley, MA.

Ibrahimbegovic, A. ,Frey, F. & Kozar, I. (1995). Computational aspects of vector-like parameterization of three-dimensional finite rotations. *International Journal of Numerical Methods in Engineering* 38, 3653-3673.

Ibrahimbegovic, A. & Mikad, M. A. (1998). Finite rotations in dynamics of beams and implicit time-stepping schemes. *International Journal of Numerical Methods in Engineering* 41, 781-814.

Lee, S. Y. & Lee, C. W. (1999). Modeling and vibration analysis of misaligned rotor-ball bearing system *Journal of Sound and Vibration* 224, 17-32.

Piotrowski, J. (1995) *Shaft Alignment Handbook* (2nd ed). Marcel Dekker Inc., New York - Basel- Hong Kong.

Saavedra, P. N. & Ramirez, D. E. (2004a). Vibration analysis of rotors for the identification of shaft misalignment Part 1: theoretical analysis. *Proc. Instn. Mech. Engrs., IMechE Part C* 218, 971-985.

Saavedra, P. N. & Ramirez, D. E. (2004b). Vibration analysis of rotors for the identification of shaft misalignment Part 2: experimental validation. *Proc. Instn. Mech. Engrs., IMechE Part C* 218, 987-999.

Sekhar, A. S. & Prabhu, B. S. (1995). Effects of coupling misalignment on vibrations of rotating machinery. *Journal of Sound and Vibration* 185, 655-671.

Simo, J. C. (1985). A Finite strain beam formulation. The three-dimensional dynamic problem. Part I. *Computer Methods in Applied Mechanics and Engineering* 49, 55-70.

Xu, M. & Marangoni, R. D. (1994a). Vibration analysis of a motor-flexible coupling- rotor system subject to misalignment and unbalance, Part I: theoretical model and analysis. *Journal of Sound and Vibration* 176, 663-679.

Xu, M. & Marangoni, R. D. (1994b). Vibration analysis of a motor-flexible coupling- rotor system subject to misalignment and unbalance, Part II: experimental validation. *Journal of Sound and Vibration* 176**,** 681-691.

APPENDICES

APPENDIX 1

LINEARIZED VIRTUAL WORK EQUATION

In order to alleviate notation, the subscript '**n+1**' (denoting that the variable is evaluated at time $\mathbf{t_{n+1}}$) and superscript '**i**' (denoting the iteration counter) are dropped.

The first term on the right side in Equation (3.128) give rise residual:

$$\int_S \left(\boldsymbol{L}_\delta(\boldsymbol{\gamma})\cdot\mathbf{n}+\boldsymbol{L}_\delta(\boldsymbol{\omega})\cdot\mathbf{m}\right)\mathrm{ds}=\int_S\begin{bmatrix}\delta\boldsymbol{\varphi}'\\ \delta\boldsymbol{\theta}\\ \delta\boldsymbol{\theta}'\end{bmatrix}^{\mathrm{T}}[\mathbf{R}]\ \mathrm{ds}$$

where

$$[\mathbf{R}]=\begin{bmatrix}\mathbf{I}_{3x3} & (\boldsymbol{\varphi}'\times)\cdot\tilde{\mathbf{T}}(\boldsymbol{\theta}) & \mathbf{0}\\ \mathbf{0} & \mathbf{R}+(\boldsymbol{\omega}'\times)\cdot\tilde{\mathbf{T}}(\boldsymbol{\theta}) & \tilde{\mathbf{T}}(\boldsymbol{\theta})\end{bmatrix}^{\mathrm{T}}\begin{bmatrix}\mathbf{n}^{\varphi}\\ \mathbf{m}^{\varphi}\end{bmatrix}$$

The second and third terms on the right side in Equation (3.128) lead to material and geometric parts of the stiffness matrix, respectively:

$$\int_S\left(\boldsymbol{L}_\delta(\boldsymbol{\gamma})\cdot\boldsymbol{L}_\Delta\left(\mathbf{n}^{\varphi}\right)+\mathrm{L}_\delta(\boldsymbol{\omega})\cdot\boldsymbol{L}_\Delta\left(\mathbf{m}^{\varphi}\right)\right)\mathrm{ds}=\int_S\begin{bmatrix}\delta\boldsymbol{\varphi}'\\ \delta\boldsymbol{\theta}\\ \delta\boldsymbol{\theta}'\end{bmatrix}^{\mathrm{T}}\left[\mathbf{K}^{\mathrm{M}}\right]\begin{bmatrix}\Delta\boldsymbol{\varphi}'\\ \Delta\boldsymbol{\theta}\\ \Delta\boldsymbol{\theta}'\end{bmatrix}\ \mathrm{ds}$$

where

$$\left[\mathbf{K}^{\mathrm{M}}\right]=\begin{bmatrix}\mathbf{I}_{3\times3} & (\boldsymbol{\varphi}'\times)\cdot\tilde{\mathbf{T}}(\boldsymbol{\theta}) & \mathbf{0}\\ \mathbf{0} & \mathbf{R}+(\boldsymbol{\omega}'\times)\cdot\tilde{\mathbf{T}}(\boldsymbol{\theta}) & \tilde{\mathbf{T}}(\boldsymbol{\theta})\end{bmatrix}^{\mathbf{T}}\begin{bmatrix}\boldsymbol{\Lambda}^{\mathrm{T}}\mathbf{C}_{\mathbf{n}}\boldsymbol{\Lambda} & \mathbf{0}\\ \mathbf{0} & \boldsymbol{\Lambda}^{\mathrm{T}}\mathbf{C}_{\mathbf{m}}\boldsymbol{\Lambda}\end{bmatrix}\begin{bmatrix}\mathbf{I}_{3\times3} & (\boldsymbol{\varphi}'\times)\cdot\tilde{\mathbf{T}}(\boldsymbol{\theta}) & \mathbf{0}\\ \mathbf{0} & \mathbf{R}+(\boldsymbol{\omega}\times)\cdot\tilde{\mathbf{T}}(\boldsymbol{\theta}) & \tilde{\mathbf{T}}(\boldsymbol{\theta})\end{bmatrix}$$

and

$$\int_S\left(\boldsymbol{L}_\Delta\left(\boldsymbol{L}_\delta(\boldsymbol{\gamma})\right)\cdot\mathbf{n}+\boldsymbol{L}_\Delta\left(\boldsymbol{L}_\delta(\boldsymbol{\omega})\right)\cdot\mathbf{m}\right)\mathrm{ds}=\int_S\begin{bmatrix}\delta\boldsymbol{\varphi}'\\ \delta\boldsymbol{\theta}\\ \delta\boldsymbol{\theta}'\end{bmatrix}^{\mathrm{T}}\left[\mathbf{K}_1^{\mathrm{G}}+\mathbf{K}_2^{\mathrm{G}}\right]\begin{bmatrix}\Delta\boldsymbol{\varphi}'\\ \Delta\boldsymbol{\theta}\\ \Delta\boldsymbol{\theta}'\end{bmatrix}\ \mathrm{ds}$$

where

$$\left[\mathbf{K}_1^{\mathrm{G}}\right]=\begin{bmatrix}\mathbf{0} & -(\mathbf{n}^{\varphi}\times)\cdot\tilde{\mathbf{T}}(\boldsymbol{\theta}) & \mathbf{0}\\ \tilde{\mathbf{T}}^{\mathbf{T}}(\boldsymbol{\theta})\cdot(\mathbf{n}^{\varphi}\times) & \tilde{\mathbf{T}}^{\mathbf{T}}(\boldsymbol{\theta})(\boldsymbol{\varphi}'\times)(\mathbf{n}^{\varphi}\times)\tilde{\mathbf{T}}(\boldsymbol{\theta})+\boldsymbol{\Xi}(\mathbf{n}^{\varphi}\times\boldsymbol{\varphi}') & \mathbf{0}\\ \mathbf{0} & \mathbf{0} & \mathbf{0}\end{bmatrix}^{\mathrm{T}}$$

$$\left[\mathbf{K}_2^G\right]=\begin{bmatrix} \mathbf{0} & \mathbf{0} & \mathbf{0} \\ \mathbf{0} & \tilde{\mathbf{T}}^{\mathrm{T}}(\boldsymbol{\theta})(\boldsymbol{\omega}\times)(\mathbf{m}^{\varphi}\times)\tilde{\mathbf{T}}(\boldsymbol{\theta})+\boldsymbol{\Xi}(\mathbf{m}^{\varphi}\times\boldsymbol{\omega}) & \tilde{\mathbf{T}}^{\mathrm{T}}(\boldsymbol{\theta})(\mathbf{m}^{\varphi}\times)\tilde{\mathbf{T}}(\boldsymbol{\theta})+\boldsymbol{\Xi}^{\mathrm{T}}(\mathbf{m}^{\varphi}) \\ \mathbf{0} & \tilde{\mathbf{T}}^{\mathrm{T}}(\boldsymbol{\theta})(\mathbf{m}^{\varphi}\times)\mathbf{R}-\mathbf{R}^{\mathrm{T}}(\mathbf{m}^{\varphi}\times)\tilde{\mathbf{T}}(\boldsymbol{\theta})+\mathbf{H} & \\ \mathbf{0} & -\tilde{\mathbf{T}}^{\mathrm{T}}(\boldsymbol{\theta})(\mathbf{m}^{\varphi}\times)\tilde{\mathbf{T}}(\boldsymbol{\theta})+\boldsymbol{\Xi}(\mathbf{m}^{\varphi}) & \mathbf{0} \end{bmatrix}$$

with

$$\tilde{\mathbf{T}}(\boldsymbol{\theta})=\frac{\sin\theta}{\theta}\mathbf{I}+\frac{1-\cos\theta}{\theta^2}\boldsymbol{\Theta}+\frac{\theta-\sin\theta}{\theta^3}\boldsymbol{\theta}\otimes\boldsymbol{\theta}\quad\text{in }(\boldsymbol{\Theta}\cdot\boldsymbol{\theta}=\mathbf{0})$$

$$\mathbf{R}=c_1[\boldsymbol{\theta}'\otimes\boldsymbol{\theta}]+c_2[(\boldsymbol{\theta}\times\boldsymbol{\theta}')\otimes\boldsymbol{\theta}]+c_3(\boldsymbol{\theta}\cdot\boldsymbol{\theta}')[\boldsymbol{\theta}\otimes\boldsymbol{\theta}]-c_4[\boldsymbol{\Theta}']+c_5(\boldsymbol{\theta}\cdot\boldsymbol{\theta}')[\mathbf{I}]+c_5[\boldsymbol{\theta}\otimes\boldsymbol{\theta}']$$

$$\boldsymbol{\Xi}(\mathbf{a})=[c_1\mathbf{a}-c_2(\boldsymbol{\theta}\times\mathbf{a})+c_3(\boldsymbol{\theta}\cdot\mathbf{a})\boldsymbol{\theta}]\otimes\boldsymbol{\theta}+c_4[\mathbf{a}\times]+c_5[(\boldsymbol{\theta}\times\mathbf{a})\mathbf{I}+(\boldsymbol{\theta}\otimes\mathbf{a})]$$

$$\begin{aligned}\mathbf{H}=&\left(c_1(\mathbf{m}^{\varphi}\cdot\boldsymbol{\theta}')+c_2\mathbf{m}^{\varphi}\cdot(\boldsymbol{\theta}\times\boldsymbol{\theta}')+c_3(\mathbf{m}^{\varphi}\cdot\boldsymbol{\theta})(\boldsymbol{\theta}\cdot\boldsymbol{\theta}')\right)[\mathbf{I}]\\&+\left(a_1(\mathbf{m}^{\varphi}\cdot\boldsymbol{\theta}')+a_2\mathbf{m}^{\varphi}\cdot(\boldsymbol{\theta}\times\boldsymbol{\theta}')+a_3(\mathbf{m}^{\varphi}\cdot\boldsymbol{\theta})(\boldsymbol{\theta}\cdot\boldsymbol{\theta}')\right)[\boldsymbol{\theta}\otimes\boldsymbol{\theta}]\\&+c_5[\boldsymbol{\theta}'\otimes\mathbf{m}^{\varphi}+\mathbf{m}^{\varphi}\otimes\boldsymbol{\theta}']+c_3(\mathbf{m}^{\varphi}\cdot\boldsymbol{\theta})[\boldsymbol{\theta}'\otimes\boldsymbol{\theta}+\boldsymbol{\theta}\otimes\boldsymbol{\theta}']\\&+c_3(\boldsymbol{\theta}\cdot\boldsymbol{\theta}')[\boldsymbol{\theta}\otimes\mathbf{m}^{\varphi}+\mathbf{m}^{\varphi}\otimes\boldsymbol{\theta}]+c_2[(\boldsymbol{\theta}'\times\mathbf{m}^{\varphi})\otimes\boldsymbol{\theta}+\boldsymbol{\theta}\otimes(\boldsymbol{\theta}'\times\mathbf{m}^{\varphi})]\end{aligned}$$

and

$$c_1=\frac{\theta\cos\theta-\sin\theta}{\theta^3}\qquad c_2=\frac{\theta\sin\theta+2\cos\theta-2}{\theta^4}$$

$$c_3=\frac{3\sin\theta-2\theta-\theta\cos\theta}{\theta^5}\qquad c_4=\frac{1-\cos\theta}{\theta^2}\qquad c_5=\frac{\theta-\sin\theta}{\theta^3}$$

$$a_1=c_3-c_2\qquad a_2=(c_1-4c_2)/\theta^2\qquad a_3=(c_2-5c3)/\theta^2$$

APPENDIX 2
EXPLICIT FORM OF CONSTRAINT EQUATION

$$L_{aug} = \frac{1}{2} I_r \dot{\theta}_r^2 n_r - \frac{1}{2}\int_0^L (\boldsymbol{\varepsilon} \cdot n + k \cdot m) ds + \boldsymbol{\lambda}(t) \cdot \hbar(t)$$

where

$$\hbar(t) = \Im(\theta_\ell(t), \theta'_\ell(t), \varphi_\ell(t), \varphi'_\ell(t)) + I_r \ddot{\theta}_r(t)$$

and

$$\Im(\bullet) = \left[\mathbf{r}_\ell \times \left(\boldsymbol{\Lambda}(\theta_\ell) \cdot \mathbf{C}_n \cdot \boldsymbol{\Lambda}^T(\theta_\ell) \cdot \boldsymbol{\gamma}(\theta_\ell, \varphi'_\ell)\right) + \left(\boldsymbol{\Lambda}(\theta_\ell) \cdot \mathbf{C}_m \cdot \boldsymbol{\Lambda}^T(\theta_\ell) \cdot \boldsymbol{\omega}(\theta_\ell, \theta'_\ell)\right)\right] \cdot \mathbf{n}_r + \mathbf{I}_r \ddot{\boldsymbol{\theta}}_r$$

Variation of constraint equation is given as:

$$\delta L_{aug} = \delta\Pi + I_r \ddot{\theta}_r(t)\delta\theta_r + I_r \ddot{\lambda}(t)\delta\theta_r + \hbar(t)\delta\lambda(t) + \lambda(t)\delta\Im(\bullet) = 0$$

and

Linearized form Constraint Equation is obtained as:

$$L_\Delta[\delta L_{aug}] = L_\Delta[\delta\Pi] + \delta\theta_r\left[\frac{I_r}{\Delta t^2}\right]\Delta\theta_r + \delta\theta_r\left[\frac{I_r}{\Delta t^2}\right]\Delta\lambda + \delta\lambda\left[\frac{I_r}{\Delta t^2}\right]\Delta\theta_r + \delta\lambda \cdot L_\Delta[\Im(\bullet)] + \lambda(t) \cdot L_\Delta[\delta\Im(\bullet)] + \Im(\bullet)\Delta\lambda$$

where

explicit form of $\delta\Pi$ and $L_\Delta[\delta\Pi]$ are given in Appendix 1.

$$\delta\Im(\bullet) = \begin{bmatrix} \delta\varphi'_\ell \\ \delta\theta_\ell \\ \delta\theta'_\ell \end{bmatrix}^T \cdot \mathbf{R}_{\delta\Im}\, L_\Delta[\Im(\bullet)] = \mathbf{R}_{\delta\Im}^T \cdot \begin{bmatrix} \Delta\varphi'_\ell \\ \Delta\theta \\ \Delta\theta'^T_\ell \end{bmatrix}$$

$$L_\Delta[\delta\Im(\bullet)] = \begin{bmatrix} \delta\varphi'_\ell \\ \delta\theta_\ell \end{bmatrix}^T \cdot \left[\mathbf{T}_1^{\Delta\Im}\right] \cdot \begin{bmatrix} \Delta\varphi'_\ell \\ \Delta\theta_\ell \end{bmatrix} + \begin{bmatrix} \delta\theta_\ell \\ \delta\theta'_\ell \end{bmatrix}^T \cdot \left[\mathbf{T}_2^{\Delta\Im}\right] \cdot \begin{bmatrix} \Delta\theta_\ell \\ \Delta\theta'_\ell \end{bmatrix}$$

$$\mathbf{R}_{\delta\mathfrak{I}} = \begin{bmatrix} \mathbf{b_1} \\ \widetilde{\mathbf{T}}_\ell^{\mathrm{T}} \boldsymbol{\Phi}'^{\mathrm{T}}_\ell \mathbf{b_1} + \widetilde{\mathbf{T}}_\ell^{\mathrm{T}} \boldsymbol{\Omega}_\ell^{\mathrm{T}} \mathbf{b_2} + \mathbf{R}_\ell^{\mathrm{T}} \mathbf{b_2} \\ \widetilde{\mathbf{T}}_\ell^{\mathrm{T}} \mathbf{b_2} \end{bmatrix}$$

$$\mathbf{T}_1^{\Delta\mathfrak{I}} = \begin{bmatrix} \mathbf{0} & \mathbf{B}_1^T \widetilde{\mathbf{T}}_\ell^T \\ \widetilde{\mathbf{T}}_\ell \mathbf{B}_1 & \widetilde{\mathbf{T}}_\ell^T (\boldsymbol{\varphi}'_\ell \times) \mathbf{B}_1 \widetilde{\mathbf{T}}_\ell + \sum \left(\mathbf{b}_1 \times \boldsymbol{\varphi}'_\ell \right) \end{bmatrix}$$

$$\mathbf{T}_2^{\Delta\mathfrak{I}} = \begin{bmatrix} \widetilde{\mathbf{T}}_\ell^T (\boldsymbol{\omega}_\ell \times) \mathbf{B}_2 \widetilde{\mathbf{T}}_\ell + \Xi\left(\left(\mathbf{b}_2 \times \boldsymbol{\omega}_\ell \right) + \widetilde{\mathbf{T}}_\ell \mathbf{B}_2 \mathbf{R}_\ell - \mathbf{R}_\ell^T \mathbf{B}_2 \widetilde{\mathbf{T}}_\ell + \mathbf{H} \right) & \widetilde{\mathbf{T}}_\ell^T \mathbf{B}_2 \widetilde{\mathbf{T}}_\ell + \Xi\left(\mathbf{b}_2 \right)^{\mathrm{T}} \\ - \widetilde{\mathbf{T}}_\ell^T \mathbf{B}_2 \widetilde{\mathbf{T}}_\ell + & \mathbf{0} \end{bmatrix}$$

with

$$\mathbf{b}_1 = \boldsymbol{\Lambda}_\ell \mathbf{C}^T \boldsymbol{\Lambda}_\ell^T \cdot \left(\mathbf{n}_\ell \times \mathbf{r}_\ell \right)$$

$$\mathbf{b}_2 = \boldsymbol{\Lambda}_\ell \mathbf{D}^T \boldsymbol{\Lambda}_\ell^T \mathbf{n}_\ell$$

$$\boldsymbol{\Omega} \cdot \boldsymbol{\omega} = \mathbf{0}, \qquad \mathbf{B}_1 \cdot \mathbf{b}_1 = \mathbf{0}, \qquad \mathbf{B}_2 \cdot \mathbf{b}_2 = \mathbf{0}$$

$$\boldsymbol{\Lambda}_\ell = \boldsymbol{\Lambda}(\theta_\ell), \quad \widetilde{\mathbf{T}}_\ell = \widetilde{\mathbf{T}}(\theta_\ell), \; \mathbf{R}_\ell = \mathbf{R}(\theta_\ell, \theta'_\ell)$$

APPENDIX 3

IMPLEMENTATION OF PROPOSED SCHEME

Assign Initial Values

Geometric Properties of Coupling Element

D_{cp}= 50 mm (Bore Diameter)

d_r= 19 mm (Rotor Diamater)

$$b = \frac{D_{cp} - d_r}{2}$$

$$r_{cp} = \frac{D_{cp} + d_r}{4}$$

P= 3.18 mm (Pitch)

t= 2.4 mm (Coil Thickness)

L_{cp}=54 mm (Coupling Length)

N_c= 3.5 (Number of Coils)

$A_{xx} = b \cdot t$ (Area of the Helical Beam)

$A_{yx} = \frac{5}{6} A_{xx}$ (Effective Shear Area)

$A_{zx} = \frac{5}{6} A_{xx}$ (Effective Shear Area)

$$I_y = \frac{b^3 \cdot t}{12}$$

$$I_z = \frac{b \cdot t^3}{12}$$

$J_x = I_y + I_z$

Material Properties of Couplinh Element (Al 7075-T6)

$\rho_{cp} = 2100$ kg/m^3 (Density)

E_{cp}= 72x10^9 Pa (Young Modulus)

ν= 0.33 (Poision Ratio)

$$G_{cp} = \frac{E_{cp}}{2 \cdot (1 + \nu)}$$ (Shear Modulus)

Constitutive Matrices of Helical Beam

$\mathbf{C_n}$=diag[$E_{cp}A_{xx}$, $G_{cp}A_{yx}$, $G_{cp}A_{zx}$]

$\mathbf{C_m}$=diag[$G_{cp}J_x$, $E_{cp}I_y$, $E_{cp}I_z$]

Assign Misalignment Values (see Figure 6)

$\delta = [0 \quad 0 \quad \delta]^T$ (Parallel Misalignment)

$\alpha = [\alpha \quad 0 \quad 0]^T$ (Angular Misalignment)

Radius Vectors (Undeformed Configurations) (see Figure 6)

$$\mathbf{r_m} = \begin{bmatrix} 0 & 0 & r_{cp} \end{bmatrix}^T$$

$$\mathbf{r_L} = \begin{bmatrix} 0 & 0 & -r_{cp} \end{bmatrix}^T$$

Radius Vector (Initial Configurations) (see Figure 6)

$$\mathbf{r}_\ell = \Lambda(\alpha) \cdot \mathbf{r_L}$$

Unit Vectors (See Figure 6)

$$\mathbf{n_m} = \begin{bmatrix} 0 & 1 & 0 \end{bmatrix}^T$$

$$\mathbf{n_{r,0}} = \begin{bmatrix} 0 & 1 & 0 \end{bmatrix}^T$$

$$\mathbf{n_r} = \Lambda(\alpha) \cdot \mathbf{n_{r,0}}$$

Calculate position vectors of undeformed configuration (φ_0)

$$\Delta\beta = \frac{2N_c\pi}{n_{elm}(n_l - 1)}$$

where

n_{elm} – number of finite element

n_l –total local node (n_l=4)

$$\varphi_{0,m} = \left[r_{cp} \sin\Delta\beta \quad \frac{P \cdot (m\Delta\beta)}{2\pi} \quad r_{cp} \cos\Delta\beta \right]^T \quad m=1,2,3 \ldots. n_t$$

where

$n_t = (n_{elm}-1)(n_l-1)+n_l$ (total global node)

Length Vector (see Figure 6)

$$\mathbf{L} = \left[0 \quad \frac{P \cdot (n_t \Delta\beta)}{2\pi} \quad 0 \right]^T$$

Calculate Deformed Configuration

Step 1: Assign specified values to total displacement and incremental rotation vectors at first global node:

$$\theta_{l,n+1} = \Delta\theta_m \mathbf{n}_m$$

$$\mathbf{u}_l = \Lambda(\theta_{l,n+1}) \cdot \Lambda(\theta_{l,n}) \cdot \mathbf{r}_m - \varphi_{0,l}$$

where $\Delta\theta_m$ is user specified motor rotation angle from time step n to time step n+1.

If displacements and rotations are calculated for new time step (n+1)

Assign predicted values to total displacement and incremental rotation vectors for global nodes 2 to (n_t-1):

$\mathbf{u}_a$ and θ_a where a=2,3, .. (n_t-1)

Calculate nodal position vectors:

$\varphi_a = \mathbf{u}_a + \varphi_{0,a}$ where a=2,3, .. (n_t-1)

Assign predicted value to rotor rotation angle from time step n to time step n+1: $\theta_{r,n+1}$

Calculate position and incremental rotation vectors for last node

$$\boldsymbol{\theta}_{\ell,n+1} = \theta_r \mathbf{n}_r$$
$$\boldsymbol{\varphi}_\ell = \mathbf{L} + \boldsymbol{\delta} + \exp(\boldsymbol{\theta}_{\ell,n+1}) \cdot \boldsymbol{\Lambda}_{\ell,n} \cdot \mathbf{r}_{\ell,0}$$

Calculate Angular velocity and acceleration of rotor

$$\dot{\theta}_{r,n+1} = \frac{\theta_{r,n+1}}{\Delta t} \quad \ddot{\theta}_r = \frac{\dot{\theta}_{r,n+1} - \dot{\theta}_{r,n}}{\Delta t}$$

Assign predicted value to Lagrange multiplier: λ

Calculate first and second derivative of Lagrange multiplier

$$\dot{\lambda}_{n+1} = \frac{\lambda}{\Delta t} \quad \ddot{\lambda}_{n+1} = \frac{\dot{\lambda}_{n+1} - \dot{\lambda}_n}{\Delta t}$$

If displacements and rotations are computed (iterated) for time step n+1

Retrieve computed iterative values of incremental displacement and rotation vectors for global nodes of 2 to (n_t-1): $\Delta\mathbf{u}_a, \Delta\boldsymbol{\theta}_a$ where a=2,3, .. (n_t-1)

Update total displacement and incremental rotation vectors for global nodes of 2 to (n_t-1):

$$\mathbf{u}_a \leftarrow \mathbf{u}_a + \Delta\mathbf{u}_a$$
$$\boldsymbol{\theta}_a \leftarrow \boldsymbol{\theta}_a + \Delta\boldsymbol{\theta}_a$$

Update position vectors (except first and last node)

$$\boldsymbol{\varphi}_a = \mathbf{u}_a + \boldsymbol{\varphi}_{a,0}$$

Retrive computed iterative value of incremental rotor angle: $\Delta\theta_r$

Update incremental rotor angle: $\theta_r \leftarrow \theta_r + \Delta\theta_r$

Calculate iterative value of incremental rotation vector for last node :

$$\Delta\boldsymbol{\theta}_\ell = \Delta\theta_r \mathbf{n}_r$$

Update incremental rotation and position vector for last node:

$$\boldsymbol{\theta}_\ell \leftarrow \boldsymbol{\theta}_\ell + \Delta\boldsymbol{\theta}_\ell$$
$$\boldsymbol{\varphi}_\ell = \mathbf{L} + \boldsymbol{\delta} + \exp(\boldsymbol{\theta}_\ell) \cdot \boldsymbol{\Lambda}_{\ell,n} \cdot \mathbf{r}_{\ell,0}$$

Update Angular velocity and acceleration of rotor

$$\dot{\theta}_{r,n+1} = \frac{\theta_{r,n+1}}{\Delta t} \quad \ddot{\theta}_r = \frac{\dot{\theta}_{r,n+1} - \dot{\theta}_{r,n}}{\Delta t}$$

Retrieve computed iterative value of Lagrange multiplier: $\Delta\lambda$

Update incremental Lagrange multiplier: $\lambda \leftarrow \lambda + \Delta\lambda$

Update first and second derivative of Lagrange multiplier

$$\dot{\lambda}_{n+1} = \frac{\lambda}{\Delta t} \quad \ddot{\lambda}_{n+1} = \frac{\dot{\lambda}_{n+1} - \dot{\lambda}_n}{\Delta t}$$

Step 2: Compute total strains and stress resultants for elements (at each Gauss points)

Compute position and incremental rotation vectors:

$$\boldsymbol{\varphi}_{el} = \sum_{b=1}^{4} \mathbf{N}_b(\xi_l) \boldsymbol{\varphi}_b^{el}$$

$$\boldsymbol{\theta}_{el} = \sum_{b=1}^{4} \mathbf{N}_b(\xi_I)\boldsymbol{\theta}_b^{el}$$

Compute position and incremental rotation vector derivatives:

$$\boldsymbol{\varphi}'_{el} = \sum_{b=1}^{4} \mathbf{N}'_b(\xi_I)\boldsymbol{\varphi}_b^{el}$$

$$\boldsymbol{\theta}'_{el} = \sum_{b=1}^{4} \mathbf{N}'_b(\xi_I)\boldsymbol{\theta}_b^{el}$$

Compute (total) rotation tensors:

$$\boldsymbol{\Lambda} = \exp(\boldsymbol{\theta}_{el}) \cdot \boldsymbol{\Lambda}_n$$

Compute section unit normals:

$$\mathbf{a} = \boldsymbol{\Lambda} \cdot \mathbf{g} \qquad \mathbf{g} = \boldsymbol{\varphi}'_0$$

Compute axial, shear and bending strains:

$$\boldsymbol{\gamma} = \boldsymbol{\varphi}' - \mathbf{a}$$

$$\boldsymbol{\omega} = \mathrm{T}(\boldsymbol{\theta}_{el}) \cdot \boldsymbol{\theta}'_{el} + \exp(\boldsymbol{\theta}_{el}) \cdot \boldsymbol{\omega}_n$$

Compute stress resultants:

$$\mathbf{n} = \boldsymbol{\Lambda} \cdot \mathbf{C}_\mathbf{n} \cdot \boldsymbol{\Lambda}^{\mathrm{T}} \cdot \boldsymbol{\gamma}$$

$$\mathbf{m} = \boldsymbol{\Lambda} \cdot \mathbf{C}_\mathbf{m} \cdot \boldsymbol{\Lambda}^{\mathrm{T}} \cdot \boldsymbol{\omega}$$

Step 3: Compute residual and tangent stiffness matrix of beam without imposing any boundary condition:

$$\mathbf{r}_b^{el} = \sum_{i=1}^{3} j_W(i) \begin{bmatrix} \mathrm{N}'_b\mathbf{I}_{3X3} & \mathbf{0} \\ \mathbf{0} & \mathrm{N}_b\mathbf{I}_{3X3} \\ \mathbf{0} & \mathrm{N}'_b\mathbf{I}_{3X3} \end{bmatrix}^{\mathrm{T}} [\mathbf{R}]^{el}$$

$$\mathbf{K}_{bc}^{M,el} = \sum_{i=1}^{3} j_W(i) \begin{bmatrix} \mathrm{N}'_b\mathbf{I}_{3X3} & \mathbf{0} \\ \mathbf{0} & \mathrm{N}_b\mathbf{I}_{3X3} \\ \mathbf{0} & \mathrm{N}'_b\mathbf{I}_{3X3} \end{bmatrix}^{\mathrm{T}} [\mathbf{K}^{M}]^{el} \begin{bmatrix} \mathrm{N}'_c\mathbf{I}_{3X3} & \mathbf{0} \\ \mathbf{0} & \mathrm{N}_c\mathbf{I}_{3X3} \\ \mathbf{0} & \mathrm{N}'_c\mathbf{I}_{3X3} \end{bmatrix}$$

$$\mathbf{K}_{bc}^{G,el} = \sum_{i=1}^{3} j_W(i) \begin{bmatrix} \mathrm{N}'_b\mathbf{I}_{3X3} & \mathbf{0} \\ \mathbf{0} & \mathrm{N}_b\mathbf{I}_{3X3} \\ \mathbf{0} & \mathrm{N}'_b\mathbf{I}_{3X3} \end{bmatrix}^{\mathrm{T}} [\mathbf{K}_1^{G} + \mathbf{K}_2^{G}]^{el} \begin{bmatrix} \mathrm{N}'_c\mathbf{I}_{3X3} & \mathbf{0} \\ \mathbf{0} & \mathrm{N}_c\mathbf{I}_{3X3} \\ \mathbf{0} & \mathrm{N}'_c\mathbf{I}_{3X3} \end{bmatrix}$$

where $j_W(i)$ are the Gauss weights.

Compute Global residual and tangent stiffness matrices:

$$\mathbf{r} = \sum_{el=1}^{n_{el}} \mathbf{I}_{el}^{r} \left(\sum_{b=1}^{4} \mathbf{I}_b^{r} \mathbf{r}_b^{el} \right)$$

$$\mathbf{K} = \sum_{el_i=1}^{n_{el}} \sum_{el_j=1}^{n_{el}} \mathbf{I}_{el_i}^{r} \left(\sum_{b=1}^{4} \sum_{c=1}^{4} \mathbf{I}_b^{r} \left(\mathbf{K}_{bc}^{M} + \mathbf{K}_{bc}^{G} \right) \mathbf{I}_c^{r} \right) \mathbf{I}_{el_j}^{r}$$

where

$\mathbf{I}_\bullet^\star$: Coefficient matrix with elements 0 and 1.

Step 4: Compute forces and moments at the end of the beam (last element):

Compute position and incremental rotation vectors:

$$\boldsymbol{\varphi}_\ell = \sum_{b=1}^{4} N_b(1)\boldsymbol{\varphi}_b \qquad \boldsymbol{\theta}_\ell = \sum_{b=1}^{4} N_b(1)\boldsymbol{\theta}_b$$

Compute position and incremental rotation vector derivatives:

$$\boldsymbol{\varphi}'_\ell = \sum_{b=1}^{4} N'_b(1)\boldsymbol{\varphi}_b \qquad \boldsymbol{\theta}'_\ell = \sum_{b=1}^{4} N'_b(1)\boldsymbol{\theta}_b$$

Compute (total) rotation tensors:

$$\boldsymbol{\Lambda}_\ell = \exp(\boldsymbol{\theta}_\ell)\cdot\boldsymbol{\Lambda}_{\ell,n}$$

Compute section unit normals:

$$\mathbf{a}_\ell = \boldsymbol{\Lambda}_\ell \cdot \mathbf{g}_\ell \qquad \mathbf{g}_\ell = \boldsymbol{\varphi}'_{0,\ell}$$

Compute axial, shear and bending strains:

$$\boldsymbol{\gamma}_\ell = \boldsymbol{\varphi}'_\ell - \mathbf{a}_\ell$$

$$\boldsymbol{\omega}_\ell = \mathbf{T}(\theta_\ell)\cdot\boldsymbol{\theta}'_\ell + \exp(\boldsymbol{\theta}_\ell)\cdot\omega_{\ell,n}$$

Compute stress resultants:

$$\mathbf{F}_\ell = \boldsymbol{\Lambda}_\ell \cdot \mathbf{C} \cdot \boldsymbol{\Lambda}_\ell^{\mathrm{T}} \cdot \boldsymbol{\gamma}_\ell \qquad \mathbf{M}_\ell = \boldsymbol{\Lambda}_\ell \cdot \mathbf{D} \cdot \boldsymbol{\Lambda}_\ell^{\mathrm{T}} \cdot \boldsymbol{\omega}_\ell$$

Compute constraint

$$\hbar = (\mathbf{r}_\ell \times \mathbf{F}_\ell + \mathbf{M}_\ell)\cdot\mathbf{n}_r$$

Step 5: Compute residual and tangent part of constraint equation:

$$\begin{bmatrix}\delta\theta_r\\ \delta\lambda\end{bmatrix}^{\mathrm{T}} \mathbf{r}_{\mathfrak{I}}^1 = \begin{bmatrix}\delta\theta_r\\ \delta\lambda\end{bmatrix}^{\mathrm{T}} \begin{bmatrix} I_r(\ddot{\theta}_r + \ddot{\lambda})\\ \hbar(t)\end{bmatrix}$$

$$\begin{bmatrix}\delta\boldsymbol{\varphi}_\ell\\ \delta\boldsymbol{\theta}_\ell\end{bmatrix}^{\mathrm{T}} \mathbf{r}_{\mathfrak{I}}^2 = \begin{bmatrix}\delta\boldsymbol{\varphi}_\ell\\ \delta\boldsymbol{\theta}_\ell\end{bmatrix}^{\mathrm{T}} \left(\begin{bmatrix}\mathbf{I_{3X3}} & \mathbf{0}\\ \mathbf{0} & \mathbf{I_{3X3}}\\ \mathbf{0} & \mathbf{I_{3X3}}\end{bmatrix}^{\mathrm{T}} \lambda(t)\mathbf{R}_{\delta\mathfrak{I}} \right)$$

$$\begin{bmatrix}\delta\theta_r\\ \delta\lambda\end{bmatrix}^{\mathrm{T}} \mathbf{K}_{\mathfrak{I}}^1 \begin{bmatrix}\Delta\theta_r\\ \Delta\lambda\end{bmatrix} = \begin{bmatrix}\delta\theta_r\\ \delta\lambda\end{bmatrix}^{\mathrm{T}} \begin{bmatrix}\frac{I_r}{\Delta t^2} & \frac{I_r}{\Delta t^2}\\ \frac{I_r}{\Delta t^2} & 0\end{bmatrix} \begin{bmatrix}\Delta\theta_r\\ \Delta\lambda\end{bmatrix}$$

$$\begin{bmatrix}\delta\boldsymbol{\varphi}_\ell\\ \delta\boldsymbol{\theta}_\ell\\ \delta\lambda\end{bmatrix}^{\mathrm{T}} \mathbf{K}_{\mathfrak{I}}^2 \begin{bmatrix}\Delta\boldsymbol{\varphi}_\ell\\ \Delta\boldsymbol{\theta}_\ell\\ \Delta\lambda\end{bmatrix} = \begin{bmatrix}\delta\boldsymbol{\varphi}_\ell\\ \delta\boldsymbol{\theta}_\ell\\ \delta\lambda\end{bmatrix}^{\mathrm{T}} \left(\begin{bmatrix}\mathbf{I_{3X3}} & \mathbf{0} & \mathbf{0}\\ \mathbf{0} & \mathbf{I_{3X3}} & \mathbf{0}\\ \mathbf{0} & \mathbf{I_{3X3}} & \mathbf{0}\\ \mathbf{0} & \mathbf{0} & 1\end{bmatrix}^{\mathrm{T}} \begin{bmatrix}\mathbf{0} & \mathbf{R}_{\delta\mathfrak{I}}\\ \mathbf{R}_{\delta\mathfrak{I}}^{\mathrm{T}} & \mathbf{0}\end{bmatrix} \begin{bmatrix}\mathbf{I_{3X3}} & \mathbf{0} & \mathbf{0}\\ \mathbf{0} & \mathbf{I_{3X3}} & \mathbf{0}\\ \mathbf{0} & \mathbf{I_{3X3}} & \mathbf{0}\\ \mathbf{0} & \mathbf{0} & 1\end{bmatrix} \right) \begin{bmatrix}\Delta\boldsymbol{\varphi}_\ell\\ \Delta\boldsymbol{\theta}_\ell\\ \Delta\lambda\end{bmatrix}$$

Step 6: Rearrange residual and tangent (stiffness) matrices according to boundary conditions:

Delete rows and colums corresponding to first node (since $\boldsymbol{\theta}_1$ and $\boldsymbol{\varphi}_1$ are specified):

$$\delta\boldsymbol{\theta}_0 \to 0\,,\ \delta\boldsymbol{\varphi}_0 \to 0$$

$\Delta\boldsymbol{\theta}_0 \to 0$, $\Delta\boldsymbol{\varphi}_0 \to 0$

Express variations on last node in terms of θ_r and $\mathbf{n}_r$ (see Equations (-) and (-)):

$\delta\boldsymbol{\theta}_\ell = \mathbf{n}_r \delta\theta_r$, $\Delta\boldsymbol{\theta}_\ell = \mathbf{n}_r \Delta\theta_r$

$\delta\boldsymbol{\varphi}_\ell = \Xi\left(\boldsymbol{\Lambda}_{\ell,n} \cdot \mathbf{r}_{\ell,0}\right) \cdot \mathbf{n}_r \delta\theta_r$, $\Delta\boldsymbol{\varphi}_\ell = \Xi\left(\boldsymbol{\Lambda}_{\ell,n} \cdot \mathbf{r}_{\ell,0}\right) \cdot \mathbf{n}_r \Delta\theta_r$

Modify residual and tangent (stiffness) matrices:

$\mathbf{r}^{New} \leftarrow \mathbf{r}$, $\mathbf{K}^{New} \leftarrow \mathbf{K}$

$\mathbf{r}_{\mathfrak{I}}^{2,New} \leftarrow \mathbf{r}_{\mathfrak{I}}^{2}$, $\mathbf{K}_{\mathfrak{I}}^{2,New} \leftarrow \mathbf{K}_{\mathfrak{I}}^{2}$

Step 7: Compute total residual and tangent (stiffness) matrices:

$$\mathbf{r}_{\text{Total}} = \mathbf{r}^{New} + \mathbf{I}_{\mathfrak{I}}^{1}\ \mathbf{r}_{\mathfrak{I}}^{1} + \mathbf{I}_{\mathfrak{I}}^{2}\ \mathbf{r}_{\mathfrak{I}}^{2,New}\ ,\ \mathbf{K}_{\text{total}} = \mathbf{K}^{New} + \mathbf{I}_{\mathfrak{I}}^{\sigma}\ \mathbf{K}_{\mathfrak{I}}^{1}\ \mathbf{I}_{\mathfrak{I}}^{\eta} + \mathbf{I}_{\mathfrak{I}}^{\Delta}\ \mathbf{K}_{\mathfrak{I}}^{2,New}\mathbf{I}_{\mathfrak{I}}^{\nabla}$$

$\mathbf{I}_{\bullet}^{\bullet}$: Coefficient matrix with elements 0 and 1.

Step 8: Solve for incremental displacements and rotations:

$$\mathbf{K}_{\text{Total}} \cdot \begin{bmatrix} \Delta\mathbf{u}_a \\ \Delta\boldsymbol{\theta}_a \\ \Delta\theta_\ell \\ \Delta\lambda \end{bmatrix} = -\mathbf{r}_{\text{Total}}$$

APPENDIX 4

GEOMETRIC AND MATERIAL PROPERTIES OF HELICAL COUPLING

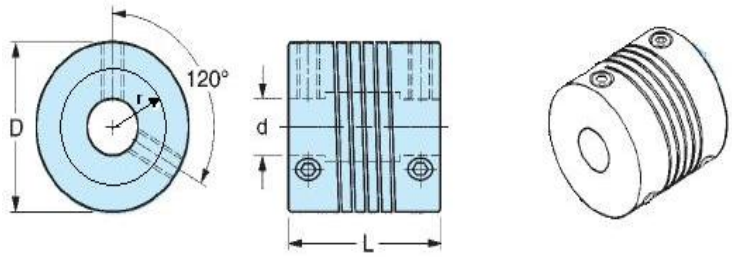

Geometric Properties of coupling:

D= 50 mm (Outside diameter)

d= 19 mm (Inside diameter)

Pitch= 3.18 mm

t= 2.4 mm (Thickness of coil)

b= 34.5 mm

N_c=3.5 (Number of coil)

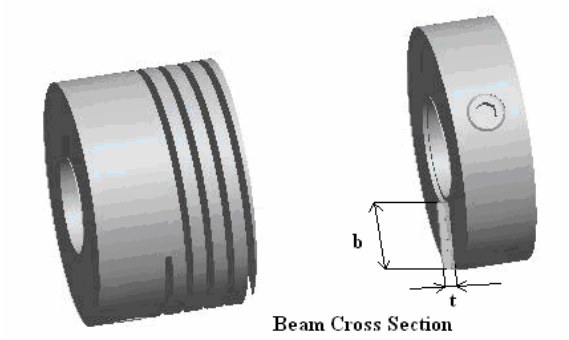

Material Properties of coupling:

Material: 7074-T6 Aluminum

E=72x10^9 N/m^2 (Young Modulus)

Nu=0.33 (Possion Ratio)

G=E/(2+2*Nu) (Shear Modulus)

APPENDIX 5

ANSYS SIMULATIONS

Hypothecial System

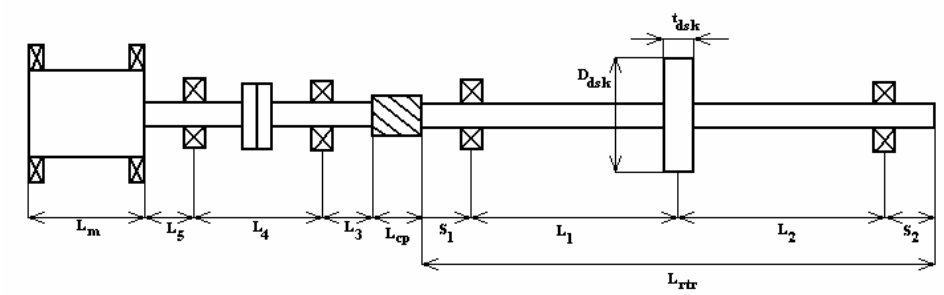

ANSYS Model

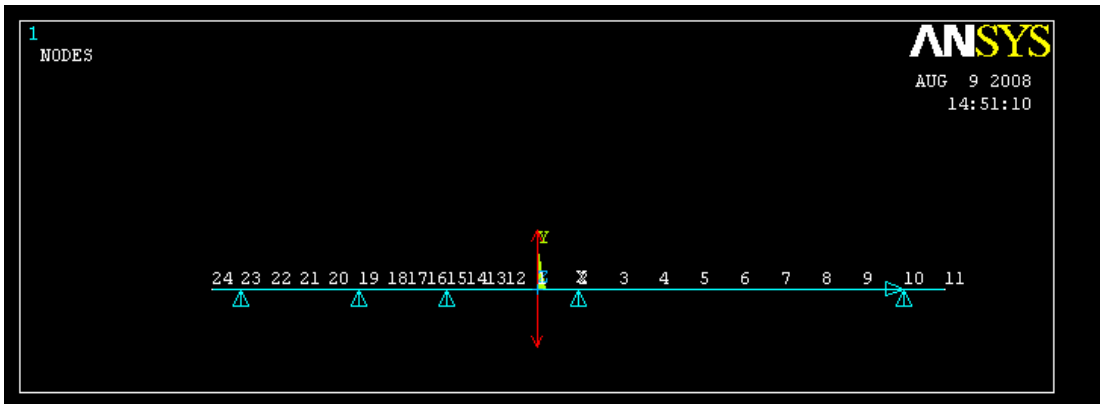

Hypothecial System Parameters:

Common Parameters:

L_m= 300 mm (motor length)
L_3= 15 mm
L_4= 170 mm
L_5= 15 mm
L_{cp}= 54 mm

Paramaters for Inertia Value of 0.1Ir

t_{dsk}= - (no disk)
D_{dsk}= - (no disk)
d_{rtr}= 19 mm (rotor diameter)
L_{rtr}= 693 mm (rotor length)
L_1= 277.2 mm
L_2= 277.2 mm
S_1= 69.3 mm
S_2=69.3 mm

0.1Ir= 6.53×10^{-5} kg-m^2
Natural Frequencies=166.47, 535.41, 990.89, 1051.4 Hz

Paramaters for Inertia Value of Ir

t_{dsk}= 25 mm (disk thickness)
D_{dsk}= 75 mm (disk diameter)
d_{rtr}= 19 mm (rotor diameter)
L_{rtr}= 535 mm (rotor length)
L_1= 214 mm
L_2= 214 mm
S_1= 53.5 mm
S_2=53.5 mm

Ir= 6.53×10^{-4} kg-m^2
Natural Frequencies=166.29, 812.22, 1056.9, 1159.1 Hz

Paramaters for Inertia Value of 10Ir

t_{dsk}= 25 mm (disk thickness)
D_{dsk}= 133.33 mm (disk diameter)
d_{rtr}= 19 mm (rotor diameter)
L_{rtr}= 1203 mm (rotor length)
L_1= 481.2 mm
L_2= 481.2 mm
S_1= 120.3 mm
S_2= 120.3 mm

10Ir= 6.53×10^{-3} kg-m^2
Natural Frequencies= 29.71, 166.31, 290.01, 467.25, 620.65 Hz

ANSYS Simulation Files:

Beam Model (for inertia value of 0.1I_r)

```
/com, Beam3 element
pi=3.14159        !value of pi
C*** Constant Parameters
C*************************************
Lr=535e-3                 !m Rotor Length
Lbs=490e-3                !m Bearing Span
Lcp=54e-3         !m Length of Coupling
Lbm2=200e-3       !m Length of 2nd Beam
Lmtr=300e-3       !Length of motor beam

dr=19e-3                  !m rotor diameter
dd=75e-3                  !m disk diameter
dt=25e-3                  !m disk thickness
dCpBg=50e-3       !m Coupling Outside diamater
dCpSml=19e-3      !m Coupling Inside Diameter
dCp=dCpBg-dCpSml        !Thickness of Coupling

Ar=pi*dr*dr/4     !m2 Rotor Area
Ad=pi*dd*dd/4     !m2 Disk Area
ACp=pi*(dCpBg*dCpBg-dCpSml*dCpSml)/4 !m2 Coupling Area

Vr=Ar*Lr                  !m3 Rotor volume
Vd=Ad*dt-Ar*dt !m3 Disk Volume

ro=7800                   !kg/m3 Density of rotor material
md=ro*Vd                  !kg Disk Weigth
mr=ro*Vr                  !kg rotor weigth
roCp=2810         !Kg/m3 Density of Coupling Material

Id=pi*dr*dr*dr*dr/64              !m4 Area moment of inertia of rotor
Jd=pi*dr*dr*dr*dr/32              !m4 Polar moment of inertia of rotor
```

```
Ipr=ro*pi*Lr*dr*dr*dr*dr/32         !kg-m2 Mass moment of inertia of rotor
Ipd=ro*pi*dt*(dd*dd*dd*dd-dt*dt*dt*dt)/32  !kg-m2 Mass moment of inertia of disk

ICpBg=pi*dCpBg*dCpBg*dCpBg*dCpBg/64
ICpSml=pi*dCpSml*dCpSml*dCpSml*dCpSml/64
ICp=ICpBg-ICpSml         !m4 Coupling Area Moment of Inertia
JCp=2*ICp         !Polar Moment of Inertia of Coupling

C**********************************
/config,nres,10000
/prep7
/COM Beam Element Generation

ET,1,beam3
ET,2,mass21,,,3
R,1,Ar,Id,dr !Rotor %2D
R,2,md,Ipd/2 !Disk
R,3,Acp,ICp,dCpBg !Coupling 2D

Mp,EX,1,2e11
Mp,DENS,1,ro
Mp,PRXY,1,0.33

!Coupling Material
Mp,EX,2,72e9
Mp,DENS,2,roCp
Mp,PRXY,2,0.33

!Beam Nodes
N,1,0,0
N,11,Lr,0
FILL
!Coupling Node
N,12,-Lcp,0
!2nd Beam
N,18,(-Lcp-Lbm2),0
FILL
N,24,(-Lcp-Lbm2-Lmtr),0
FILL

Type,1
Real,1
Mat,1
E,1,2
EGEN,10,1,1

!Add disk mass and inertia

Type,2
REAL,2
E,6

Type,1
Real,3
Mat,2
E,1,12

Type,1
```

```
Real,1
Mat,1
E,12,13
E,13,14
E,14,15
E,15,16
E,16,17
E,17,18
E,18,19
E,19,20
E,20,21
E,21,22
E,22,23
E,23,24

C*** Constraints
C**********************************
D,2,UY,0.0
!D,2,UZ,0.0
D,10,UX,0.0
D,10,UY,0.0
!D,10,UZ,0.0
D,15,UY,0.0
!D,15,UZ,0.0
D,19,UY,0.0
!D,19,UZ,0.0
D,23,UY,0.0
!D,23,UZ,0.0
Finish
```

Loading File

```
deltim, 3.333333e-005
Time, 3.333333e-005
F,1,FY, 0.000000e+000
F,1,MZ, 0.000000e+000
SOLVE
Time, 6.666667e-005
F,1,FY, 2.972797e-003
F,1,MZ, -3.071657e-002
SOLVE
Time, 1.000000e-004
F,1,FY, 4.664149e-003
F,1,MZ, -3.070769e-002
SOLVE
Time, 1.333333e-004
F,1,FY, 6.328986e-003
F,1,MZ, -3.069938e-002
SOLVE
.
.
.
.
Time, 2.590000e-001
F,1,FY, 3.594390e-002
F,1,MZ, -3.068341e-002
SOLVE
Time, 2.590333e-001
```

```
F,1,FY, 3.623576e-002
F,1,MZ, -3.069182e-002
SOLVE
FINISH
```

Solution
/input, ***Beam Model***

```
C**********************************
C***Solution

C**********************************
/SOLU
ANTYPE,trans          ! Transient ANALYSIS


OUTPR,NSOL,1
OUTRES,NSOL,1
```

/input, ***Loading File***

```
/post26
NSOL,2,6,u,x,DX6
NSOL,3,6,u,y,DY6
NSOL,5,4,u,x,DX4
NSOL,6,4,u,y,DY4
Finish
```

APPENDIX 6

MATLAB CODE

%Assign initial Values

```
clear all
% Calculate Initial Geometric Data of Coupling Element

Smld=19e-3; % m Coupling smal Diamater
BigD=50e-3; % m Couplşng big Diamater
Pitch=3.18e-3; %m
Nc=7; %  2*Number of coil
N_angle=5;%degree rotation angle of constant speed shaft
k=1/16;
b=(BigD-Smld)/2;
t=2.4e-3; %m coil thickness
r=(Smld+BigD)/4;

% Geometric and Material Properties of Couping Element

roSt=7800;% Kg/m3 Density of  Steel (for Rotor - Dsik)
E=72e9;% Pa Young Modulus of Al 7075-T6
Nu=0.33;% Possion Ratio
G=E/(2+2*Nu); % Pa  Shear Modulus
Ax=b*t; % m2 Area
A2x=5/6*Ax; % m2 Efective Shear Area
A3x=5/6*Ax;% m2 Effective Area
Iy=b*b*b*t/12;
Iz=t*t*t*b/12;
Jx=Iy+Iz;

 % Input Inertia

input('Specify inertia values:', Inertia)

% Constitutive Matrices:Cn Cm

Cn=diag([E*Ax,G*A2x,G*A3x]);
Cm=diag([G*Jx,E*Iy,E*Iz]);

% Specify Angular Velocity

VelRPM=5000; % RPM

%  Specify Number of Elements, Number of Local  Nodes and Number of Gauss Points

n_Gauss=3;
n_elm=2*Nc/k; %Number of Element
totallocalnode=4;
totalglobalnode=(n_elm-1)*(totallocalnode-1)+totallocalnode;

% Initialize Total Rotation and Displacement Cell arrays

PrevROTMTRX=cell(n_elm,n_Gauss);
InlRTMTRX=cell(n_elm,n_Gauss);
Omega_alfa=cell(n_elm,n_step,n_Gauss);
for i_elm=1:n_elm
   for i_Gauss=1:n_Gauss
      PrevROTMTRX{i_elm,i_Gauss}=eye(3);
   end
end

% Initialize Rotation matrices

firstROTMTRX=eye(3);
EndROTMTRX=eye(3);
for i_elm=1:n_elm
   for i_Gauss=1:n_Gauss
      Omega_alfa{i_elm,1,i_Gauss}=[0;0;0];
   end
end
Omega_alfaEND=zeros(3,x_step);

% Calculate Position Vectors for Undeformed Configuration
```

```
teta=0;
dteta=k*pi/2/(totallocalnode-1);
for i_globalnode=1:totalglobalnode
      InitialPhiVls(1:3,i_globalnode)=[r*sin(teta);Pitch*teta/2/pi;r*cos(teta)];
      teta=teta+dteta;
end

%*************************************************************************
% Assign BC Values to the arrays
%sSpecify  global nodes, elements and  local nodes

BCNode1=[1,totalglobalnode];%Global Nodes
BCElm1=[1;n_elm];
BClocal1=[1,4];
BCNode2=[1];%Global Nodes
BCElm2=[1];
BClocaL2=[1];
%*************************************************************************
%Initial Load Steps

%Apply Angular Misalignment
x_stepAng=0;
%Apply Parallel Misalignment
x_stepPrl=1;
%Total Initial load steps
x_step=x_stepAng+x_stepPrl; %First Load Step
%Specify ANGULAR misalignmentangle
MisalignmentAngle=0*pi/180;%rad
%Specify PARALLEL misalignment value
PrlMis=0.25e-3;%m
%*************************************************************************
%Incremental values for End of coupling
%Angular Misalignment

if x_stepAng~=0
DROT1=MisalignmentAngle/x_stepAng;%radian, 1 degree increment
elseif x_stepAng==0
DROT1=0;
End

%Parralel Misalignment

if x_stepPrl~=0
DPMis=PrlMis/x_stepPrl;%radian, 1 degree increment
elseif x_stepPrl==0
DPMis=0;
end
%*************************************************************************
%Inctemental Values for Rotation

DROT2=1*pi/180;

%Specify (rotation) Unit  Vectors

n_rot1=[1;0;0]; %First step rotation vector
n_rot2=[[0;1;0],[0;cos(MisalignmentAngle);sin(MisalignmentAngle)]];%Second step rotation vectors
%Specify velocity acceleration
DTime=DROT2/(VelRPM/60*2*pi);
for i_acc=1
angVel(i_acc)=0
angAcc(i_acc)=0;
end
angVel(x_step)=DROT2/DTime;%rad/sec
angAcc(x_step)=0;
%*************************************************************************
% Radius Vectors (Undeformed Configuration)

r1zero=[0;0;InitialPhiVls(3,totalglobalnode)];
r2zero=[0;0;InitialPhiVls(3,1)];
lzero=[0;InitialPhiVls(2,totalglobalnode);0];

% BC values

r1=r1zero; %radius at the END of coupling
r2=r2zero;%radius at the tip of coupling
%*************************************************************************
```

```
%Initial Values

TotalDisp=zeros(3,totalglobalnode);
IncRot=zeros(3,totalglobalnode);
%Angular misalignment not zero
if DROT1~=0
   IncRot(1:3,totalglobalnode)=DROT1*n_rot1;
   [antROT,dummyROT]=rotation(IncRot(1:3,totalglobalnode));
   TotalDisp(1:3,totalglobalnode)=lzero+antROT*EndROTMTRX*r1zero ...
                    -InitialPhiVls(1:3,totalglobalnode);
%Angular misalignment is zero and parallel misalignmentis not zero
elseif ((DROT1==0)&(DPMis~=0))
   IncRot(1:3,totalglobalnode)=[0;0;0];
   TotalDisp(1:3,totalglobalnode)=[0;0;DPMis];
end
%*************************************************************************
% Shape Function Values at given GAUSS Point

GaussPnts=[0.774596669241483; ...
         0.0; ...
         -0.774596669241483];
GaussWgths=[0.555555555555556; ...
          0.888888888888889; ...
          0.555555555555556];
W=GaussWgths;
for i_Gauss=1:3
   t=GaussPnts(i_Gauss);
   N(i_Gauss,1)=0.5*(1-t)-0.5*(1-t*t)+(-9*t*t*t+t*t+9*t-1)/16;
   N_prime(i_Gauss,1)=-0.5+t+(-27*t*t+2*t+9)/16;
   N_scnd(i_Gauss,1)=1+(-2*27*t+2)/16;
   N(i_Gauss,2)=(1-t*t)+(27*t*t*t+7*t*t-27*t-7)/16;
   N_prime(i_Gauss,2)=-2*t+(3*27*t*t+14*t-27)/16;
   N_scnd(i_Gauss,2)=-2+(6*27*t+14)/16;
   N(i_Gauss,3)=(-27*t*t*t-9*t*t+27*t+9)/16;
   N_prime(i_Gauss,3)=(-3*27*t*t-18*t+27)/16;
   N_scnd(i_Gauss,3)=(-6*27*t-18)/16;
   N(i_Gauss,4)=0.5*(1+t)-0.5*(1-t*t)+(9*t*t*t+t*t-9*t-1)/16;
   N_prime(i_Gauss,4)=0.5+t+(27*t*t+2*t-9)/16;
   N_scnd(i_Gauss,4)=1+(2*27*t+2)/16;
end
%*************************************************************
% Shape Function Values at Fourth Point

   tEND=1;
   N_END(1)=0.5*(1-tEND)-0.5*(1-tEND*tEND)+(-9*tEND*tEND*tEND+tEND*tEND+9*tEND-1)/16;
   N_primeEND(1)=-0.5+tEND+(-27*tEND*tEND+2*tEND+9)/16;
   N_scndEND(1)=1+(-2*27*tEND+2)/16;
   N_END(2)=(1-tEND*tEND)+(27*tEND*tEND*tEND+7*tEND*tEND-27*tEND-7)/16;
   N_primeEND(2)=-2*tEND+(3*27*tEND*tEND+14*tEND-27)/16;
   N_scndEND(2)=-2+(6*27*tEND+14)/16;
   N_END(3)=(-27*tEND*tEND*tEND-9*tEND*tEND+27*tEND+9)/16;
   N_primeEND(3)=(-3*27*tEND*tEND-18*tEND+27)/16;
   N_scndEND(3)=(-6*27*tEND-18)/16;
   N_END(4)=0.5*(1+tEND)-0.5*(1-tEND*tEND)+(9*tEND*tEND*tEND+tEND*tEND-9*tEND-1)/16;
   N_primeEND(4)=0.5+tEND+(27*tEND*tEND+2*tEND-9)/16;
   N_scndEND(4)=1+(2*27*tEND+2)/16;
%*********************************************************************
% Calculate Initial Rotation Matrix and Determinant of det(dPhi/ds)

for i_elm=1:n_elm
   for i_Gauss=1:3
      i_g1=(i_elm-1)*(totallocalnode-1)+1;
      i_g2=(i_elm-1)*(totallocalnode-1)+totallocalnode;
      [InlRTMTRX{i_elm,i_Gauss},detPhi(i_elm,i_Gauss)]=Rot_Ini(InitialPhiVls(1:3,i_g1:i_g2),N,N_prime,N_scnd,i_Gauss);
   end
end
%*********************************************************************

% Calculate Initial Rotation Matrix Forth Fourth node of last element
ENDi_g1=(n_elm-1)*(totallocalnode-1)+1;
ENDi_g2=(n_elm-1)*(totallocalnode-1)+totallocalnode;
[InlRTMTRXEND,detPhiEND]=Rot_IniEND(InitialPhiVls(1:3,ENDi_g1:ENDi_g2),N_END,N_primeEND,N_scndEND);
%*********************************************************************
%Write Initial Phi Values to the file

   %Displacenent Data
```

```
   fidDisp=fopen('TDFrMm5000Al19_I1_01XExp_0025Inc1deg.txt','w');
   fprintf(fidDisp,'%4d\n',0);
   for i_glbnode=1:totalglobalnode
      fprintf(fidDisp,'%4d %+5.25e %+5.25e %+5.25e\n', ...
           [i_glbnode InitialPhiVls(1,i_glbnode) InitialPhiVls(2,i_glbnode) InitialPhiVls(3,i_glbnode)]);
   end
   fprintf(fidDisp,'%4d %+5.25e %+5.25e\n',[0 angVel(1) angAcc(1)]);
   fclose(fidDisp);

   %Create Rotation file

   fidROT=fopen('IRFrMm5000Al19_I1_01XExp_0025Inc1deg.txt','w');
   fprintf(fidROT,'%4d\n',0);
   fclose(fidROT);
%*************************************************************************

MalngNr(1:x_step)=zeros(1,x_step);
for i_step=1:n_step %1i_step
  DTheta=0;
  DeltaTheta=0;
  Lambda=0;
  if i_step<=x_step
        BCNodes=BCNode1;
  elseif i_step>x_step
        BCNodes=BCNode2;
        angVel(i_step)=angVel(i_step-1);
        angAcc(i_step)=0;
   end


   cnvrg=[1];
   i_Itr=1;
   n_step=8000; %Total Load Step
%*************************************************************************
```

% Calculate Deformed Configuration

```
while cnvrg(length(cnvrg))>1e-14 %cnvrg
      %Initialize Global Stiffness and Residual Matrices
      GlobalRsdlMtrx=sparse(6*(n_elm-1)*(totallocalnode-1)+6*totallocalnode,1);
      GlobalStiffMAT=sparse(6*(n_elm-1)*(totallocalnode-1)+6*totallocalnode, ...
                  6*(n_elm-1)*(totallocalnode-1)+6*totallocalnode);
      GlobalStiffGEO=sparse(6*(n_elm-1)*(totallocalnode-1)+6*totallocalnode, ...
                  6*(n_elm-1)*(totallocalnode-1)+6*totallocalnode);
      GlobalForce=sparse(6*(n_elm-1)*(totallocalnode-1)+6*totallocalnode,1);
      %*********************************************************************
      for i_elm=1:n_elm% 1i_elm
         i_g1=(i_elm-1)*(totallocalnode-1)+1;
         i_g2=(i_elm-1)*(totallocalnode-1)+totallocalnode;
         PhiIntmdt=InitialPhiVls(1:3,i_g1:i_g2)+ ...
               TotalDisp(1:3,i_g1:i_g2);
         ThetaIntmdt=IncRot(1:3,i_g1:i_g2);

         %Initialize Element Stiffness and Residual Matrices
         RsdlMtrx=sparse(totallocalnode*6,1);
         stiffMAT=sparse(totallocalnode*6,totallocalnode*6);
         stiffGEO=sparse(totallocalnode*6,totallocalnode*6);
       %*********************************************************************
         for i_Gauss=1:3 %FOR 1i_Gauss
            [Phi,PhiS,Theta,ThetaS]=ShpFnc(PhiIntmdt,ThetaIntmdt,N,N_prime,detPhi(i_elm,i_Gauss),i_Gauss);
            R=R_Mtrx(Theta,ThetaS);
            [ROT{i_elm,i_Gauss},T_ROT]=rotation(Theta);

            ROTMTRX=ROT{i_elm,i_Gauss}*PrevROTMTRX{i_elm,i_Gauss};
            epsilon_alfa=PhiS-ROTMTRX*InlRTMTRX{i_elm,i_Gauss}(:,1);
            Omega_alfa{i_elm,i_step+1,i_Gauss}=T_ROT*ThetaS+ROT{i_elm,i_Gauss}*Omega_alfa{i_elm,i_step,i_Gauss};
            k_alfa=Omega_alfa{i_elm,i_step+1,i_Gauss};
            n_alfa=ROTMTRX*InlRTMTRX{i_elm,i_Gauss}*Cn ...
                 *transpose(ROTMTRX*InlRTMTRX{i_elm,i_Gauss})*epsilon_alfa;
            m_alfa=ROTMTRX*InlRTMTRX{i_elm,i_Gauss}*Cm ...
                 *transpose(ROTMTRX*InlRTMTRX{i_elm,i_Gauss})*k_alfa;
           %*********************************************************************
             %Record Forces and Moments
            FORCE(i_elm,i_step,i_Gauss,1)=n_alfa(1);
```

```
  FORCE(i_elm,i_step,i_Gauss,2)=n_alfa(2);
  FORCE(i_elm,i_step,i_Gauss,3)=n_alfa(3);
  MOMENT(i_elm,i_step,i_Gauss,1)=m_alfa(1);
  MOMENT(i_elm,i_step,i_Gauss,2)=m_alfa(2);
  MOMENT(i_elm,i_step,i_Gauss,3)=m_alfa(3);
  %************************************************************************

  H=H_MTRX(m_alfa,Theta,ThetaS);
```

%ELement Residual Vector

```
A1=n_alfa;
A2=transpose(SKEW(PhiS)*T_ROT)*n_alfa+ ...
       (transpose(R+SKEW(k_alfa)*T_ROT))*m_alfa;
A3=transpose(T_ROT)*m_alfa;
for ii=1:totallocalnode %FOR 1_ii
   for i=1:3 %x y z %for 1xyz_i
      RsdlMtrx(6*(ii-1)+i)=RsdlMtrx(6*(ii-1)+i)+ ...
                  W(i_Gauss)*N_prime(i_Gauss,ii)*A1(i);
      RsdlMtrx(6*(ii-1)+3+i)=RsdlMtrx(6*(ii-1)+3+i)+ ...
                   W(i_Gauss)*A2(i)*N(i_Gauss,ii)*detPhi(i_elm,i_Gauss)+ ...
                   W(i_Gauss)*A3(i)*N_prime(i_Gauss,ii);
   end %END 1xyz_i
end %END 1_ii
```

%Element Tangent Material Matrix

```
 B1=ROTMTRX*InlRTMTRX{i_elm,i_Gauss}*Cn*transpose(ROTMTRX*InlRTMTRX{i_elm,i_Gauss});
 B11=ROTMTRX*InlRTMTRX{i_elm,i_Gauss}*Cm*transpose(ROTMTRX*InlRTMTRX{i_elm,i_Gauss});
 B2=B1*SKEW(PhiS)*T_ROT;
 A1=transpose(SKEW(PhiS)*T_ROT)*B1;
 B3=transpose(SKEW(PhiS)*T_ROT)*B1*(SKEW(PhiS)*T_ROT)+ ...
   transpose(R+SKEW(k_alfa)*T_ROT)*B11*(R+SKEW(k_alfa)*T_ROT);
 B4=transpose(R+SKEW(k_alfa)*T_ROT)*B11*T_ROT;
 B5=transpose(T_ROT)*B11*(R+SKEW(k_alfa)*T_ROT);
 B6=transpose(T_ROT)*B11*T_ROT;

for ii=1:totallocalnode %2_ii
   for jj=1:totallocalnode %1_jj
      for i=1:3 %2xyz_i
         for j=1:3 %1xyz_j
            stiffMAT(6*(ii-1)+i,6*(jj-1)+j)=stiffMAT(6*(ii-1)+i,6*(jj-1)+j)+ ...
                                 W(i_Gauss)*B1(i,j)*N_prime(i_Gauss,ii)*N_prime(i_Gauss,jj)/ ...
                                 detPhi(i_elm,i_Gauss);
            stiffMAT(6*(ii-1)+3+i,6*(jj-1)+j)=stiffMAT(6*(ii-1)+3+i,6*(jj-1)+j)+ ...
                                  W(i_Gauss)*A1(i,j)*N(i_Gauss,ii)*N_prime(i_Gauss,jj);
            stiffMAT(6*(ii-1)+i,6*(jj-1)+3+j)=stiffMAT(6*(ii-1)+i,6*(jj-1)+3+j)+ ...
                                  W(i_Gauss)*B2(i,j)*N_prime(i_Gauss,ii)*N(i_Gauss,jj);
            stiffMAT(6*(ii-1)+3+i,6*(jj-1)+3+j)=stiffMAT(6*(ii-1)+3+i,6*(jj-1)+3+j)+ ...
                                  W(i_Gauss)*B3(i,j)*N(i_Gauss,ii)*N(i_Gauss,jj)*detPhi(i_elm,i_Gauss)+ ...
                                  W(i_Gauss)*B5(i,j)*N_prime(i_Gauss,ii)*N(i_Gauss,jj)+ ...
                                  W(i_Gauss)*B4(i,j)*N(i_Gauss,ii)*N_prime(i_Gauss,jj)+ ...
                                  W(i_Gauss)*B6(i,j)*N_prime(i_Gauss,ii)*N_prime(i_Gauss,jj)/ ...
                                   detPhi(i_elm,i_Gauss);
         end %1xyz_j
      end %2xyz_i
   end %1_jj
end %2_ii
```

% Element Tangent Geometric Matrix

```
 B2=-SKEW(n_alfa)*T_ROT;
 A1=transpose(T_ROT)*SKEW(n_alfa);
 B3=transpose(T_ROT)*SKEW(k_alfa)*skew(m_alfa)*T_ROT+ ...
   Sum_Mtrx(Theta,SKEW(m_alfa)*k_alfa)+ ...
   transpose(T_ROT)*SKEW(m_alfa)*R-transpose(R)*SKEW(m_alfa)*T_ROT+ ...
   H+ ...
   transpose(T_ROT)*SKEW(PhiS)*SKEW(n_alfa)*T_ROT+ ...
   Sum_Mtrx(Theta,SKEW(n_alfa)*PhiS);
 B4=transpose(T_ROT)*SKEW(m_alfa)*T_ROT+transpose(Sum_Mtrx(Theta,m_alfa));
 B5=-transpose(T_ROT)*SKEW(m_alfa)*T_ROT+Sum_Mtrx(Theta,m_alfa);

for ii=1:totallocalnode %3_ii
   for jj=1:totallocalnode %2_jj
      for i=1:3 %3xyz_i
         for j=1:3 %2xyz_j
```

```
                stiffGEO(6*(ii-1)+i,6*(jj-1)+j)=stiffGEO(6*(ii-1)+i,6*(jj-1)+j)+0;
                stiffGEO(6*(ii-1)+3+i,6*(jj-1)+j)=stiffGEO(6*(ii-1)+3+i,6*(jj-1)+j)+ ...
                                W(i_Gauss)*A1(i,j)*N(i_Gauss,ii)*N_prime(i_Gauss,jj);
                stiffGEO(6*(ii-1)+i,6*(jj-1)+3+j)=stiffGEO(6*(ii-1)+i,6*(jj-1)+3+j)+ ...
                                W(i_Gauss)*B2(i,j)*N_prime(i_Gauss,ii)*N(i_Gauss,jj);
                stiffGEO(6*(ii-1)+3+i,6*(jj-1)+3+j)=stiffGEO(6*(ii-1)+3+i,6*(jj-1)+3+j)+ ...
                                W(i_Gauss)*B3(i,j)*N(i_Gauss,ii)*N(i_Gauss,jj)*detPhi(i_elm,i_Gauss)+ ...
                                W(i_Gauss)*B5(i,j)*N_prime(i_Gauss,ii)*N(i_Gauss,jj)+ ...
                                W(i_Gauss)*B4(i,j)*N(i_Gauss,ii)*N_prime(i_Gauss,jj);

              end %2xyz_j
            end %3xyz_i
          end %2_jj
        end %3_ii


    end %1_i_Gauss
    %Update Global Stiffness Matrix
    GlobalNode1=6*(i_elm-1)*(totallocalnode-1)+1;
    GlobalNode2=6*(i_elm-1)*(totallocalnode-1)+6*totallocalnode;
    GlobalRsdlMtrx(GlobalNode1:GlobalNode2)=GlobalRsdlMtrx(GlobalNode1:GlobalNode2)+ ...
                        RsdlMtrx;
    GlobalStiffMAT(GlobalNode1:GlobalNode2,GlobalNode1:GlobalNode2)= ...
        GlobalStiffMAT(GlobalNode1:GlobalNode2,GlobalNode1:GlobalNode2)+ ...
        stiffMAT;
    GlobalStiffGEO(GlobalNode1:GlobalNode2,GlobalNode1:GlobalNode2)= ...
        GlobalStiffGEO(GlobalNode1:GlobalNode2,GlobalNode1:GlobalNode2)+ ...
        stiffGEO;
end %1i_elm

%Assemble Global Stfiness

GlobalStiff=GlobalStiffMAT+GlobalStiffGEO;
[glbSN,glbSM]=size(GlobalStiff);

%Calculate total Force Vector

TotalForceVec=-GlobalRsdlMtrx;
[glbFN,glbFM]=size(TotalForceVec);
if i_step<=x_step %IFxxx
    GlobalStiff=GlobalStiff(7:(glbSN-6),7:(glbSM-6));
    TotalForceVec=TotalForceVec(7:(glbFN-6),1);
elseif i_step>x_step

 %Update according to constraints

    r1vec=EndROTMTRX*r1zero;
    DRrot=[DeltaR(ThetaIntmdt(:,4),r1vec)*n_rot2(:,2);n_rot2(:,2)];
    S1=GlobalStiff(1:(6*totalglobalnode-6),1:(6*totalglobalnode-6));
    S2=GlobalStiff(1:(6*totalglobalnode-6),(6*totalglobalnode-6+1):6*totalglobalnode);
    S3=GlobalStiff((6*totalglobalnode-6+1):6*totalglobalnode,1:(6*totalglobalnode-6));
    S4=GlobalStiff((6*totalglobalnode-6+1):6*totalglobalnode,(6*totalglobalnode-6+1):6*totalglobalnode);
    GlobalStiff=[S1,S2*DRrot;transpose(DRrot)*S3,transpose(DRrot)*S4*DRrot];

    %Update according to constraints

    F1=TotalForceVec(1:(6*totalglobalnode-6),1);
    F2=TotalForceVec((6*totalglobalnode-6+1):6*totalglobalnode,1);
    TotalForceVec=[F1;transpose(DRrot)*F2];

    %Apply BCs

    BCNodes1=6*(n_elm-1)*(totallocalnode-1)+6*totallocalnode;
    TotalForceVec=TotalForceVec(7:(BCNodes1-6+1),1);
    GlobalStiff=GlobalStiff(7:(BCNodes1-6+1),7:(BCNodes1-6+1));
%************************************************************
%Calculate Forces and Moments at the end of beam

ENDi_g1=(n_elm-1)*(totallocalnode-1)+1;
ENDi_g2=(n_elm-1)*(totallocalnode-1)+totallocalnode;
PhiIntmdtEND=InitialPhiVls(1:3,ENDi_g1:ENDi_g2)+ ...
             TotalDisp(1:3,ENDi_g1:ENDi_g2);
ThetaIntmdtEND=IncRot(1:3,ENDi_g1:ENDi_g2);
[PhiEND,PhiSEND,ThetaEND,ThetaSEND]=ShpFncEND(PhiIntmdtEND,ThetaIntmdtEND,N_END,N_primeEND,detPhiEND);
[ROTEND,T_ROTEND]=rotation(ThetaEND);
```

```
%Strains at the end of coupling

epsilon_alfaEND=PhiSEND-ROTEND*EndROTMTRX*InlRTMTRXEND(:,1);
Omega_alfaEND(:,i_step+1)=T_ROTEND*ThetaSEND+ROTEND*Omega_alfaEND(:,i_step);
k_alfaEND=Omega_alfaEND(:,i_step+1);
%Forces and Moment at the end of coupling

n_alfaEND=ROTEND*EndROTMTRX*InlRTMTRXEND*Cn ...
            *transpose(ROTEND*EndROTMTRX*InlRTMTRXEND)*epsilon_alfaEND;
m_alfaEND=ROTEND*EndROTMTRX*InlRTMTRXEND*Cm ...
            *transpose(ROTEND*EndROTMTRX*InlRTMTRXEND)*k_alfaEND;

%New location of END Radius Vector

RdsEND=ROTEND*EndROTMTRX*r1zero;
%Save Force- Moment- r

MomentEND(:,i_step)=m_alfaEND;
ForceEND(:,i_step)=n_alfaEND;
RValuesEND(:,i_step)=RdsEND;
%Moment along rotation axis=Inertia*(Theta'')

MalngNr(i_step)=transpose(n_rot2(:,2))*(SKEW(RdsEND)*(n_alfaEND)+m_alfaEND)+Inertia*angAcc(i_step);

%*****************************************************************
b1=(ROTEND*EndROTMTRX*InlRTMTRXEND*transpose(Cn)*transpose(ROTEND*EndROTMTRX*InlRTMTRXEND)) ...
  *SKEW(n_rot2(:,2))*RdsEND;
b2=(ROTEND*EndROTMTRX*InlRTMTRXEND*transpose(Cm)*transpose(ROTEND*EndROTMTRX*InlRTMTRXEND))*n_rot2(:,2);
X=SKEW(RdsEND);
F1=b1;
F2=transpose(SKEW(PhiSEND)*T_ROTEND)*b1;
OmTH=SKEW(T_ROTEND*ThetaSEND);
REnd=R_Mtrx(ThetaEND,ThetaSEND);
F3=transpose(OmTH*T_ROTEND)*b2+transpose(REnd)*b2;
F4=transpose(T_ROTEND)*b2;
G1=transpose(SKEW(b1))*T_ROTEND;
G2=transpose(G1);
G3=transpose(T_ROTEND)*SKEW(PhiSEND)*SKEW(b1)*T_ROTEND+Sum_Mtrx(ThetaEND,SKEW(b1)*PhiSEND);
G4=transpose(T_ROTEND)*OmTH*SKEW(b2)*T_ROTEND+Sum_Mtrx(ThetaEND,SKEW(b2)*PhiSEND)+ ...
  transpose(T_ROTEND)*SKEW(b2)*REnd-transpose(REnd)*SKEW(b2)*T_ROTEND+ ...
  H_MTRX(b2,ThetaEND,ThetaSEND);
G5=transpose(T_ROTEND)*SKEW(b2)*T_ROTEND+transpose(Sum_Mtrx(ThetaEND,b2));
G6=-transpose(T_ROTEND)*SKEW(b2)*T_ROTEND+Sum_Mtrx(ThetaEND,b2);
%ADD Variations
%TotalForce Vector
[ROW,CLM]=size(GlobalStiff);
%Add Lamda Part
TotalForceVec=[TotalForceVec;0];
GlobalStiff=[[GlobalStiff;zeros(1,CLM)],zeros(ROW+1,1)];
%Update Total Force Vector
%DPhi1-DTheta1
iCk1Phi=6*(n_elm-1)*(totallocalnode-1)+1-6;%First Node Deleted
iCk1ndPhi=iCk1Phi+2;
iCk1RT=6*(n_elm-1)*(totallocalnode-1)+3+1-6;%First Node Deleted
iCk1ndRT=iCk1RT+2;
TotalForceVec(iCk1Phi:iCk1ndPhi,1)=TotalForceVec(iCk1Phi:iCk1ndPhi,1)- ...
                Lambda*N_primeEND(1)/detPhiEND*F1;
TotalForceVec(iCk1RT:iCk1ndRT,1)=TotalForceVec(iCk1RT:iCk1ndRT,1)- ...
                Lambda*N_primeEND(1)/detPhiEND*F4;
%DPhi2-DTheta2
iCk2Phi=iCk1Phi+6;
iCk2ndPhi=iCk2Phi+2;
iCk2RT=iCk1RT+6;
iCk2ndRT=iCk2RT+2;
TotalForceVec(iCk2Phi:iCk2ndPhi,1)=TotalForceVec(iCk2Phi:iCk2ndPhi,1)- ...
                Lambda*N_primeEND(2)/detPhiEND*F1;
TotalForceVec(iCk2RT:iCk2ndRT,1)=TotalForceVec(iCk2RT:iCk2ndRT,1)- ...
                Lambda*N_primeEND(2)/detPhiEND*F4;
%DPhi3-DTheta3
iCk3Phi=iCk2Phi+6;
iCk3ndPhi=iCk3Phi+2;
iCk3RT=iCk2RT+6;
iCk3ndRT=iCk3RT+2;
TotalForceVec(iCk3Phi:iCk3ndPhi,1)=TotalForceVec(iCk3Phi:iCk3ndPhi,1)- ...
                Lambda*N_primeEND(3)/detPhiEND*F1;
```

```
TotalForceVec(iCk3RT:iCk3ndRT,1)=TotalForceVec(iCk3RT:iCk3ndRT,1)- ...
                    Lambda*N_primeEND(3)/detPhiEND*F4;
%DThetaR
TotalForceVec(ROW,1)=TotalForceVec(ROW,1)-Lambda*Inertia/DTime/DTime- ...
   Lambda*(N_primeEND(4)/detPhiEND*transpose(n_rot2(:,2))*(-transpose(X*T_ROTEND)*F1+F4)- ...
         transpose(n_rot2(:,2))*(F2+F3))- ...
         Inertia*angAcc(i_step);
%DLamda
TotalForceVec(ROW+1,1)=TotalForceVec(ROW+1,1)-MalngNr(i_step);
%
%GlobalStiffness Matrix
%
%DLamda*[XX]*DeltaPhi1
GlobalStiff(ROW+1,iCk1Phi:iCk1ndPhi)=GlobalStiff(ROW+1,iCk1Phi:iCk1ndPhi)+ ...
                    N_primeEND(1)/detPhiEND*transpose(F1);
%DPhi1*[XX]*DeltaLambda
GlobalStiff(iCk1Phi:iCk1ndPhi,CLM+1)=GlobalStiff(iCk1Phi:iCk1ndPhi,CLM+1)+ ...
                    N_primeEND(1)/detPhiEND*(F1);

%DLamda*[XX]*DeltaTheta1
GlobalStiff(ROW+1,iCk1RT:iCk1ndRT)=GlobalStiff(ROW+1,iCk1RT:iCk1ndRT)+ ...
                    N_primeEND(1)/detPhiEND*transpose(F4);
%DTheta1*[XX]*DeltaLambda
GlobalStiff(iCk1RT:iCk1ndRT,CLM+1)=GlobalStiff(iCk1RT:iCk1ndRT,CLM+1)+ ...
                    N_primeEND(1)/detPhiEND*(F4);
%DLamda*[XX]*DeltaPhi2
GlobalStiff(ROW+1,iCk2Phi:iCk2ndPhi)=GlobalStiff(ROW+1,iCk2Phi:iCk2ndPhi)+ ...
                    N_primeEND(2)/detPhiEND*transpose(F1);

%DPhi2*[XX]*DeltaLambda
GlobalStiff(iCk2Phi:iCk2ndPhi,CLM+1)=GlobalStiff(iCk2Phi:iCk2ndPhi,CLM+1)+ ...
                    N_primeEND(2)/detPhiEND*(F1);
%DLamda*[XX]*DeltaTheta2
GlobalStiff(ROW+1,iCk2RT:iCk2ndRT)=GlobalStiff(ROW+1,iCk2RT:iCk2ndRT)+ ...
                    N_primeEND(2)/detPhiEND*transpose(F4);
%DTheta2*[XX]*DeltaLambda
GlobalStiff(iCk2RT:iCk2ndRT,CLM+1)=GlobalStiff(iCk2RT:iCk2ndRT,CLM+1)+ ...
                    N_primeEND(2)/detPhiEND*(F4);
%DLamda*[XX]*DeltaPhi3
GlobalStiff(ROW+1,iCk3Phi:iCk3ndPhi)=GlobalStiff(ROW+1,iCk3Phi:iCk3ndPhi)+ ...
                    N_primeEND(3)/detPhiEND*transpose(F1);
%DPhi3*[XX]*DeltaLambda
GlobalStiff(iCk3Phi:iCk3ndPhi,CLM+1)=GlobalStiff(iCk3Phi:iCk3ndPhi,CLM+1)+ ...
                    N_primeEND(3)/detPhiEND*(F1);

%DLamda*[XX]*DeltaTheta3
GlobalStiff(ROW+1,iCk3RT:iCk3ndRT)=GlobalStiff(ROW+1,iCk3RT:iCk3ndRT)+ ...
                    N_primeEND(3)/detPhiEND*transpose(F4);
%DTheta3*[XX]*DeltaLambda
GlobalStiff(iCk3RT:iCk3ndRT,CLM+1)=GlobalStiff(iCk3RT:iCk3ndRT,CLM+1)+ ...
                    N_primeEND(3)/detPhiEND*(F4);
%DLambda[XX]DeltaThetaR
GlobalStiff(ROW+1,CLM)=GlobalStiff(ROW+1,CLM)+Inertia/DTime/DTime+ ...
   transpose(F2+F3)*n_rot2(:,2)+ ...
   N_primeEND(4)/detPhiEND*(-transpose(F1)*X*T_ROTEND+transpose(F4))*n_rot2(:,2);
%DThetaR*[XX]*DeltaLamda
GlobalStiff(ROW,CLM+1)=GlobalStiff(ROW,CLM+1)+Inertia/DTime/DTime+  ...
  transpose(n_rot2(:,2))*(F2+F3)+ ...
  N_primeEND(4)/detPhiEND*transpose(n_rot2(:,2))*(-transpose(X*T_ROTEND)*F1+F4);
%DPhi1*[XX]*DeltaThetaR
GlobalStiff(iCk1Phi:iCk1ndPhi,CLM)=GlobalStiff(iCk1Phi:iCk1ndPhi,CLM)+ ...
   Lambda*N_primeEND(1)/detPhiEND*G1*n_rot2(:,2);
%DPhi2*[XX]*DeltaThetaR
GlobalStiff(iCk2Phi:iCk2ndPhi,CLM)=GlobalStiff(iCk2Phi:iCk2ndPhi,CLM)+ ...
   Lambda*N_primeEND(2)/detPhiEND*G1*n_rot2(:,2);
%DPhi3*[XX]*DeltaThetaR
GlobalStiff(iCk3Phi:iCk3ndPhi,CLM)=GlobalStiff(iCk3Phi:iCk3ndPhi,CLM)+ ...
   Lambda*N_primeEND(2)/detPhiEND*G1*n_rot2(:,2);
%DThetaR*[XX]*DeltaPhi1
GlobalStiff(ROW,iCk1Phi:iCk1ndPhi)=GlobalStiff(ROW,iCk1Phi:iCk1ndPhi)+...
   Lambda*N_primeEND(1)/detPhiEND*transpose(n_rot2(:,2))*G2;
%DThetaR*[XX]*DeltaPhi2
GlobalStiff(ROW,iCk2Phi:iCk2ndPhi)=GlobalStiff(ROW,iCk2Phi:iCk2ndPhi)+...
   Lambda*N_primeEND(2)/detPhiEND*transpose(n_rot2(:,2))*G2;
%DThetaR*[XX]*DeltaPhi3
GlobalStiff(ROW,iCk3Phi:iCk3ndPhi)=GlobalStiff(ROW,iCk3Phi:iCk3ndPhi)+...
```

```
   Lambda*N_primeEND(3)/detPhiEND*transpose(n_rot2(:,2))*G2;
%DTheta1*[XX]*DeltaThetaR
GlobalStiff(iCk1RT:iCk1ndRT,CLM)=GlobalStiff(iCk1RT:iCk1ndRT,CLM)+ ...
   Lambda*N_primeEND(1)/detPhiEND*G6*n_rot2(:,2);
%DTheta2*[XX]*DeltaThetaR
GlobalStiff(iCk2RT:iCk2ndRT,CLM)=GlobalStiff(iCk2RT:iCk2ndRT,CLM)+ ...
   Lambda*N_primeEND(2)/detPhiEND*G6*n_rot2(:,2);
%DTheta3*[XX]*DeltaThetaR
GlobalStiff(iCk3RT:iCk3ndRT,CLM)=GlobalStiff(iCk3RT:iCk3ndRT,CLM)+ ...
   Lambda*N_primeEND(3)/detPhiEND*G6*n_rot2(:,2);
%DThetaR*[XX]*DeltaTheta1
GlobalStiff(ROW,iCk1RT:iCk1ndRT)=GlobalStiff(ROW,iCk1RT:iCk1ndRT)+...
   Lambda*N_primeEND(1)/detPhiEND*transpose(n_rot2(:,2))*G5;
%DThetaR*[XX]*DeltaTheta2
GlobalStiff(ROW,iCk2RT:iCk2ndRT)=GlobalStiff(ROW,iCk2RT:iCk2ndRT)+...
   Lambda*N_primeEND(2)/detPhiEND*transpose(n_rot2(:,2))*G5;
%DThetaR*[XX]*DeltaTheta3
GlobalStiff(ROW,iCk3RT:iCk3ndRT)=GlobalStiff(ROW,iCk3RT:iCk3ndRT)+...
   Lambda*N_primeEND(1)/detPhiEND*transpose(n_rot2(:,2))*G5;
%DthetaR*[XX]*DeltaThetaR
GlobalStiff(ROW,CLM)=GlobalStiff(ROW,CLM)+ ...
   Lambda*N_primeEND(4)/detPhiEND*transpose(n_rot2(:,2))* ...
      (-transpose(X*T_ROTEND)*G1-G2*X*T_ROTEND+G5+G6)*n_rot2(:,2)+ ...
   Lambda*transpose(n_rot2(:,2))*(G3+G4)*n_rot2(:,2)+ ...
   Inertia/DTime/DTime;

%*************************************************************************
    end% END of Ifxxx

    %Solve for Increments
    DeltaInc=GlobalStiff\TotalForceVec;
    %Update
    BCnumber=0;
    i_BC=0;
    BCcntr=1;
     if i_step>x_step
     Lambda=Lambda+DeltaInc(ROW+1);
     DeltaInc=DeltaInc(1:ROW);
     end
    for i_globalnode=1:totalglobalnode
      if any(i_globalnode==(BCNodes))
         DeltaDisp((3*(i_globalnode-1)+1):3*i_globalnode,1)=[0;0;0];
         DeltaRot((3*(i_globalnode-1)+1):3*i_globalnode,1)=[0;0;0];
         BCnumber=BCnumber+1;
         i_BC=i_BC+1;
         BCcntr=BCcntr+1;
      elseif all(i_globalnode~=BCNodes)&(i_globalnode~=totalglobalnode)
         Check1=(i_globalnode>=BCNodes(i_BC));
         iChecknode1=6*(i_globalnode-1)+1-6*BCnumber*Check1;
         iChecknode2=6*i_globalnode-3-6*BCnumber*Check1;
         iChecknode3=6*(i_globalnode-1)+4-6*BCnumber*Check1;
         iChecknode4=6*i_globalnode-6*BCnumber*Check1;
         DeltaDisp((3*(i_globalnode-1)+1):3*i_globalnode,1)= ...
            DeltaInc(iChecknode1:iChecknode2);
         TotalDisp(1:3,i_globalnode)=TotalDisp(1:3,i_globalnode)+ ...
            DeltaInc(iChecknode1:iChecknode2);
         DeltaRot((3*(i_globalnode-1)+1):3*i_globalnode,1)= ...
            DeltaInc(iChecknode3:iChecknode4);
         IncRot(1:3,i_globalnode)=IncRot(1:3,i_globalnode)+ ...
            DeltaInc(iChecknode3:iChecknode4);

      elseif (i_globalnode==totalglobalnode)&(i_step>x_step)
         %Update last node
         IncRot(1:3,totalglobalnode)=IncRot(1:3,totalglobalnode)+ ...
            DeltaInc(length(DeltaInc))*n_rot2(:,2);

         [updROT,dummyT]=rotation(IncRot(1:3,totalglobalnode));
         TotalDisp(1:3,totalglobalnode)=lzero+updROT*EndROTMTRX*r1zero ...
                +[0;0;PrlMis]-InitialPhiVls(1:3,totalglobalnode);
         DeltaTheta=DeltaInc(length(DeltaInc));
         DTheta=DTheta+DeltaTheta;
         angVel(i_step)=DTheta/DTime;
         angAcc(i_step)=(angVel(i_step)-angVel(i_step-1))/DTime;
      end %END of if
    end %end of for
    %Update Lambda
```

```
    cnvrg=[cnvrg;sqrt(transpose(DeltaDisp)*DeltaDisp)+ ...
          sqrt(transpose(DeltaRot)*DeltaRot)];
    disp([' i_step=',num2str(i_step,'%d')]);
    disp(['cnvrg=',num2str(cnvrg(length(cnvrg)),'%0.10e')])
    disp(['DTheta=',num2str(DTheta,'%0.15e')])
    disp([' DROT2=',num2str(DROT2,'%0.15e')])
    disp(['DTheta-DROT2=',num2str((DTheta-DROT2),'%0.15e')])
    disp(['Inital  Velocity=',num2str(angVel(x_step),'%0.15e')])
    disp(['Angular Velocity=',num2str(angVel(i_step),'%0.15e')])
    disp(['Angular Acceleration=',num2str(angAcc(i_step),'%0.15e')])
    disp(['MomentAlong_Nr=',num2str(MalngNr(i_step),'%0.15e')])
    disp(['Lambda=',num2str(Lambda,'%0.15e')]);
    i_Itr=i_Itr+1;

  end %End of While
  %Write to file
   %Displacenent Data
  fidDisp=fopen('TDFrMm5000Al19_I1_01XExp_0025Inc1deg.txt','a');
  fprintf(fidDisp,'%4d\n',i_step);
  for i_glbnode=1:totalglobalnode
     fprintf(fidDisp,'%4d %+5.25e %+5.25e %+5.25e\n', ...
           [i_glbnode TotalDisp(1,i_glbnode) TotalDisp(2,i_glbnode) TotalDisp(3,i_glbnode)]);
  end
  fprintf(fidDisp,'%4d %+5.25e %+5.25e\n',[i_step angVel(i_step) angAcc(i_step)]);
  fclose(fidDisp);
   %Rotation Data
  fidROT=fopen('IRFrMm5000Al19_I1_01XExp_0025Inc1deg.txt','a');
  fprintf(fidROT,'%4d\n',i_step);
  for i_glbnode=1:totalglobalnode
     fprintf(fidROT,'%4d %+5.25e %+5.25e %+5.25e\n', ...
           [i_glbnode IncRot(1,i_glbnode) IncRot(2,i_glbnode) IncRot(3,i_glbnode)]);
  end
  fclose(fidROT);
 %Update for next iteration
  %Update EndROTMTRX
      [EndROT,dummT]=rotation(IncRot(1:3,totalglobalnode));
      EndROTMTRX=EndROT*EndROTMTRX;
      %update Omega_alfaEND
      if i_step<=x_step
       ENDi_g1=(n_elm-1)*(totallocalnode-1)+1;
       ENDi_g2=(n_elm-1)*(totallocalnode-1)+totallocalnode;
       PhiIntmdtEND=InitialPhiVls(1:3,ENDi_g1:ENDi_g2)+ ...
              TotalDisp(1:3,ENDi_g1:ENDi_g2);
       ThetaIntmdtEND=IncRot(1:3,ENDi_g1:ENDi_g2);
       [PhiEND,PhiSEND,ThetaEND,ThetaSEND]=ShpFncEND(PhiIntmdtEND,ThetaIntmdtEND,N_END,N_primeEND,detPhiEND);
       [ROTEND,T_ROTEND]=rotation(ThetaEND);
       Omega_alfaEND(:,i_step+1)=T_ROTEND*ThetaSEND+ROTEND*Omega_alfaEND(:,i_step);
      end
      %************************
      IncRot=zeros(3,totalglobalnode);
      for i_elm=1:n_elm
       for i_Gauss=1:n_Gauss
        PrevROTMTRX{i_elm,i_Gauss}=ROT{i_elm,i_Gauss}*PrevROTMTRX{i_elm,i_Gauss};
       end
      end
      if i_step<x_step
        if (i_step<x_stepAng)
         IncRot(1:3,totalglobalnode)=DROT1*n_rot1;
         [antROT,dummyROT]=rotation(IncRot(1:3,totalglobalnode));
         TotalDisp(1:3,totalglobalnode)=lzero+antROT*EndROTMTRX*r1zero ...
                                  -InitialPhiVls(1:3,totalglobalnode);
        elseif (i_step>=x_stepAng)
            IncRot(1:3,totalglobalnode)=[0;0;0];
            TotalDisp(1:3,totalglobalnode)=TotalDisp(1:3,totalglobalnode)+[0;0;DPMis];
        end
      elseif i_step>=x_step
        IncRot(1:3,1)=DROT2*n_rot2(:,1);
        [firstROT,dummyT]=rotation(IncRot(1:3,1));
        firstROTMTRX=firstROT*firstROTMTRX;
        TotalDisp(1:3,1)=firstROTMTRX*r2zero-InitialPhiVls(1:3,1);
      end

if any(i_step==[1:35:n_step])
save TFrcMmt5000Al19_I1_01XExp_0025Inc1deg.mat
end
end %1i_step
```